# AN INVESTIGATION OF A
# TWO-STEP, TEMPERATURE-STAGED,
# DIRECT COAL LIQUEFACTION PROCESS

Reyna Singh

[BSc. (Eng.), UKZN]

University of KwaZulu-Natal

Durban

Dissertation submitted in the School of Chemical Engineering

in fulfilment of the requirements for the degree

Master of Science in Engineering, Chemical Engineering

11 December 2015

Supervisors: Dr David Lokhat and Prof. Milan Carsky

**Declaration**

I, Reyna Singh declare that:

The research reported in this dissertation/thesis, except where otherwise indicated, is my original work.

(i) This dissertation/thesis has not been submitted for any degree or examination at any other university.

(ii) This dissertation/thesis does not contain other persons' data, pictures, graphs or other information, unless specifically acknowledged as being sourced from other persons.

(iii)This dissertation/thesis does not contain other persons' writing, unless specifically acknowledged as being sourced from other researchers. Where other written sources have been quoted, then:

    a) their words have been re-written but the general information attributed to them has been referenced;

    b) Where their exact words have been used, their writing has been placed inside quotation marks, and referenced.

(iv)Where I have reproduced a publication of which I am an author, co-author or editor, I have indicated in detail which part of the publication was actually written by myself alone and have fully referenced such publications.

(v) This dissertation/thesis does not contain text, graphics or tables copied and pasted from the Internet, unless specifically acknowledged, and the source being detailed in the dissertation/thesis and in the References sections.

(vi) This dissertation has been approved for submission by the supervisor of this work

Signed (Candidate):_____            Date: <u>08  Decemeber 2015</u>

Signed (Supervisor):_____          Date: <u>11 December 2015</u>

## Acknowledgment

**Research Outputs**

Peer reviewed conference paper:

Singh, R; Lokhat, D; Carsky M., A two-step, temperature staged direct coal liquefaction process*, International Journal of Chemical, Molecular, Nuclear, Materials and Metallurgy Engineering*, Vol.9, No. 7, 2015 873-879, World Academy of Science, Engineering and Technology conference –Zurich, Switzerland July 2015

# Abstract

From its inception in the 1700's, deriving fuel from the Direct Coal Liquefaction (DCL) process has spawned numerous pursuits. While coal is an abundant fossil fuel in many countries and represents approximately 70% of the world's total energy reserves (Birol, 2004), the DCL process is synonymous with the use of severe operating conditions and catalysts of poor activity.

This work is an investigation of a two-step, temperature-staged DCL process and aimed at producing a high value liquid hydrocarbon product at, relatively, mild operating conditions.

This stepwise process was initially carried out in a batch reactor. In this first stage, the aim was to maximise on the liquid product (oil) yield by enhancing the thermal dissolution of high grade bituminous type coal in tetralin as the hydrogen donor solvent, using 2:1 and 3:1 solvent: coal ratios. The oil obtained was refined by hydrotreating in a catalytic fixed bed reactor. Both stages were carried out isobarically at 100 barg and, in the first stage, temperatures of 250 ℃ and 300 °C were used. Thereafter, operating temperatures were staged with a 50 °C increase in the second stage reactor. In the first stage, molybdenum doped magnetite was used as the catalyst. The performances of cobalt-molybdenum (Co-Mo) and nickel-molybdenum (Ni-Mo) were trialled in the second-stage reactor. In order to assess the potential value of the oil between the stages, the oil was analysed using Gas Chromatography –Mass Spectrometry (GC-MS).

Within the actual experimental boundary; oil yield, alkane and cycloalkane selectivity response data was fitted to linear models. In the first stage the liquid yield was increased with the use of molybdenum doped magnetite catalyst and affected mainly by the temperature and solvent: coal ratios. An oil yield of approximately 51.26% was obtained for blank runs and up to 54.77% for catalysed runs. As a hydrodesulphurisation (HDS) performer and selectivity to the production of long and branched chain alkanes, Ni-Mo had an improved performance over Co-Mo. Co-Mo is selective to a higher concentration of cycloalkanes. For 16 days on stream each, Ni-Mo had a higher activity than Co-Mo.

A comparison of the actual data with a literature baseline, showed similarities for the results obtained using 2:1 solvent: coal ratios for both the blank and catalysed runs. As literature made use of severe operating conditions, the performance of the experimental batch reactor system was superior to literature.

While there remains room for improvement in the design of the two-stage system, evidence exists that the potential to cover the demand for low–sulphur, crude diesel and solvents from the production of high value hydrocarbon liquid in the said process, is demonstrated.

# Table of Contents

# I List of Figures

Below the list of figures included in the main body of the report

## II. List of Tables

Below the list of figures included in the main body of the report.

**Chapter 3**

**Chapter 4**

# Chapter One: Introduction

**Chapter Overview:**

This chapter provides background of the DCL process, including insight into the studies which have developed from the foundation of Bergius process. In summary, it provides facts and figures relating to the shortfalls of the process; and by overcoming these shortfalls substantiates for further research and commercial implementation of DCL. The main research aims and objectives are included in section 1.2.

## 1.1 Background and Importance of Topic

### 1.1.1   History of Direct Coal Liquefaction

Coal has been the world's main source of energy since the beginning of the French Revolution in the 1700's.

Direct coal liquefaction technology first developed from work on hydrogenating coal tar by Bergius in Germany in the 1920s. The first brown coal was hydrogenated in 1929 by Bergius, who operated the direct coal liquefaction process under severe operating conditions, including a pressure and temperature of approximately 70MPa and 500°C respectively (Robinson, 2009). The original Bergius plants consisted of liquid phase catalytic hydrogenation of a coal recycle slurry followed by vapour-phase catalytic hydrogenation of middle oils. Apart from the severe operating conditions, another disadvantage of the process was its use of an iron-based catalyst of poor activity. In the 1930s, several plants were built in Germany, and one in Billingham, England. German capacity increased to the point that during World War II, eight additional plants were built in Germany. In 1943, the installed capacity was over 100 000 barrels (approximately 16 million litres) per stream per day in 15 plants which processed 50 000 tons of dry coal per day. The United States Bureau of Mines tested the German technology after World War II in a 200 barrel (approximately 31 796 litres) per day pilot plant. All of the German efforts were proved technically successful but could not compete economically with inexpensive petroleum from the Middle East in the early 1950's (Robinson, 2009).

Further development of the process developed from the Bergius technology, with the major objectives being relaxing of operating conditions, increasing the liquid yield and lowering the hydrogen consumption. Hydrogen donor solvents, catalyst and stepwise hydrogen addition (two or three stages in various combinations) have been explored with plant sizes including 200 tonnes of coal per day.

China is the only country with a commercialised coal to liquid plant. In Shenhua, Inner Mongolia, this plant  is based on the Hydrogen Research, Inc. (HRI) integrated two-stage liquefaction (ITSL) process and the New Energy and Industrial Technology Development Organization (NEDOL) processes (Robinson, 2009).

### 1.1.2 Second Generation Technologies

The Bergius process spawned second generation technologies which were introduced between the 1970s and 1980s. The pilot plants to develop these processes included:

1.    SRC-II (solvent refined coal) in Tacoma, Washington

2.    EDS (Exxon Donor Solvent) in Baytown, Texas and

3.    H-Coal in Catlettsburg, Kentucky

Both the SRC-II and EDS processes depended on a donor solvent for hydrogen during the liquefaction and used the mineral iron containing ores in the coal for a catalyst.

The EDS process used a catalytic stage to hydrotreat part of the recycle solvent in a second reactor. However, no catalyst was used in the coal liquefaction unit.

The H-Coal process was developed by HRI and was derived from their H-Oil process for petroleum residual upgrading. The basis of the process was a novel catalytic reactor in which the catalyst was ebullated in the liquid phase, similar to the gas-phase fluidized bed processes used in the petroleum industry (Robinson, 2009).

The U.S. Department of Energy (DOE) built a 250 tonne per day pilot plant at Catlettsburg, Kentucky which ran from 1980 to 1983. The plant was a technical success and confirmed yields by smaller scale equipment and a wide variety of mechanical equipment was tested including ebbulation pumps, pressure let-down and block valves, and hydrocyclones to concentrate the solids containing product. Although the process was not economical, two developments promised further cost reductions. The first was a catalyst developed by Amoco researchers. This process used a unique bimodal pore size distribution resulting in less catalyst deactivation and most importantly higher liquid yields. The second improvement, from Chevron Research, was a two stage liquefaction scheme which lowered hydrogen consumption by tailoring reaction conditions in each stage to favour the reactions of coal dissolution, hydrogenation of the donor solvent, thermal and catalytic conversion of the high molecular weight species and removal of sulphur, nitrogen and oxygen (Robinson, 2009).

### 1.1.3 Importance of Direct Coal Liquefaction

Oil provides 35% of global energy consumption and driven by population growth and economic development, the global energy demand is rising (Birol, 2004). While petroleum has been the primary feedstock for the production of liquid fuels for decades, it is becoming increasingly evident that petroleum reserves are declining and hence petroleum prices are on the rise.

Coal, a solid fossil fuel, is an abundant resource in many countries and represents approximately 70% of the world's total energy reserves (Birol, 2004). Thus coal will be available for the foreseeable future without raising geopolitical concerns. The cost of converting coal into useful liquid fuel is higher than the cost of refining crude oil; however it is the relative price of the raw coal feedstocks that provides the main incentive to pursue the technology (Birol, 2004).

There are vast coal reserves in countries such as the United States, China and South Africa. Coal constitutes the largest single fossil fuel resource in the U.S. South Africa has been producing coal-derived fuels since 1955 and today, about 30% of the country's gasoline and diesel needs are produced from indigenous coal (Birol, 2004).

Until recently, the use of coal-to-liquids did not increase with increased fuel demands because of environmental restrictions and the ready availability of petroleum and natural gas. Compared to petroleum, coal is hydrogen deficient and can be converted into liquid fuel by the process of hydrogenation. It also contains a higher oxygen, nitrogen and ash content. Thus, coal cannot be considered the most attractive energy source when comparing the chemistry of petroleum and natural gas. Most plants use petroleum or natural gas to fuel the process, whereas coal has not reached that level yet.

There are a number of problems associated with production of liquid fuels from coal such as loss of expensive catalyst, high pressure equipment, high equipment cost, and environmental pollution. Carbon dioxide ($CO_2$) capture and storage is an emerging technology with vast amounts of research already done in this field, it offers the potential for major reductions in $CO_2$ emissions from coal plants. Carbon dioxide emissions, over the full fuel cycle, can be reduced by as much as 20% compared to conventional oil products, through the use of carbon capture and storage (Williams and Larson, 2003).

Hydrocarbons, including natural gas, liquid petroleum gas (LPG), naphtha, are the principal process raw materials for the manufacture of hydrogen. The high cost of these raw materials for the manufacture of hydrogen is one of the reasons for the synthetic liquid fuel from coal to be more expensive than natural crude oil. Production of hydrogen from coal, which is a proven technology, will make the coal liquefaction more attractive. Furthermore, by using highly active catalysts, hydrogenation pressure has been cut down to 130-210 bar, which considerably reduces the cost of commercial reactors (Robinson, 2009).

Most sources state that one of the greatest problems in the direct hydrogenation yet to be solved is the use of commercial catalysts which are expensive, with short life and cannot be recovered

or regenerated. The difficulty lies in finding a low cost disposable catalyst(s). Literature has well established that cobalt and molybdenum are good catalysts for hydrogenation and hydrodesulphurization of coal, whereas nickel and molybdenum are effective for coal hydrodenitrogenation.

The transition of the main petroleum source to coal will not occur rapidly and will have to be justified substantially both economically and politically. The technology for the production of fuel from coal already exists, as improved coal technology starts to emerge which overcomes the current disadvantages of the process, the commercialization of such technologies will undoubtedly increase.

Coal may be used to produce liquid fuels suitable for transportation applications by the removal of carbon or the addition of hydrogen, either directly or indirectly. The first approach is usually known as carbonisation or pyrolysis and has low yields. The second is called liquefaction. The less efficient, but commercially proven, indirect liquefaction process relies on the gasification of coal to produce synthesis gas ( a mixture of carbon monoxide and hydrogen) which is then reacted over a catalyst at temperature and pressure to produce the desired liquid products. It is this indirect process, using well-established Fischer-Tropsch synthesis that has been commercialised by Sasol in South Africa and will be used in several new projects proposed in China (Robinson, 2009). Direct liquefaction is the most efficient route currently available (Akash, 2013).

**1.1.3.1 Direct versus Indirect Coal Liquefaction**

Carbon monoxide can be produced by gasification or using another carbon rich compound. The necessary reaction energy is supplied by steam or oxygen.

$$C + \frac{1}{2}O_2 \rightarrow CO \qquad\qquad (1.1.3.1)$$

The resulting mixture of carbon monoxide and hydrogen is called synthesis gas (syngas). In the presence of a suitable catalyst, syngas is used to construct hydrocarbon chains of different lengths. Generally, the Fischer Tropsch (FT) process yields two product types, described by (1.1.3.2) and (1.1.3.2).

$$nCO + 2nH_2 \rightarrow nH_2O + C_nH_{2n} \text{ (olefins)} \qquad (1.1.3.2)$$

$$nCO + (2n+1)H_2 \rightarrow nH_2O + C_nH_{2n+2} \text{ (paraffins)} \quad (1.1.3.3)$$
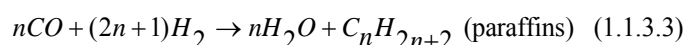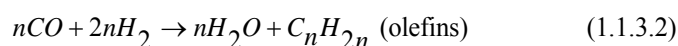
The selectivity to olefins or paraffins depends on the catalysts used and the reactor operating conditions. Olefin-rich products with 'n' in the range of 12-19 are suitable for making synthetic diesel and solvents in the low temperature FT-process.

In the DCL process, the coal is split into shorter hydrocarbons; resembling ordinary crude oil. This process occurs by adding $H_2$ under high pressure and temperature, thus eliminating the need for a gaseous middle stage.

$$nC + (n+1)H_2 \rightarrow C_nH_{2n+2} \qquad\qquad (1.1.3.4)$$

The main advantages of developing the coal-to-liquid technologies can be summarised as follows:

- Coal is the leading fossil fuel in terms of affordability and is widely distributed around the world. Thus, coal benefits from a well-established global market, with a large number of suppliers.
- The production of liquid fuels from coal will not require vast land resources or cause competition with food production.
- Coal is mined in over 50 countries worldwide and presently in over 70-infrastructure systems exists for utilising this resource to provide liquid fuels. There are a number of Coal-to-liquid (CTL) projects around the world at various stages of development, the most advanced being in China, the USA and Australia. There is also strong interest from other countries including Indonesia, Germany and India. Much like South Africa, all of these countries have large domestic reserves of coal.
- The capital cost of CTL plants is also expected to decrease through the ongoing development of the technology.
- The development of a coal to liquids (CTL) industry can serve to overcome oil-related energy security risks. Using domestic coal reserves, or accessing the relatively stable international coal market, can allow countries to minimise their exposure to oil price volatility while providing the liquid fuels needed for economic growth.
- Liquid fuels from coal can be delivered from an existing pump at a filling station via existing distribution infrastructure and used, without modification, in the current vehicle fleet.
- The use of carbon capture and storage, recycles and closed loop processes can minimise emissions from the manufacturing process.

## 1.2 Research Aims and Objectives

The research carried out in this work was aimed at:

- Producing a high value, liquid hydrocarbon product by means of the two-step, temperature-staged, DCL process
- Assessing the performance of a two-step temperature staged reaction system
- Assessing the performance of catalysts by studying and comparing product distributions obtained from GC-MS chromatograms and differences in liquid yields

The following specific tasks allowed the research to be executed in such a manner so as to gain insight into the specifics of the process in relation to operating conditions, reactor and catalyst type.

- To carry-out the two-step DCL process, using the temperature-staged approach, bituminous coal and tetralin as the hydrogen-donor solvent.
- To carry-out the first-stage of the DCL process in a high-pressure, batch reactor with molybdenum doped magnetite as the catalyst.
- To carry-out the second-stage of the process in a fixed bed reactor, using the liquid product of the first stage
- To perform a factorial design of the experimental runs and respective responses in order to assess optimum operating conditions.
- To determine the statistical significance of the data and fit the data to a model which would predict both yield and selectivity
- To compare actual experimental results to literature in order to assess the performance of the two systems relative to documented baselines
- To compare the performance of the second-stage catalysts viz. Ni-Mo and Co-Mo
- To qualitatively and quantitatively analyse the liquid products from both stages using Gas-Chromatography Mass-Spectrometry (GC-MS) techniques

# Chapter Two: Literature Survey

**Chapter Overview:** The direct coal liquefaction process is chemically very complex. This is owing to the complex structure of coal. This chapter attempts to unravel the chemistry of various coal types by an analytical comparison of their chemical constituents. In terms of investigating the process, temperature, multi-staged facilities are discussed. The reaction mechanism and advantages of using tetralin as the hydrogen donor solvent are explained. The main process variables used in this experiment including temperature, reaction time and catalyst type are put into a theoretical context in terms of their effects on the DCL process.

## 2.1 Coal

### 2.1.1 Chemistry of Coal

Robinson (2009) emphasised the importance of understanding the chemistry of coal liquefaction in order to optimize the processes for converting the carbonaceous matter in coal to environmentally acceptable liquids.

Akash (2013) suggested that coal is made up of complex macromolecules without repeating monomer units. These macromolecules are composed primarily of carbon and hydrogen and also consist of significant amounts of oxygen, nitrogen and sulphur. The constituent units are mostly substituted aromatics or hydro-aromatics, and the degree of condensation increases as the coal matures.

With reference to figure 2.1.1, the overall macromolecular structure of a bituminous coal can be considered as condensed and highly substituted cyclic carbon structures that are mutually linked together by alkyl and ether bridges.
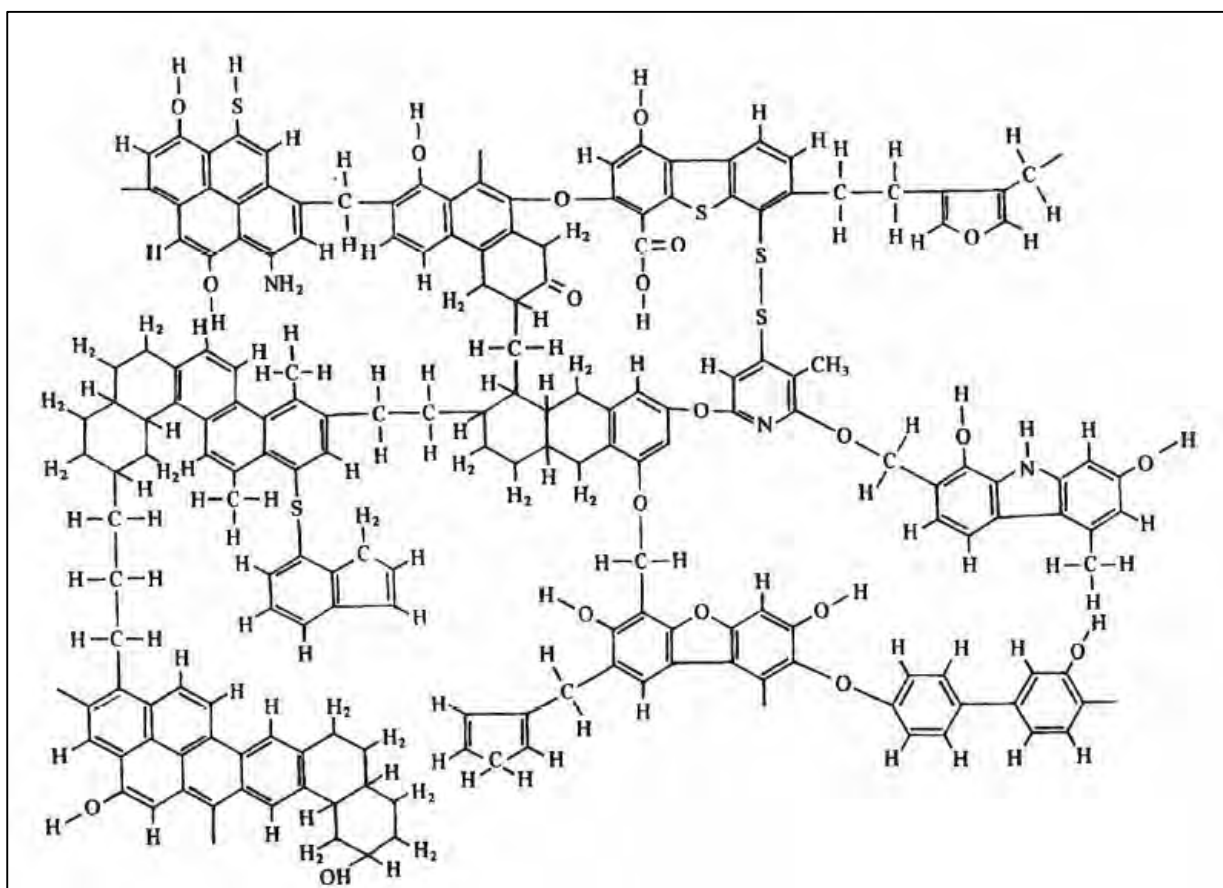
Figure 2.1.1: Schematic representation of structural groups in bituminous coal **(Akash, 2013)**

Bituminous, subbituminous, and lignite coals can be converted into liquids. Bituminous coals produce the highest liquid yields, while Anthracite produces mostly gases and is therefore more difficult to liquefy (Robinson, 2009).

**2.1.2 Properties and Ranking of Coal**

According to Robinson (2009), there are at least seven characteristics of coals that may influence their behaviour in conversion processes. These seven characteristics are rank, geological history, mineral content, trace element distribution, petrographic composition, chemical structural parameters and pore structure. The coal 'series' allows coals to be classified by the carbon content as:

**Peat ⟶ Lignite ⟶ Sub-bituminous ⟶ Bituminous ⟶ Anthracite**

**Lowest Rank ⟵⟶ Highest Rank**
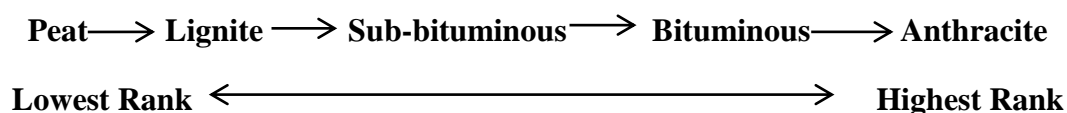
Figure 2.1.2: Hierarchy of coal series

The process of alteration from living plant material through dead material, as in from the peat stage onward is called metamorphism, and the term "rank", a qualitative concept, is a scientific indication of this degree of alteration or metamorphism.

There are however other means used to determine the quality of coal. The American Society of Testing and Materials (A.S.T.M) system used for commercial purposes in the U.S., and the International systems used in Europe, use volatile matter to classify the higher rank coals, and calorific values for the lower (Robinson, 2009).

Geological history is a further characteristic of coal which is of importance. For any particular geological age, coals were deposited in a number of distinct basins in different parts of the world and experienced distinctly different geological histories (Robinson, 2009).

The relative amounts of oxygen-containing compounds with the chemical composition $C_nH_{2n}O$, decrease with increasing coal rank. The relative amounts of aromatic hydrocarbons such as napthalenes, phenanthrenes, and pyrenes increase with increasing coal rank. The higher stability of aromatic relative to aliphatic compounds may contribute to the increase in the temperature of maximum volatile matter evolution with increasing coal rank (Robinson, 2009).

Schobert (1987) described the various coal ranks as follows:

*Peat (Brown coal):*

Compared to lignite, peat has very high moisture content (up to 60%) and geologically, it is a younger coal. Deposits of peat show distinct layering, which are distinguishable by colour. When this coal dries on exposure to air, slacking readily occurs resulting in large pieces of coal disintegrating. When stored in stockpiles or bins, peat occasionally catches fire by spontaneous combustion, making it easy to ignite but with a low heating value. Brown coal is abundant in the state of Victoria, Australia as well as in central and Eastern Europe.

*Lignite:*

Among the coals of the United States, lignite is the lowest in rank containing less than 75% carbon on moisture free and ash free basis. The moisture content of the lignite is high, but not as high as that of brown coals. The highest moisture content of lignite mined in the United States is between 40-42%. Lignite is relatively soft and ranges from brown to black. Because lignite has not progressed very far in maturation, many lignite deposits contain easily recognisable plant material. Two major lignite deposits occur in the United States, one of which is the largest in the world.

*Sub-bituminous Coal:*

Subbituminous coal holds an intermediate position in the rank between the lignite and bituminous coal. Subbituminous coals have matured to a point where the woody plant material often visible in peat and lignite, is not seen. Subbituminous coals have the same tendency toward slacking and spontaneous combustion as lignite and brown coal possesses.

*Bituminous Coal:*

Bituminous coal supplies most of the energy that comes from coal. Until the 1970s, the low-rank coals provided the only about 2% of the national coal consumption, bituminous and anthracite occupied the remainder. Bituminous coal is black, but frequently appears to be banded with alternating layers of glossy black and dull black. It breaks into prismatic blocks. The moisture and volatile matter contents are lower and the heating value is higher than those of subbituminous coal. Bituminous coal shows little tendency to disintegrate on weathering or experience spontaneous combustion.

When some varieties of bituminous coal are heated in the absence of air, they soften. Heating also removes volatile matter as gases, which bubble through the softened mass of coal. The product resolidifies as a porous, hard black solid known as coke. Coke is the fuel used in the blast furnaces to make iron.

Bituminous coal is widespread throughout the world. The principal countries having bituminous coal include Great Britain, Germany, the Soviet Union, China, Australia and South Africa.

The structure of bituminous coal is better understood than that of other coal types. It consists of clusters of aromatic carbon rings with appreciable amounts of hydroaromatic carbon. An average of 65 to 75 percent of the carbon is aromatic, 15 to 25 percent is hydroaromatic, and 5 to 10 percent is aliphatic carbon. The individual groups or clusters contain from one to probably not more than five or six rings, an average cluster containing about three rings. The individual clusters are joined together chemically in layers or lamellae by various types of bonds including short aliphatic bridges (e.g. methylene), ether linkages, sulphide or disulphide linkages and even biphenyl linkages. The lamellae appear to be held together in more or less parallel layers for physical interactions (e.g., hydrogen bonding or Van der Waals forces) in a "graphite-like" structure. A cluster may be randomly orientated with respect to its nearest neighbour (i.e. it may not necessarily lie in the same plane as its neighbour). A schematic representation of the principal types of structural groups in bituminous coal and the manner in which these groups are joined are shown in the Figure 2 above.

The ratio of atomic hydrogen to carbon in a typical bituminous coal is in the range of 0.8 to 0.9. With increasing coal rank; carbon content increases, hydrogen to carbon atomic ratio decreases, oxygen content decreases, aromatic character increases, and the volatile fraction decreases.

Bituminous coals can manifest a phenomenon known as plasticity. When a bituminous coal is heated to between 325℃ and 350℃, the coal mass begins to soften or become plastic. When in this state, the coal sticks to almost anything and may plug the reactor or cause other problems that may terminate the liquefaction operation. Gas-fluidized bed operation becomes very difficult or impossible. Much of the technology associated with the bituminous coal types has been directed towards the solution of this problem (Robinson, 2009).

Most theories conclude that the plastic state results from a thermal rupture of the coal's structural bonds, both the physical forces holding the lamellae together and the chemical bonds between the clusters within the lamellae. Neither the higher rank coals such as anthracites nor the lower rank coals such as subbituminous and lignite manifest the plastic behaviour; however, subjecting the low rank coals to liquefaction temperatures under hydrogen pressure often induces a degree of plasticity with the resultant problems.

Liquefaction of bituminous coal involves passing through the plastic state because the rate of liquefaction is too slow at temperatures below the initiation of the plastic state. Viable single-stage liquefaction processes operate between 400 and 550℃. Temperatures above 550℃ cause extensive cracking which results in high gas yields. Typically, cracking can be described as the process whereby complex long chain molecules are broken down, via the breaking of carbon-carbon bonds, into simpler molecules such as light hydrocarbon compounds and gases (University of York, 2014).

When bituminous coal is heated to a suitable liquefaction temperature the following changes occur:

1.  Rupture of the physical bonds (Van Der Waals forces and hydrogen bonds) between the layers (lamellae) in the coal and formation of smaller organic fragments.
2.  Rupture of a sufficient number of chemical bonds linking clusters together to free these clusters and at the same time form free radicals.
3.  Stabilization of the free radical fragments. The production of a significant yield to liquids requires stabilization of these fragments as small entities to inhibit polymerization that would form a less reactive mass.

Anthracite:

Anthracite is jet black and usually has a high lustre. It is the hardest, most dense coal and is also known as black diamond because of its hardness, lustre and commercial value.

Anthracite ranks highest among coals, a position merited for several reasons. Having very low volatile matter content, anthracite burns with a hot clean flame with no smoke or soot. This feature makes it an ideal domestic fuel. Compared with bituminous coal, anthracite burns more slowly and gives off heat more uniformly. Anthracite is very low in moisture, about 3%, and is low in sulphur. It is stable in storage and, unlike other coals, can be handled without dust forming. Its heating value comes close to that of bituminous coals.

The many good qualities of anthracite make it a premium fuel; however its geographic distribution limits its use. Therefore, it is not as readily available on the market as are other coals and thus commands a premium price.

### 2.1.3 Sulphur and Ash

Of the approximately 80 elements found in coal, the one besides carbon having the most significant effect on coal is sulphur. When coal or coal liquids are burned, the sulphur oxide

formed causes air pollution if allowed to escape to the environment. The sulphur in coal occurs in the following three forms:

1. Organic Sulphur: This is a part of the molecular composition of the coal itself
2. Pyritic Sulphur: Occurs in the mineral pyrite and some related minerals
3. Sulphate sulphur: This type of sulphur mostly presents as iron sulphates

In most cases, sulphate sulphur is a small fraction of the total sulphur content in low-rank coals, organic sulphur may contribute half or more of the total sulphur.

When coal is burned it leaves behind the inconsumable inorganic residue known as ash. The ash is the product of reactions or transformations of the inorganic components of coal caused by the high temperatures of the combustion process.

**2.1.4 Petrography**

Coal petrography specifically deals with the analysis of the maceral composition and rank of coal and therefore plays an essential part of coal analysis. The fundamentals of organic petrography, maceral composition, classification of coal components and analytical procedures, have been well established by the international committee of coal and organic petrology. (Speight, 2005)

Speight (2005) describes coal as a rock formed by geological processes and is composed of a number of distinct organic entities called macerals. The essence of the petrographic approach to the study of coal composition and the idea that coal is composed of macerals which each have a distinct set of physical and chemical properties that control the behaviour of the coal. Macerals are organic constituents in coal and non-coal rich rocks. Macerals are the optical microscopically identifiable constituents in coal. By convention, maceral names always have been as an –inite suffix. Macerals are generally divided into vitrinite (or huminite in lower rank coals); inertinite and liptinite groups. Macerals are identified and classified on the basis of their morphology, source material, colour or level of reflectivity and nature of formation. The reflected light is the most widely used petrographic analysis technique because of the relative ease of the sample preparation (Parkash et al., 1983).

Huminite or vitrinite macerals are derived from humic substances and are altered products from lignin and cellulose. Huminite refers to macerals in lignite and sub-bituminous rank coals; and vitrinite to maceral of bituminous and anthracitic ranks (Speight, 2005). Inertinite materials are to a certain degree derived from the same starting materials as huminite and vitrinite materials. Inertinites have undergone oxidation with fire thought to be the primary cause of their formation (Speight, 2005). Macerals of the liptinite group are derived from resinous and waxy materials of plants and have the highest hydrogen content of all macerals making them the lightest component of coal (Parkash et al., 1983)

Petrographically and chemically, coal is a complex material and it is convenient to describe coal in several way. Most commonly, coal is described in terms of the elemental (ultimate) composition where coal may accurately be classified on the basis of the general formula described in Speight (2005):

$C_NH_MN_xO_yS_z$ (2.1.4)

where:

N = number of carbon atoms
M = number of hydrogen atoms
x = number of nitrogen atoms
y = number of oxygen atoms
z = number of sulphur atoms

### 2.1. 5 Asphaltenes and Pre-asphaltenes

The exact chemical composition of the content of asphaltenes and pre-asphaltenes in coal remains an unknown. Asphaltenes and pre-asphaltenes are the components of coal extracts and asphaltenes are known to be the principle intermediates in the conversion of coal to oil. Asphaltenes and pre-asphaltenes are defined on the basis of solubility. Asphaltenes may be classified in terms of benzene soluble or hexane insoluble compounds. Pre-asphaltenes can be classified as pyridine soluble, but benzene insoluble.

## 2.2 Single vs. Multistage Processes

The major direct coal liquefaction (DCL) processes can be classified into single-stage processes including the SRC, EDS, H-Coal and multi-stage (mostly two-stage) processes. Multistage processes are advantageous as they can obtain higher conversions and oil yields than the single stage processes. Mechanically, the advantages of multistage processes over single-stage processes are accountable by the effects of in situ thermal pre-treatment and improved hydrogen transfer (Shui et al., 2010).

Single-stage: These processes provide the distilled liquids (distillates) through one primary reactor or reactor chain. Most of these have been superseded by two-stage processes to increase yield of lighter oils. A number of processes have been developed in single-stage technology, including Kohleoel, NEDOL, and H-Coal, Exxon donor Solvent, SRC, Imhausen and Conoco. Not all of these plants have reached commercial realisation.

Two-stage: These processes provide distillates through two reactors or reactor chains. The first reaction dissolves the coal either without a catalyst or with a disposable catalyst, producing heavy coal liquids. The product from the first stage reactor may undergo inter-stage de-ashing before being further treated in the second reactor, with hydrogen and a catalyst to produce additional distillate.

The two-stage processes are often derivatives of the single-stage reactions. For example, the catalytic two-stage liquefaction process was developed from the H-Coal single stage. This technology is the one chosen for Shenhua's Inner Mongolia plant in China, as the proprietary HTI Direct Coal Liquefaction Technology. Typically, pulverised coal is slurried in a recycled process solvent, then preheated, mixed with hydrogen and fed to the first reactor, which

operates under typical conditions of up to 430°C and 170bar (Robinson, 2009). A second reactor completes the liquefaction, operating at higher temperatures. The reaction catalyst for both stages is a nano-scale, iron-based one, dispersed in the slurry.

## 2.3 Temperature-Staged Direct Coal Liquefaction

In this study, temperature-staged direct coal liquefaction was investigated.

The first, low temperature stage can be considered to be pre-treatment. Most of the desirable liquids are still formed in the higher temperature stage. This strategy is aimed at converting net conversion to liquids, selectively improves the yield of oils and decreases gas production.

During the low-temperature stage, partial depolymerisation of the coal structure will increase the amount of extractable liquids and coal fluidity. Weaker bonds are broken and stabilized by the hydrogen transfer at low temperature. This reduces the potential for retrogressive condensation reactions at high temperatures. Effective hydrogenation at mild reaction conditions of the first stage minimizes the condensation reactions.

Multiple studies have shown that a combination of low-temperature catalytic liquefaction step followed by a higher temperature catalytic reaction significantly improved product selectivity (Robinson, 2009).

## 2.4 Two-step, temperature-staged approach

A two-step, temperature staged approach was mathematically modelled by Xu and Kandiyoti (1996) and the major findings presented in the list below. The results of their research were presented in terms of stage A (where a relatively mild temperature was used) and stage B (where a higher temperature was used viz, $350 \, °C - 450 \, °C$)

- The onset of extensive covalent bond scission (breaking of chemical bonds in long chain molecules to short chain molecule) takes place at 350°C.
- Prior to the onset of extensive chemical bond splitting (cleavage) stage A and stage B (after chemical bond cleavage) were both initially modelled as single, irreversible first order processes.
- In a more fully developed model, both stages A and B were considered to occur by means of multiple, parallel, independent first-order reactions.
- For stage A, the single reaction model gave activation energies between 35 kJ/mol and 80 kJ/mol.
- Activation energies for stage B were higher than those for stage A. For stage B activation energies were between 124 kJ/mol and 235 kJ/mol.
- The study presented by Xu and Kandiyoti (1996) is a confirmation on the validity of two stage processes.

## 2.5 Chemistry and Reaction Mechanisms of Direct Coal Liquefaction

Direct coal liquefaction (DCL) refers to the direct reaction of coal with hydrogen to form liquids Often, the process involves the addition of hydrogen to coal in solvent slurry at elevated temperature and pressure. The elevated temperature cracks the coal molecules by thermally rupturing the carbon-carbon linkages and increasing the rate of reaction. High pressure keeps the solvent and products in the liquid phase, prevents coke build-up on the reactor walls and catalyst surface, and promotes hydrogenation by maintaining a high partial pressure of hydrogen. Catalysts are normally used to increase the rates of the desirable reactions which include cracking, hydrogenation, and removal of oxygen, nitrogen, and sulphur (Mochida, 2013).

Liquid yields can be in excess of 70% of the dry weight coal feed are expected. The hydrogen reacts with oxygen, sulphur, and nitrogen in coal to remove them as water, hydrogen sulphide, and ammonia. The hydrogen is also required to substantially increase the H/C (Hydrogen-to-carbon ratio) ratio before it becomes a liquid. One of the key differences between coal and petroleum is the much lower H/C atomic ratio of coal (~0.7 vs. 1.2 for petroleum) (Akash, 2013). Consequently the conversion of coal to petroleum-like products requires direct hydrogen addition and this adds considerable expense to the product. The target of coal liquefaction is to produce substitutes for petroleum distillate fuels having an atomic ratio of 1.8-2.5, more particularly, replacements for gasoline and diesel fuel (Mochida, 2013).

Thomas (1977) investigated the DCL process according to the following reaction:

Liquefaction:  $\quad$ Coal + H$_2$ $\xrightarrow{\;\;\blacktriangle\;\;}$ C$_n$H$_{2n+2}$ + … + aromatics + … + coke $\quad\quad$ (2.4.1)
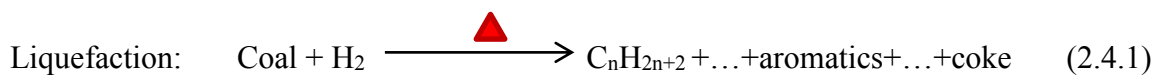
The actual amount of hydrogen consumed in the process is related to the average molecular weight (mw) of the coal liquid produced. According to Vlieger (1988) a first approximation could be presented as:

$$\text{Coal} \xrightarrow{7H_2} 2\,(\text{High MW}) \xrightarrow{2H_2} 4(\text{Intermediate MW}) \xrightarrow{13H_2} 8(\text{Low MW}) \quad (2.4.2)$$

Where $\quad\quad$ High Molecular Weight (MW) = 1000

$\quad\quad\quad\quad$ Intermediate MW = 500

$\quad\quad\quad\quad$ Low MW = 250

A high rate of hydrogen addition occurs during the initial stage of the coal conversion process in order to cap thermally induced radicals and to eliminate reactive sulphur and oxygen species. The conversion of high MW products to intermediate MW components requires only as much hydrogen as to break one bond per high MW species. As the conversion proceeds, the rate of hydrogen consumption decreases and the major part of the hydrogen is used in heteroatom removal and in the formation of low MW weight carbon gases and solvent range products.
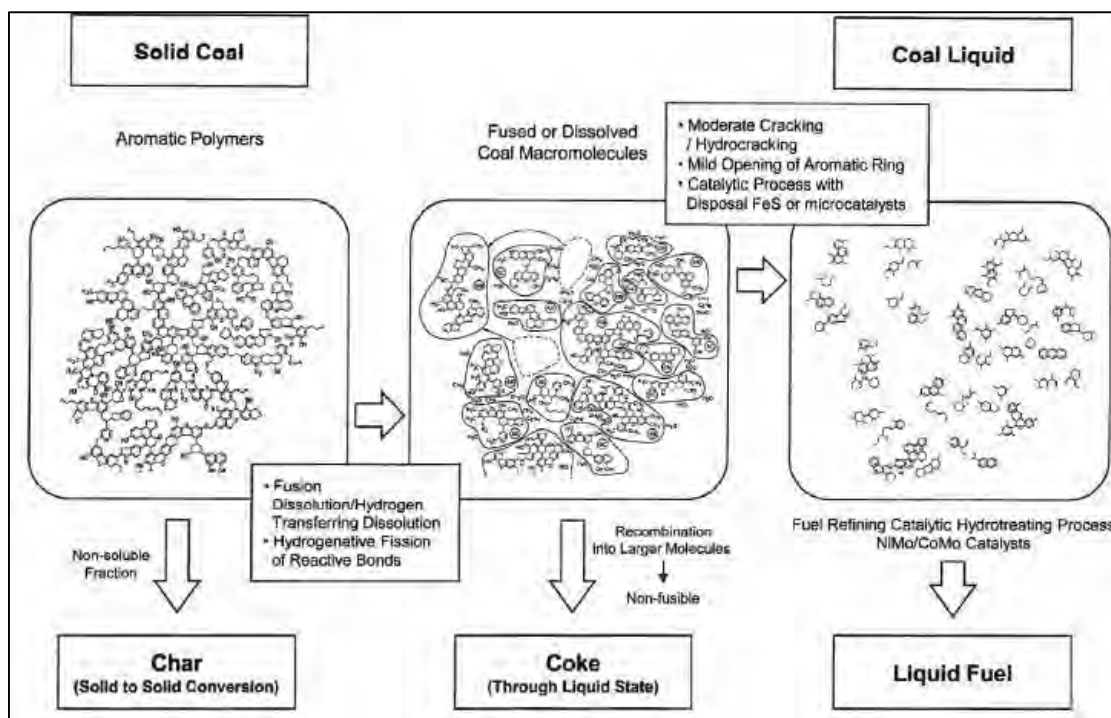
Figure 2.5.1: Chemical images of direct coal liquefaction steps (**Mochida, 2013**)

With reference to figure 2.4.1 above, Mochida (2013) explained that coal consists of polyaromatic molecules in which aromatic and heteroatomic nuclei are bonded with C-C, C-O, C-S units form the three-dimensional (3-D) networks. Depending on the rank of coal feedstock, the aromatic nuclei contain alkyl, carboxylic, carbonyl, phenol, thiol, thiophene, amine, indole, and pyridine groups.

Macromolecular interactions include aromatic stacking, hydrogen bonding, acid base and donor accepting interactions. These interactions in the coal are responsible for the formation of the 3-D networks and influence the properties and reactivities of the coal. Thus, release of the macromolecular interactions is a key to convert coal to be soluble in the solvent in the coal liquefaction process.

During liquefaction, the weakest bonds under the influence of hydrogenation, are first broken thermally into smaller aromatic units. These units present in the liquid phase, a portion of which is dissolved in the solvent, and are further thermally and catalytically cracked into smaller hydrocarbons (e.g. naphtha, kerosene, diesel and vacuum gas oil) which are similar to those compounds found in petroleum crude oil. Part of the coal macromolecules remain in the solid form and become further condensed into char or coke. Uncracked molecules, including condensed macromolecules such as tar and pitch. These products may be further hydrogenated and recycled or used in other applications.

The smaller, light gaseous components constitute the remaining portions. Light hydrocarbons, including $CH_4$, $H_2S$, $C_2H_6$, $C_1$-$C_4$, and coke should be minimized in liquefaction.
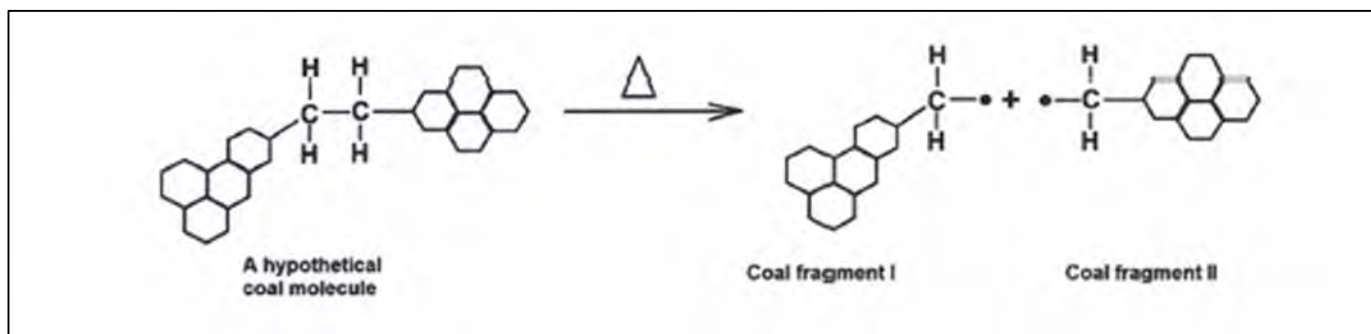


Figure 2.5.2: Chemical reaction showing the formation of free radicals **(Akash, 2013)**
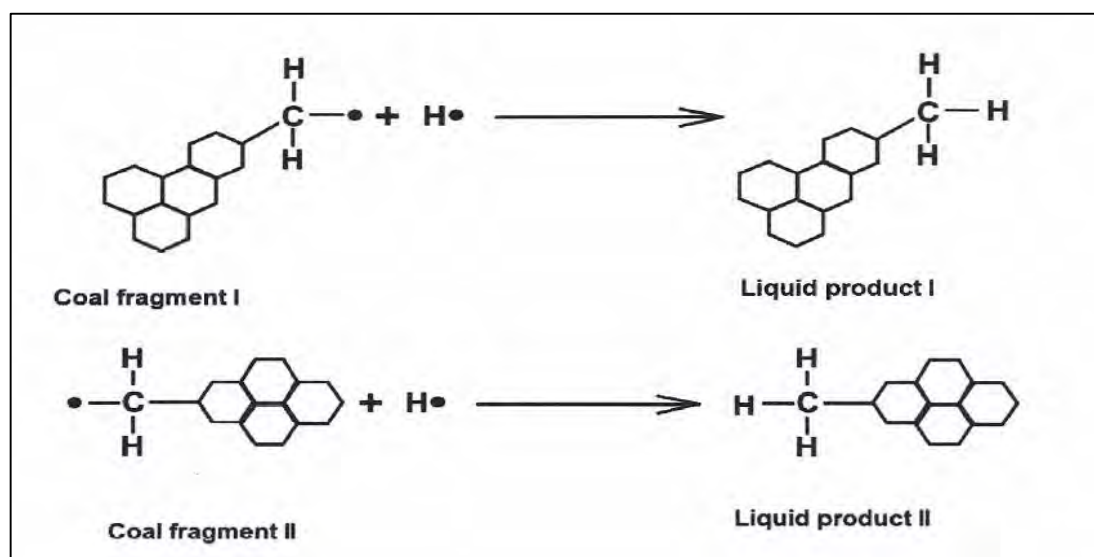


Figure 2.5.3: Chemical reactions showing the stabilization of free radicals **(Akash, 2013)**

Experimentally, it has been found that coal conversion is dependent upon the amount of hydrogen transferred to the coal. In non-catalytic coal liquefaction, conversion only takes place at temperatures high enough for thermal bond breaking to occur.

Rapid formation of free radicals occurs during coal liquefaction. It is therefore important for theses free radicals to be capped or for saturation to take place. Figure 2.4.2 and 2.4.3 are indicative of this capping process.

**2.6 Role of Tetralin as a solvent in the process**

In many DCL processes, the role of the solvent is to stabilise the free-radicals by donating hydrogen, promote the cracking of coal macromolecules, and prevent from the condensation and coking of the radicals by diluting the intermediates.

17

The solvent can be seen to have the following advantages:

- To serve as a vehicle to convey the coal into the liquefaction reactors and products from the reactor, as well as to shuttle the hydrogen from the gas phase to the coal.
- To serve as a medium for facilitating mass and heat transfer among the solid, liquid and gaseous components of the reactor inventory.
- The use or role of vehicle solvents can aid in the justification for reducing the cost of producing coals from liquids, in terms of lowering the hydrogen usage.

Coal liquefaction solvents can be classified in four distinct categories based on their effects on coals: specific, non-specific, degrading and reactive solvents.

1. Specific solvents

Specific solvents such as pyridine and NMP (N-methyl-2-pyrrolidone) can dissolve 20-40 % coal at 200 °C.

2. Non-specific solvents

Non-specific solvents such as alcohol, benzene, ether and acetone etc. can only dissolve a trace amount of coal at 100 °C. These solvents are electron donors and their dissolution of coal is a physical process as the extraction is normally performed at a low temperature ($< 200 ℃$). Chemical extraction processes employing the other two categories of solvents are commonly conducted at higher temperatures.

3. Degrading solvents

Degrading solvents, such as phenanthridine and anthracene oil etc. can extract coal more than 90 % at 400 ℃. After extraction, the solvents can be almost totally recovered from the solution. Polymerization of coal fragments may occur in the liquefaction with a degrading solvent, which can be prohibited by supply of high-pressure molecular hydrogen to stabilise the coal fragments facilitated by the solvent's hydrogen transferring and shuttling roles.

4. Reactive Solvents

Reactive solvents are solvents that can react with coal in the liquefaction, such as phenol.

DCL solvents may also be classified into donor and non-donor solvents. Typical donor solvents include tetralin, tetrahydrofluoranthene (4HFL), and dihydroanthracene (2Han), etc. and common non-donor solvents are decalin, pyrene (PY), fluoranthene (FL), and anthracene (An), etc.

Due to the different properties as discussed above, the effects of solvents on DCL are expected to be significant.

When a solvent with hydrogen donor capability is present in the system, the free radicals extract hydrogen from the solvent and thereby achieve stabilization. Re-polymerization is inhibited because the free radicals formed can continue to be stabilized by hydrogen transfer from the hydroaromatic hydrogen-donor solvent molecules.

Akash (2013) explained that if molecular hydrogen and an appropriate catalyst are added to the system, dissociative chemisorption of the hydrogen on the catalyst can yield active hydrogen that can stabilize the free radicals. It is also possible for molecular hydrogen alone to stabilize free radicals in the absence of catalyst or donor solvent but at slower reaction rates. In addition, the introduction of the catalyst and hydrogen can promote hydrogenation of a ring on a multi-ringed cluster followed by ring opening and scission thereby reducing the size of large clusters.

Most coal liquefaction processes involve the addition of a coal derived solvent to the coal prior to heating the coal to the high temperature zone. This is done to facilitate the feeding of the coal into a high-pressure region and to avoid the adhesive problems. When the coal particles are surrounded by liquid near ambient temperature, several minutes are required to bring the particle to reaction temperature (i.e. 400 °C to 500 °C), and the residence times in the preheater and the reactor in these processes are usually from 15 minutes to 1 hour. With bituminous coals, the absence of a solvent with donor capabilities requires the presence of an appropriate catalyst together with an atmosphere of sufficient hydrogen under partial pressure to permit rapid hydrogenation under partial pressure to permit rapid hydrogenation of the thermally produced free radicals.

Thus, in studying the role that tetralin plays as the hydrogen donor solvent, it is understood that as coal dissolves, hydrogen must be consumed. Free radicals are formed from the thermal disruption of weak bonds in the coal structure. For solubility to be achieved these radicals must be capped by hydrogen or they will recombine. The tetralin and naphthalene interconversion and hydrogen transfer can be described by equation 2.5.1

$$\text{Naphthalene} + 2H_2 \xrightleftharpoons{K} \text{Tetralin} \qquad\qquad (2.5.1)$$
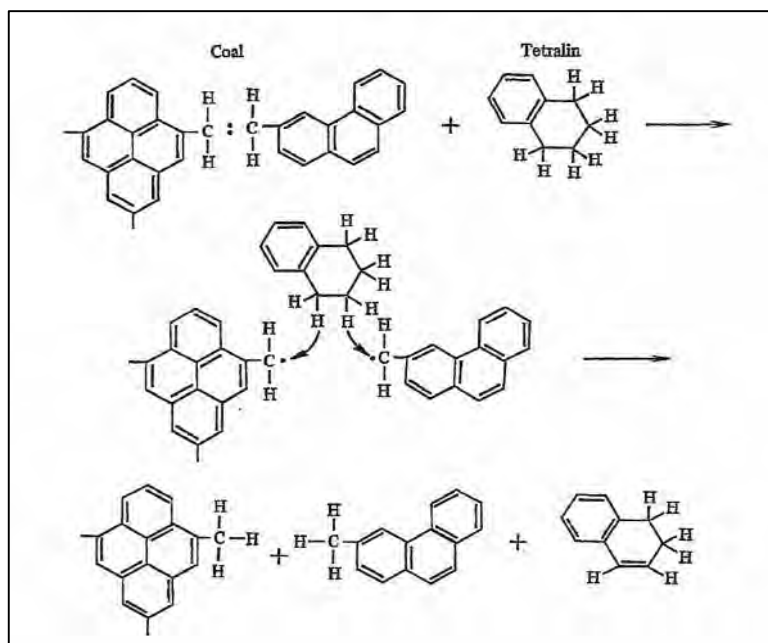


Figure 2.6: Schematic representation of the donor solvent action involving rupture of an ethylene bond in the coal structure followed by hydrogen transfer from tetralin to form stable hydrocarbon fragments **(Akash, 2013)**

Tetralin-derived products include napthalenes, alkylnaphthalene, alkyltetralins, alkylindas, cis-decalin, 1-methylindan, trans-decalin, n-butyl benzene, indan, sec-butyl benzene, 1-ethyl-2-methylbenzene, n-propyl benzene, o-xylene, isopropyl benzene, ethylbenzene and toluene (Akash, 2013).

## 2. 7 Factors Affecting the Process

### 2. 7.1 Temperature

The direct coal liquefaction mechanisms are very complex and not yet entirely known. As discussed previously, the recent DCL processes involve two steps: rupture of the macromolecular structure of coal into radical fragments at an elevated temperature and stabilization and hydrogenation of those fragments to produce molecules with lower molecular weights.

An elevated temperature would crack the coal molecules by thermally rupturing carbon-carbon linkages and enhance the reaction rates. Temperature is thus one of the most important factors that affect free radical formation and subsequent free radical reactions. These reactions do not normally occur at a low temperature, while at too high temperature undesirable coking reactions would be dominant. As such, for a specific set of reaction conditions, there exists an optimal temperature.

### 2. 7.2 Pressure

In a DCL process, high pressure is beneficial as it keeps the solvent and products in the liquid phase, prevents coke build-up on the reactor walls and catalyst surface by suppressing the retro-regressive reactions, and promotes hydrogenation by maintaining high partial pressure of hydrogen. Nevertheless, economic considerations dictate the use of a lower $H_2$ pressure in the liquefaction process.

With the advances in the DCL technology, particularly in the development of more effective catalysts and solvents such as Tetralin, the requirement for high pressure could be relaxed to about 14MPa in the first stage. It was further demonstrated that when a suitable solvent with an enough high boiling point was used, coal could be liquefied under atmospheric pressure, although most of the products were heavy fractions and the oil yield was only about 10%. In the presence of a good donor solvent, coal liquefaction could proceed under relatively lower pressure, although coal conversions could be appreciably improved by increasing the operating pressure (Robinson, 2009).

## 2. 7.3 Catalysts
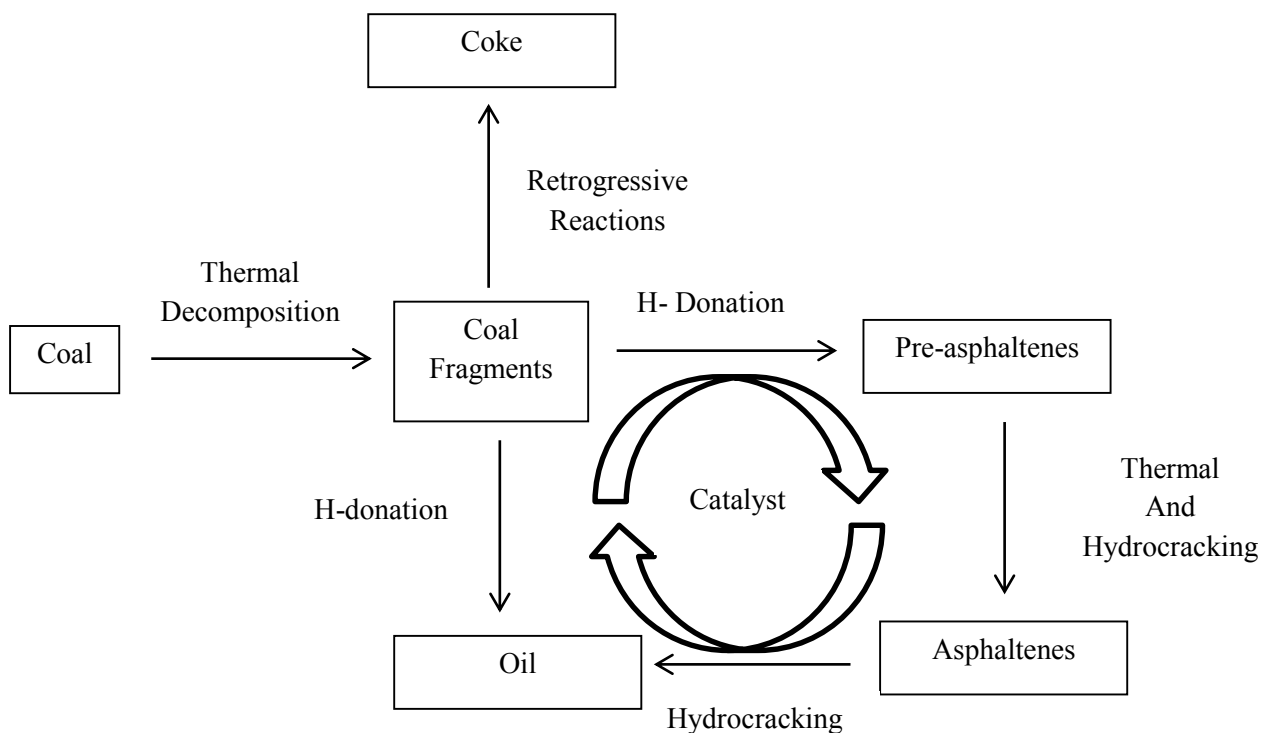


Figure 2.7.3: Schematic of reaction mechanism in catalytic coal liquefaction

With the goal of increasing the conversion of coal and the yield of oil, it is essential that operating conditions be optimised such that to minimise retrogressive reactions. Retrogressive reactions are those reactions which lead to the undesirable thermal decomposition of the coal fragments.

In the first stage of the process, the promotion of hydrogenation is a critical requirement. The use of catalysts, which are highly dispersed, aids in the transfer of the hydrogen molecules to the coal fragments in the slurry feed.

For a substance to catalyse a chemical reaction, at least one of the reactants must interact chemically with the catalyst (e.g. chemisorption of a reactant on the surface of a solid catalyst).

In the presence of the hydrogen-donor solvent it may be easier for the donor solvent itself to stabilize the free radicals from the coal with the catalyst, if present, and hydrogen acting to regenerate the donor capability of the solvent.

The removal of heteroatoms (i.e. oxygen, sulphur and nitrogen) represents an important part of coal liquefaction technology. While most of the oxygen and sulphur in coals do not occupy positions within aromatic rings, much of the nitrogen does. In the temperature range required for coal liquefaction those heteroatoms that do not occupy ring positions may be removed to a great extent through non- catalytic processes yielding water and $H_2S$, but very little nitrogen is removed under these conditions.

The removal of sulphur and nitrogen from ring positions requires catalytic hydrogenation of the ring and subsequent ring opening.

Widely documented as one of the major shortfalls associated with the CTL technology is the use of expensive catalysts which are not easily recovered from the process. The advantages in the use of magnetite ($Fe_3O_4$) as a dispersed catalyst include that it is:

-        Easily recoverable from waste coal which is unconverted
-        Abundant, inexpensive disposable catalyst
-        Known to enhance yields
-        Presents no environmental hazard
-        Proven to catalyse hydrogenation reactions


Cobalt-Molybdenum and Nickel-Molybdenum are common hydrotreating catalysts which function to achieve HDS and hydrodenitrogenation (HDN) performance. HDS is a process where a hydrogen donor reacts with coal; and a substantial amount of sulphur, oxygen, and nitrogen in the coal is eliminated as hydrogen sulphide, water and ammonia. This elimination could be a direct result of the cleavage of the hetero-bonds presents in the coal.

In this study, the focus was on HDS typically described by the reaction below:

$$[\text{R-S}] + H_2 \xrightarrow[\text{300-450°C}]{\text{Catalyst}} [\text{R-H}] + H_2S \qquad (2.6.3)$$

[R-S] can be described as the sulphur containing hydrocarbon compound and [R-H] as the resultant aliphatic hydrocarbon product. The variables which influence this reaction are the nature and the amount of the hydrogen-donor solvent, the presence and absence of hydrogen pressure, the level of this pressure, the reaction temperature, the reaction time, and the nature (rank and type) of the coal.

## 2. 7.4 Contact Time

Mixtures of coal and vehicle oil require from about 20 minutes to 1 hour at pressure and temperature for as much as 3 barrels (approximately 477 litres) of liquids per ton of coal in most hydrogen-donor solvent schemes. There is substantial evidence indicating that comparable conversion can be achieved in a much shorter time (i.e. 10 to 15 seconds) if the coal particles are heated rapidly in a high pressure hydrogen gas atmosphere and in the presence of a suitable catalyst.

## 2.8 Pyrite Decomposition

Pyrite ($FeS_2$) forms part of the mineral content present in coal. Under process conditions, pyrite rapidly transforms into a non-stoichiometric iron sulphide $Fe_{1-x}S$ where $0 \leq x \leq 0.125$ (Thomas, 1982).

The decomposition of pyrite ($FeS_2$) is dependent on temperature and the system although the activation energy has known to be approximately constant at 88 kJ/mol. A mechanism consistent with this data is the decomposition of $FeS_2$ to produce $Fe_{1-x}$ and S, thereafter the sulphur reacts with hydrogen to form $H_2S$. The onset of pyrite decomposition to pyrrohotite becomes significant at 300°C. Pyrite decomposition is proportional to the rate of $H_2S$ formed.

Thomas (1982) proposed the following reaction mechanisms for the decomposition of pyrite, where the dotted compounds represent the formation of free radicals

$$FeS_2 \rightleftharpoons Fe_{(1-x)} S + (1-x) S \tag{2.8.1}$$

With hydrogen:

$$FeS_2 \rightleftharpoons FeS + S \tag{2.8.2}$$

$$S + H_2 \rightleftharpoons HS\bullet + H\bullet \tag{2.8.3}$$

$$SH\bullet + H_2 \rightleftharpoons H_2S + H\bullet \tag{2.8.4}$$

With a solvent:

$$FeS_2 \rightleftharpoons FeS + S \tag{2.8.5}$$

$$S + Solvent \rightleftharpoons Solvent + SH\bullet \tag{2.8.6}$$

$$SH\bullet + Solvent \rightleftharpoons H_2S + Solvent \tag{2.8.7}$$

# Chapter Three: Materials and Methods

**Chapter Overview:** In this chapter, the materials, instrumentation and methods used to carry-out the said process are discussed. Particularly, the technical considerations for the first and second stage reaction systems are included. Theoretical background into the application of the best practice statistical and chemical analysis methods to the experimental data are explained.

## 3.1 Materials

### 3.1.1 Feedstock

Excluding the catalyst, the raw materials used in this lab-scale manufacturing process were coal, tetralin (Sigma Aldrich, 99%) and hydrogen gas (Afrox, >99.99 %).

The high grade bituminous coal samples used in this study were obtained from the Exxaro Grootegeluk Mine GG1 coal preparation washing plant. A petrographic and chemical analysis of the coal was conducted by the Bureau Veritas Inspectorate Laboratory for Advanced Coal Technology. Analysis results of the coal are presented in Table 3.1. The total sulphur content of 1.10 % includes the pyritic, sulphatic and organic sulphur. The proximate analysis is composed of the moisture, ash, volatile matter and fixed carbon content.

The coal was pulverised to a size fraction of between 90-100μm.

Table 3.1: Chemical Analysis of Coal Samples from Exxaro Grootegeluk GG1 Coal Mine

| Property | | Value % |
|---|---|---|
| Moisture | (adb[1]) | 2.30 |
| Ash | (db[2]) | 10.40 |
| Volatile matter | (db) | 36.90 |
| Total sulphur | (db) | 1.10 |
| Pyritic sulphur | | 0.14 |
| Sulphatic sulphur | | 0.02 |
| Organic sulphur | | 0.94 |
| Carbon | (db) | 72.86 |
| Hydrogen | (db) | 4.93 |
| Nitrogen | (db) | 1.52 |
| Oxygen | (db) | 9.15 |
| Fixed carbon | (adb) | 51.4 |
| Higher Heating Value (adb) | | 29.42 MJ/kg |

[1]adb = air-dried basis; [2] db = dry basis

Table 3.2 Petrographic properties of the coal sample used (Roux (2012))

| Maceral Composition | |
|---|---|
| Vitrinite | 85.4 % |
| Liptinite (Extinite) | 2.3 % |
| Reactive Semifusinite | 1.3 % |
| Inertinite | 5.1 % |
| Mineral Matter | 5.9 % |
| **Vitrinite Reflectance Classes** | |
| V5 (0.50 to 0.59) | 2.6% |
| V6 (0.60 to 0.69) | 22.8% |
| V7 (0.70 to 0.79) | 44.7% |
| V8 (0.80 to 0.89) | 17.6% |
| V9 (0.90 to 0.99) | 0.3% |
| V10 (1.00 to 1.09) | 0.7% |
| V11 (1.10 to 1.19) | 0.3% |
| **Petrographic Parameters** | |
| RoV (max) | 0.74% |
| RoR | 0.74% |
| Total Reactives | 89.0 % |
| Total Inerts | 11.0% |
| Optimum Inerts | 17.0% |
| Composition Balance Index | 0.65 |
| **Predicted Drum Indices** | |
| M10 Index | 10.0 |
| M40 Index | 45.0 |
| I10 Index | 24.5 |
| I20 Index | 64.3 |

With reference to Table 3.2 above, Roux (2012) states that the petrographic evaluation of the Grootegeluk GG1 sample reveals fairly normal chemical and petrographic properties. The petrographic properties exhibit a normal maceral composition and the vitrinite type results in a slightly higher rank. Fairly normal petrographic parameters are obtained from which normal coking potential is predicted in terms of drum indices.

Per 100g dry basis, the chemical analysis indicates 10.40g of ash present in the coal. Of this 10.40g, the analysis of the ash composition indicates 0.614g of iron in the form of $Fe_2O_3$ present. The amount of $Fe_2O_3$ present in the ash is 5.90 % (Roux, 2012).

### 3.1.2. Catalysts

The iron oxide nanocatalyst, molybdenum doped $Fe_3O_4$ was prepared on site at the university (Lokhat et al., 2015). The feedstock for molybdenum doped $Fe_3O_4$ production was composed of approximately 20% iron and 80 % molybdenum (Lokhat et al., 2015).

For the second stage of the process, Cobalt Molybdenum (Co-Mo) and Nickel Molybdenum (Ni-Mo) was tested in the fixed bed reactor. Cobalt Molybdenum (HDMax 200, Clariant) (C49-1-01) 3mm extrudate and Nickel Molybdenum (HDMax 300 TRX, Clariant) (C20-7); 1.3mm extrudate were used. The $Co/Mo/Al_2O_3$ was contained approximately 15 wt. % $MoO_3$ and 3wt. % $CoO$ on silica-stabilized alumina (5% SiO2). The $Ni/Mo/Al_2O_3$ contained approximately 15 wt. % $MoO_3$ and 3wt. % Ni on silica-stabilized alumina (5% SiO2).



Figure 3.1.2: Cobalt Molybdenum (HDMax 200, Clariant) (right hand side) and Nickel Molybdenum (HDMax 300 TRX, Clariant) (left hand side)

### 3.1.3 Materials used in analysis
Solvents and internal standards

The use of deuterated internal standards is considered to be standard practice for quantifying polycyclic aromatic hydrocarbon (PAH) compounds (Klee, 2013). Table 3.1.3.1 and 3.1.3.2 summarises the function and purities of the solvents and internal standards used.

Table 3.1.3.1: Solvents and Internal Standards Used in GC-MS Analysis

| Solvent | Internal Standard | Functional Organic Group |
|---------|-------------------|--------------------------|
| Propan-1-ol | Semi-volatile deuterated mixture, | PAH Compounds |
| Propan-1-ol | Ethylbenzene (Fluka, ≥98%) | Alicyclic Hydrocarbons (BTX) |
| Propan-1-ol | Pentene (Fluka, 99%) | Paraffins |
| Hexadecane | Sulfolane (Sigma Aldrich, 99%) | Sulphur |

Table 3.1.3.2: Semi-Volatile Deuterated Internal Standard Mixture Containing Certified Reference Materials Used to Quantify Compounds in Coal Derived Liquid Product

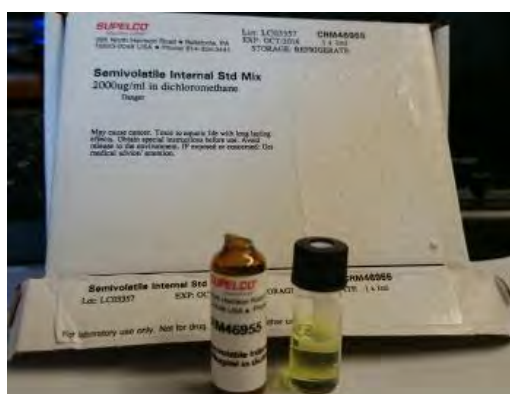| Analyte | Certified Purity (%) | Analytical Concentration (μg/ml) |
|---------|----------------------|----------------------------------|
| 1,4-Dichlorobenzene-D4 | 99.9 | 1878.5 |
| Naphthalene-D8 | 96.3 | 1919.6 |
| Acenaphthene-D10 | 99.9 | 1930.6 |
| Phenanthrene-D10 | 98.7 | 1846.6 |
| Chrysene-D12 | 98.8 | 1807.7 |
| Perylene-D12 | 99.7 | 1964.1 |



Figure 3.1.3.3:
Ampule of semi-volatile internal
standard mixture used in quantifying
PAH compounds
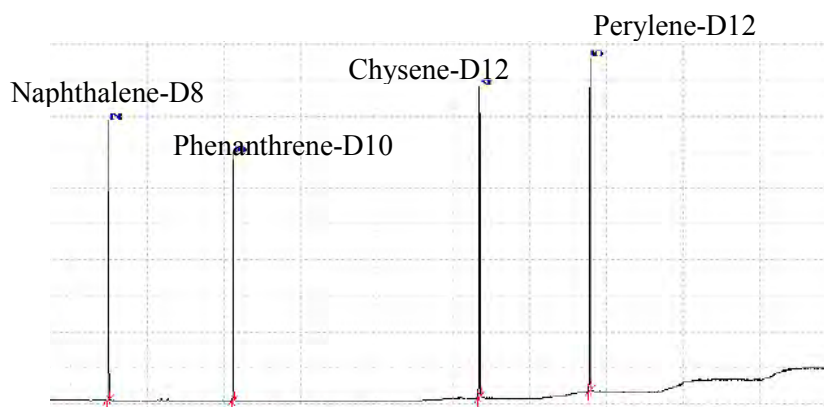
Figure 3.1.3.4:
Deuterated compounds detected from GC-MS analysis of semi-volatile mixture

## 3.2 Methods

### 3.2.1 Pre-treatment of coal

Each coal sample consisted of 100 g of bituminous coal (Roux, 2012). The coal was pulverised to an average particle size of 90-100$\mu m$. Song et al. (1987) recommended that the size of the coal particles for such experimental purposes should be approximately ≤ 60-200mesh (i.e. 74-250$\mu m$). Prior to the first-stage batch reaction, the coal samples were pre-dried at 100℃ to remove excess moisture. Song et al. (1987) also reported that by drying the coal for 2 hours at 100℃ under vacuum, the overall coal to oil conversion increases considerably.

### 3.2.2 Start-up and Hydrogenation

Pressure Test Phase:

Maintaining a high hydrogen system pressure is characteristic of coal-to-liquid processes. The start-up of the hydrogenation sequence involved pressure tests to ensure that the vessels could be properly sealed with no egress of the hydrogen into the surrounding atmosphere. While the reaction was progressing to the desired pressure of 100 barg (1450 psig), a pressure gauge reading was taken and, after a short period, another pressure reading was recorded. This value was then compared to the reading taken at the beginning of the pressure test time in order to assess whether the vessel had successfully held the pressure. On completion of the pressure test, the vent valves on both stages were opened to return the vessel to atmospheric pressure.

In particular, rubber o-rings and the replacement of the Teflon seal on the first stage batch reactor assisted in maintaining system pressure.

Hydrogen Purge Phase:

 The next phase of the hydrogenation sequence was a series of three hydrogen purges necessary to replace the nitrogen atmosphere by a hydrogen atmosphere prior to pressurization for the hydrogen addition itself. Each purge simply involved opening the hydrogen valve to pressurize the reactor followed by opening the vent valve to return the vessel to atmospheric pressure. This phase was important as hydrogen is known to easily combust in the presence of air in a confined space.

Hydrogen Addition Phase:

Soon after the hydrogen purge phase, the hydrogen addition phase was carried out.

The hydrogen valve was opened and during the addition, the hydrogen flow was controlled using a needle valve. During the hydrogen addition phase, the reactors were heated to the desired temperature. The vent valves were closed which sealed the reactor vessel. A decay in the desired system pressure was an indication that the reaction was still progressing. Hydrogenation was continued until the desired reaction pressure was reached.

### 3.2.3 First Stage Thermal Dissolution

Table 3.2.3: First stage reactor technical detail

| Reactor type | Parr Series 4521 Bench Top |
|---|---|
| Reactor volume                              [litre] | 1 |
| Maximum working pressure       [barg (psig)] | 138.91 (2000) |
| Maximum working temperature             [℃] | 350 |
| Material of construction | T316 stainless steel |
| Thermocouple type | Type J |
| Power | Electrical |

The first stage reactor facility consisted of a 1 litre Parr Series 4521 bench top reactor; with a maximum working pressure and temperature of 140barg and 350℃ respectively. With a bomb material of construction of T316 stainless steel, the reactor was suitable to withstand the expected high temperature and pressure in a corrosive environment. Operating at a high pressure, the safety rupture disc attached to the bomb head, was intended to rupture and release the bomb pressure before it exceeded a dangerous level.

The reactor was furnished with a $\frac{1}{8}$ inch outer diameter stainless steel sheath which housed a type J thermocouple. The thermocouple was inserted into the bomb head thermo-well and connected to the thermocouple socket on the rear panel of the temperature controller using an

A470E7 type wire. A pressure gauge ranging from 0-2000 psig reading with a T316 stainless steel bourdon tube was mounted on the bomb head using an attachment fitted similar to those used for the inlet sample valve assembly. The cooling for the packing was incorporated into the design of the reactor unit. Opening the bomb revealed the gas inlet valve - identifiable by its connection to a dip tube which extended to a point near the bottom of the bomb cylinder, allowing the hydrogen gas to be bubbled into the solid/liquid mixture. A liquid sampling valve was attached to the same fitting as the gas inlet valve and connected to the same dip tube. With this arrangement, incoming gas was always introduced below the surface of the liquid and the operator was provided with a means for cleaning the dip tube, to be sure that that any sample taken during a run will be a good representative of the charge. In the test phase of this work, this was achieved by opening the gas valve momentarily to force any liquid in the tube back into the reactor before withdrawing a sample from the sampling valve. In this work, the contents of the reactor were allowed to react for the full 30 and 60 minute reaction times (space times), the bomb head was then removed and the contents separated and analysed. The 3$^{rd}$ valve on the bomb head is a gas release valve connected to a plain opening on the underside of the bomb head. In order to prevent reactor pressure exceeding experiment test pressure, gas was released from this valve and drawn from the top of the reactor.

For each run, the reactor was charged with 100g of dry coal mixed with the tetralin in 2:1 and 3:1 solvent: coal ratios on a mass basis. For the first stage of the process, the catalysed runs involved adding 25g of molybdenum doped $Fe_3O_4$ catalyst to the feed mixture.

The reactor was operated electrically. The feed material was charged to the reactor, before the reactor was electrically heated to the system temperature which was set using the temperature controller.

The contents of the reactor were also well-mixed by a mechanical stirrer which was operated by an electrical driven motor.

A Teflon O-ring was fitted into the groove of the reactor head. This was to ensure that a seal was created at the interface between the head and reactor body. The head of the reactor was then secured in place by metal clamps which fit securely around the reactor head. The clamps were held in place by locking nuts and bolts. Thread tape was used on all valves and fittings secured onto the head of the reactor. New rubber o-rings were fitted as packing into the various fittings.

Prior to each run, the reactor was purged with hydrogen gas to remove excess air. The reactor was allowed to heat-up to the experimental temperature and pressurized with hydrogen gas bubbled in to the mixture. Noteworthy is the directly proportional temperature-pressure relationship observed during the reaction, hence in order to ensure safe operation in the presence of; among other gases; hydrogen formation, the reactor was gradually pressurized with hydrogen during the heating process. The reactor contents were agitated by a mechanical driven stirrer. The motor for the stirrer was powered electrically.

The reactor cooling system allowed cold water to be pumped from a tank to cool the reactor packing; and, following heat exchange with the reactor, discharged back to the cooling system.

The mass of the reacted contents was recorded. Literature highlighted the importance of interstage de-ashing in the multistage coal-to-liquid process. The liquid was separated from the unreacted solids by filtering under vacuum. The liquid mass and volume and solids masses were recorded and the conversion to gases was calculated by subtraction. Magnetite is known to be easily recoverable from the process. Thus, in calculating the solid and liquid yields of the catalysed runs, 25 g was subtracted from de-ashed mass indicated in the raw data.

Figure 3.2.3.1 provides a schematic of the stage 1 experimental set-up; with Figure 3.2.3.2 showing a flow diagram of the actual first stage process and equipment used
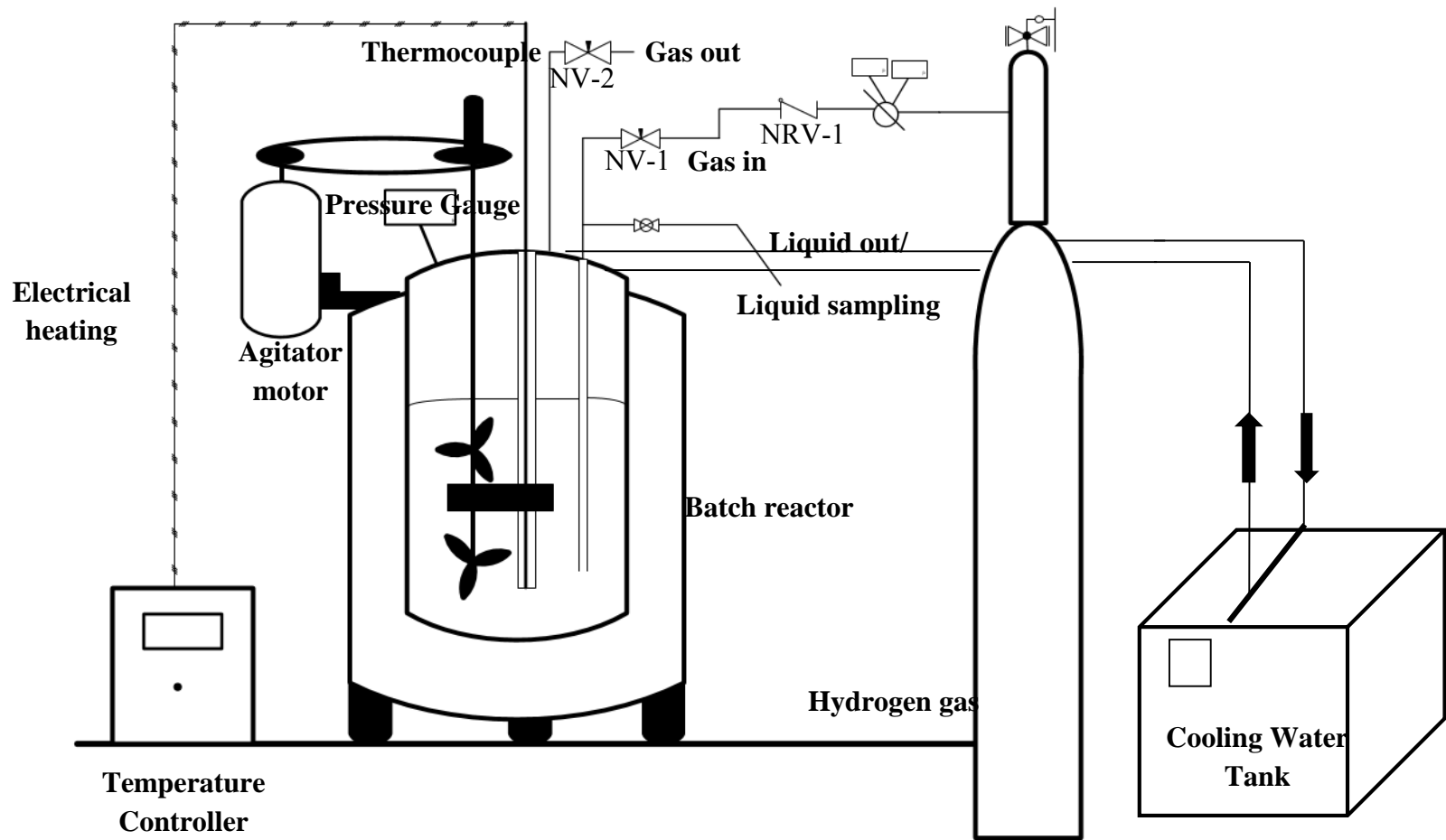
Figure 3.2.3.1: First stage reactor set-up (drawing not to scale)

Key: NV = Needle Valve; NRV = Non-return valve

**Hydrogen gas line**

**Metal clamp**

**Liquid product to be filtered**

**Cooling water lines**

**Temperature Controller**

**Batch reactor at required system pressure**

**Filtering under vacuum**

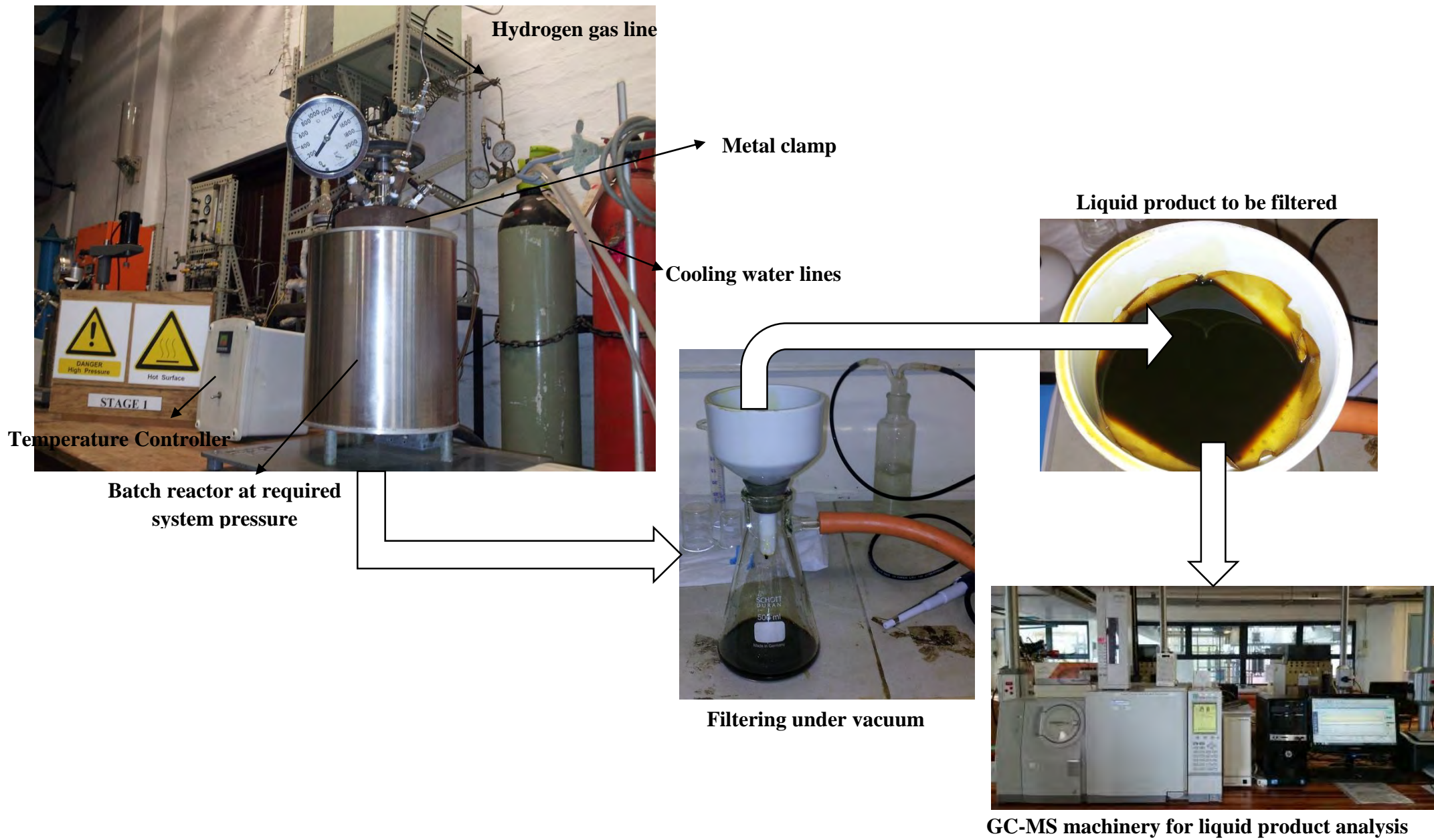**GC-MS machinery for liquid product analysis**

Figure 3.2.3.2:  First stage experimental set-up

### 3.2.4 Second Stage Refining

The filtered liquid from the first stage of the process was transferred to the second stage via the feed tank. The feed tank at room temperature was pressurized with hydrogen gas to approximately 200 kPa to aid the flow of liquid to the piston pump. The feed from the feed tank was channelled to the piston pump with the aid of gravity.

A schematic of the second stage process is shown in figure 3.2.4.3 below and figure 3.2.4.2 represents a photographic flow diagram of the actual process. The second stage of the process consisted of the first stage product being pumped into the top of the fixed-bed reactor whilst being counter-currently contacted with a stream of hydrogen gas entering through the bottom of the reactor. The fixed bed reacted had an approximate heated length of $3.35 \times 10^{-1}$ m and an inner diameter of $1.50 \times 10^{-2}$ m. Due to the constraints on the size of the fixed bed reactor with a volume of approximately 59.20 cm$^3$, only 15 ml aliquots of the first stage oil were processed per second stage run. Using the Beckman 110A positive displacement pump, experiments were conducted for flowrate of 1ml/min and the gas pressure was set at 100 barg (1450 psig) for all the runs. Aided by gravity flow of a vertical feed into the reactor, the pressure of 100 barg was sufficient to overcome any frictional losses in line before pressurizing the reactor.

Non-return valves were installed on the gas feed line as well as on the liquid feed lines. Across the heated length, the reactor was packed with Ni-Mo and Co-Mo catalyst supported by a bed of 4mm glass beads at the bed ends. It was assumed that the reaction occurred only across the heated length as outside the reactor, both the reaction temperature and catalyst bed are not maintained. It was also assumed that the pressure drop over the entire reactor (i.e. catalyst bed, glass bead beds, exit and entrance) was negligible. The liquid was channelled into the insulated reactor and electrically heated by a clam-shell furnace shown in figure 3.2.4.1. The furnace included a high temperature rating with ceramic elements, insulation and a temperature control system. In terms of sealing, all valves and fittings were correctly sized and sufficiently tightened onto the piping and equipment pieces on the rig using thread tape. This prevented any leaks and pressure losses.

By means of a thermocouple, the electrically powered furnace was capable of registering intervals of 1°C. Prior to each run, the furnace was turned on and the reactor was heated to a temperature of 300 °C, to ensure activation of the catalyst in the presence of hydrogen at a flowrate of 10 ml/min using the in-line needle valve. Beds of glass beads at the entrance and exit of the reactor ensured that the catalyst bed height was maintained. The glass bead beds also served as a distributor for the gas and liquid phases entering the catalyst bed. All experiments were conducted at a constant pressure of 100 barg to eliminate any hydrodynamic differences that might occur due to changes in pressure.

With the product valve closed, the liquid was allowed to react in the second stage reactor for the required reaction time, at a pressure of 1450 psig and the tested temperature. With the product valve open, both the liquid and gas product was allowed to enter into a collection vessel which separated the liquid product from the gas. The liquid product was collected and analysed in the GC-MS. The gas released from the process was analysed in the VarioPLUS gas analyser, which was calibrated to read the quality and quantity of the gas released in terms of methane, carbon monoxide and hydrogen. By monitoring the pressure gauge, the downstream needle valve was used to maintain the reactor pressure at 100barg.

Figure 3.2.4.1: (Left) View of the clam-shell electrically powered furnace used in heating the 2$^{nd}$-stage tube reactor. (Right) Insulation for heating contained within reactor

### 3.2.5 VARIOplusSE Gas Analyser

The non-condensable light gases released by the second-stage reaction were analysed online using the VARIOplusSE Gas Analyser from VARIOplus Industrial. This analyser was selected due to its industrial application and also since it is calibrated to identify up to nine non-condensable flue gas compounds released by the process. These compounds include hydrogen, oxygen, carbon monoxide, carbon dioxide and methane, nitrogen oxide, nitrogen dioxide and sulphur dioxide and propane.

By qualitative and quantitative analysis of these gases, it was possible to determine the extent of the pollutants released into the atmosphere by the process under investigation; and compare it to the compounds released by similar processes.

Mode of operation

MRU Vario-plus portable flue gas analyser was used to qualitatively and quantitatively analyse the non-condensable gas leaving the second stage of the process. The analyser is capable of analysis for industrial scale purposes, was equipped with a probe and filament (shown in figures 3.2.5.1 and 3.2.5.2) which were connected to the gas vent line. The gas analyser was calibrated to detect carbon monoxide, carbon dioxide, methane and H$_2$S. The gas for the Co-Mo and Ni-Mo runs was analysed as gas from a heavy fuel oil and at gas temperatures ranging from 26-27 °C. The settings available on the display shown in Figure 3.2.5.3.

Figure 3.2.5.1: Gas probe connecting second stage vent line to the gas analyser



Figure 3.2.5.2: Filament in probe used to detect the gases



Figure 3.2.5.3: MRU VarioPLUS Gas Analyser Control Panel

### 3.2.6 Piston Pump

The Beckman model 110A positive displacement piston pump was selected for this high pressure application and for controlled liquid flow through the second stage reactor. Pump specifications are indicated in Table 3.2.6. Shown in figure 3.2.4.2, at an elevated height or by increasing the head, the pump allowed adequate flow into the reactor despite the loss in head created by the in-line filter. Experimentally, sufficient head was obtained at 0.595 m. Compared to the $\frac{1}{8}$ inch diameter feed line to the pump, the discharge line had a diameter of $\frac{1}{16}$ inches, thus increasing discharge pressure considerably. Common industrial practice makes use of a pressure relief valve when positive displacement pumps are used, due to the expected high discharge pressure. A Swagelok pressure relief valve and pressure gauge were selected and installed on the feed line to the reactor to ensure that the maximum allowable pressure was not exceeded.

Since the coal liquid composition was not consistent, a mass based calibration would have posed numerous challenges. The pump was used to feed in a specific volume of liquid into the second stage reactor. This volume was based on the pump display as indicated in figure 3.2.6.

Figure 3.2.6: Beckman model 110A pump control panel

Table 3.2.6: Beckman Model 110A Pump Specifications

| Type of pump | Positive Displacement |
|---|---|
| Pressure/Flow rating | High pressure/low flow |
| Characteristic | Flow doesn't change when pressure changes |
| Flowrate  (ml/min) | 0 - 9.900 |
| Pressure psi (barg) | 0-6000 (0-413.690) |
| Feed pipe diameter (inches) | 1/8 |
| Discharge pipe diameter (inches) | 1/16 |
| Elevation height above reactor to ensure sufficient head (m) | 0.595 |

**3.2.7 Valves**

Mostly, needle, ball, 3-way and non-return valves were selected. For applications where specific flow control was required, needle valves were selected. For rapid stop-start flow action, ball valves were installed. In order to control flow in one direction while shutting of off the flow in another direction, three-way valves were selected. Non-return valves ensured directional flow control. A pressure relief valve (PRV) was also selected as a safety device in this high pressure environment. If when monitoring the pressure via pressure gauge, and fail-close or fail-open of valves doesn't work, the PRV will burst open. The PRV was calibrated to burst open passed a safe working pressure of 180 barg.
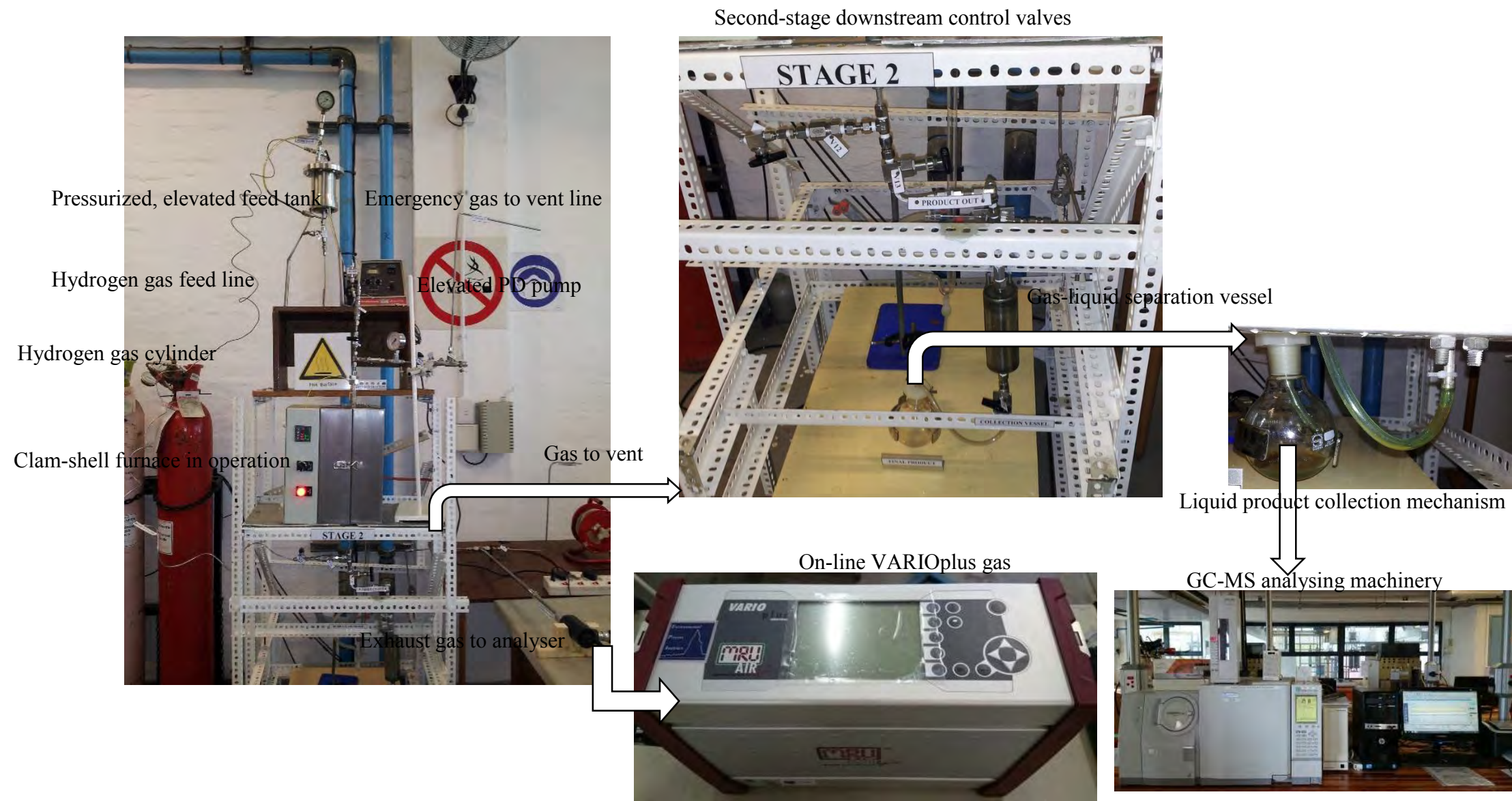
Pressurized, elevated feed tank

Emergency gas to vent line

Hydrogen gas feed line

Elevated PD pump

Hydrogen gas cylinder

Clam-shell furnace in operation

Gas to vent

Exhaust gas to analyser

Second-stage downstream control valves

STAGE 2

PRODUCT OUT

COLLECTION VESSEL

FINAL PRODUCT

Gas-liquid separation vessel

Liquid product collection mechanism

On-line VARIOplus gas

GC-MS analysing machinery
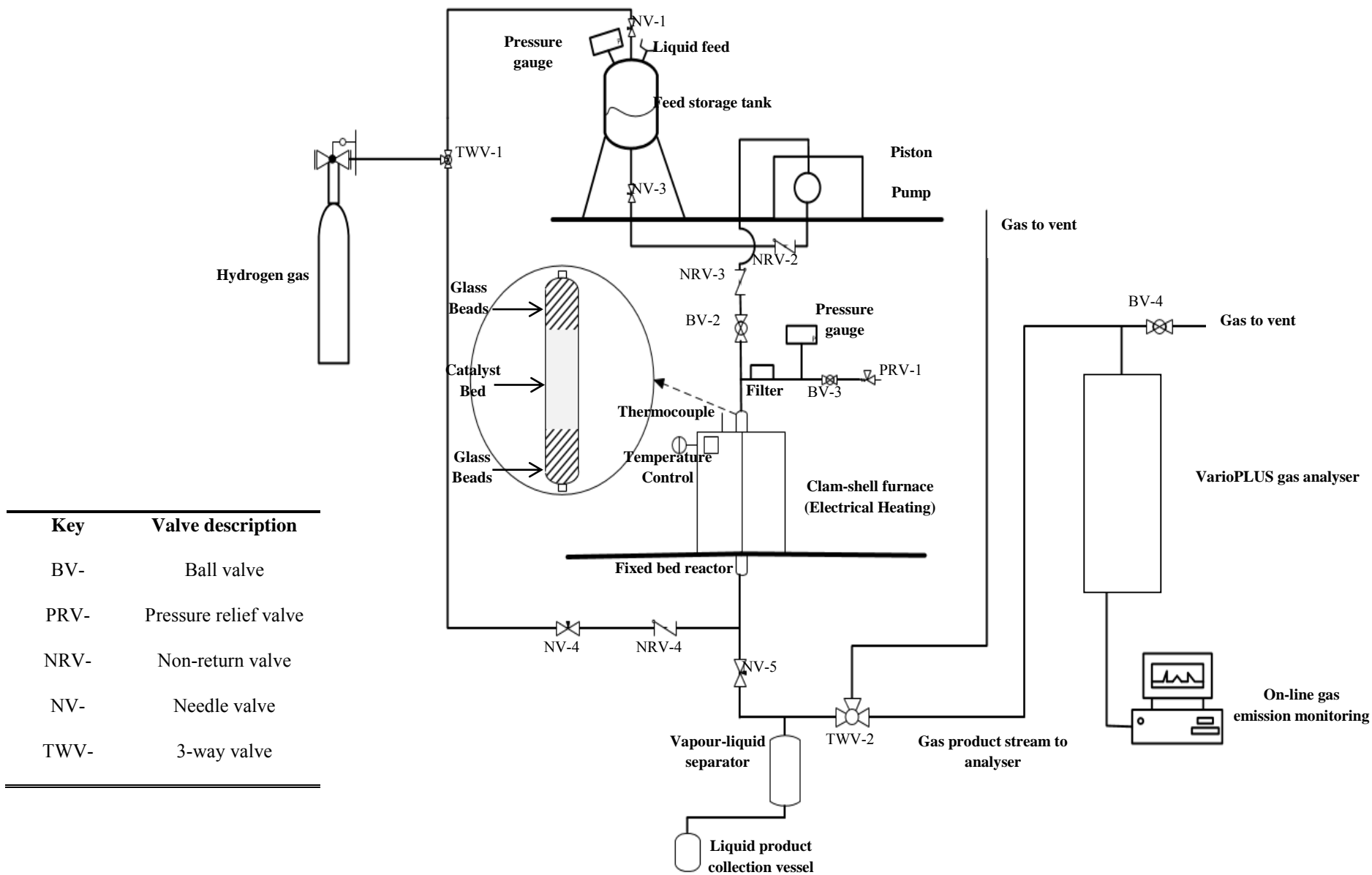
Figure 3.2.4.2 Second stage reactor set-up

Figure 3.2.4.3 Schematic of second stage reactor set-up (Drawing not to scale)

## 3.3 Analytical Techniques

### 3.3.1 Factorial Design

There are several factors of interest in this experiment viz. temperature, time and solvent: coal ratio. Hence a factorial design was used with factors being varied together. A factorial experiment allows all possible combinations of the levels of the factors in each complete trial or replicate of the experiment to be evaluated. If there are two factors A and B with 'a' levels of factor A and 'b' levels of factor B, then each replicate contains all 'ab' combinations.

The effect of a factor is defined as the change in response produced by a change in the level of the factor. This is called a main effect since it refers to the primary factors in the study. Here the primary factors are factor A which represents temperature, B which represents time and C which represents solvent: coal ratio. In this factorial design, factors A, B and C have two levels viz. "low" and "high". These two levels denoted by "-"and "+" respectively.

The number of experiments carried-out yielded a $2^3$ factorial design. This design has eight factor-level combinations and geometrically, the design can be represented as a cube (Figure 3.3.1) with the eight runs forming the corners of the cube. Indicated in Table 3.3.1. is the test design matrix which allows the 3 main effects to be estimated (A, B and C) along with three two-factor interactions (AB, AC, and BC) and one three-factor interaction (ABC). The response of the full factorial model can be approximated by the mathematical form indicated in equation 3.3.1.

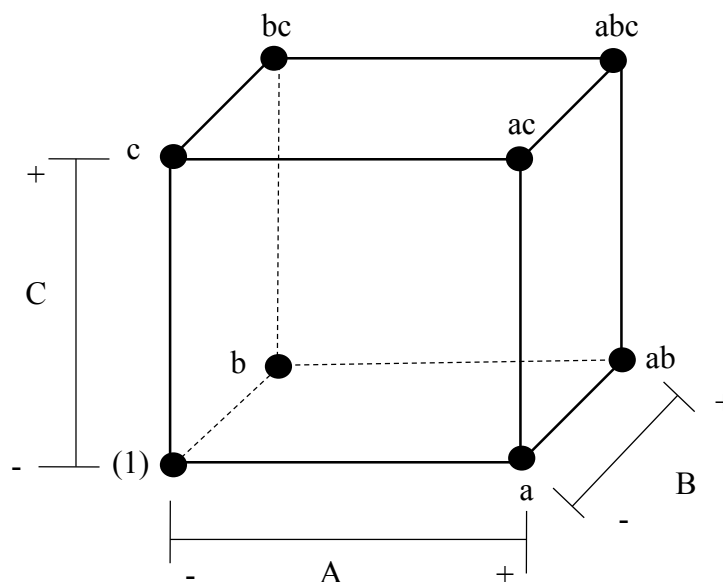$$y = \beta_o + \beta_1 x_1 + \beta_2 x_2 + \beta_{12} x_1 x_2 + \varepsilon \qquad (3.3.1)$$



Figure 3.3.1: Geometrical representation of a $2^3$ factorial design

Table 3.3.1: Signs for Effects in the $2^3$ Design

| Treatment Combination | Factorial Effect | | | | | | | |
|---|---|---|---|---|---|---|---|---|
| | I | A | B | AB | C | AC | BC | ABC |
| (I) | + | - | - | + | - | + | + | - |
| a | + | + | - | - | - | - | + | + |
| b | + | - | + | - | - | + | - | + |
| ab | + | + | + | + | - | - | - | - |
| c | + | - | - | + | + | - | - | + |
| ac | + | + | - | - | + | + | - | - |
| bc | + | - | + | - | + | - | + | - |
| abc | + | + | + | + | + | + | + | + |

## 3.3.2 Gas Chromatography-Mass Spectrometry (GC-MS)

A small amount of sample is injected into the injection port of the instrument shown in figure 3.3.2.1. The injection port is set to a temperature of approximately 250℃ which vaporizes the sample as it enters the port. The gaseous sample is then blown by a carrier gas into a thin glass tube filled with a porous material. This is called the GC column. The column is 30 metres long and coiled so that it can fit inside the oven of the instrument. In this study, the ZB-5MS column was used shown in figure 3.3.2.3. The oven regulates the temperature of the column. Since the oven is considerably cooler than the injection port, some of the molecules of the mixture condense on the porous material filling the column. The compounds then vaporize, travel a short distance through the column and condense again.

This process occurs multiple times before the substance that makes up the mixture is eluted, or exits the GC column. A compound with a higher vapour pressure (lower boiling point) will spend a greater proportion of its time in the vapour phase than a compound with a lower vapour pressure (higher boiling point). The greater the proportion of time that molecules spend in the gaseous state, the faster they will be blown through the column. This is how the GC portion of this instrument separates the components of a mixture based on their vapour pressures.

The Shimadzu GC-MS equipment used in this study is shown in Figure 3.3.2.2, and analytical conditions used in the analysis are shown in Table 3.3.2.

Numerous documented sources on GC-MS including Klee (2013) and Drews (1998), emphasise the importance of developing good techniques where the use of GC-MS time should be optimised to effect the separation process. Due to the expense of the chemicals, in particular the deuterated internal standards, four solutions were made to envelope the expected concentration range, each solution was run three times in order to ensure the most accurate response factors signals.
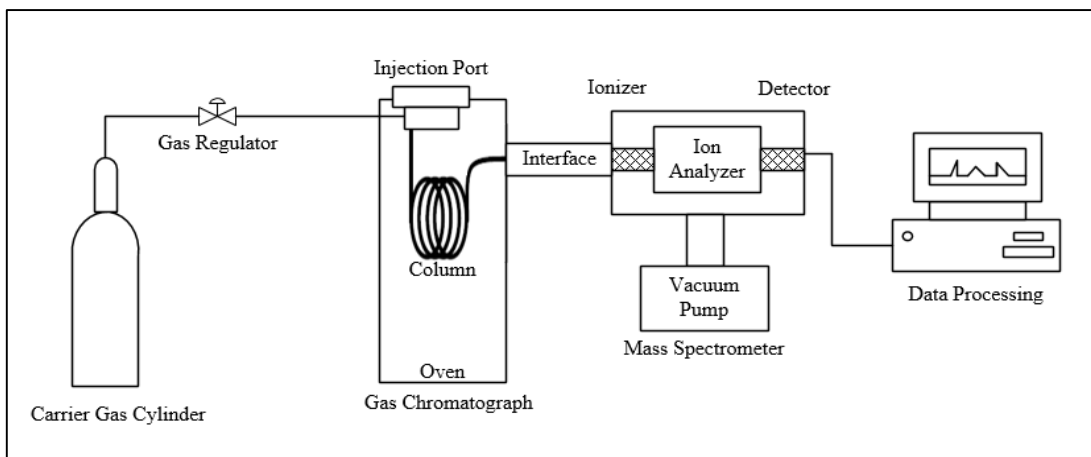
Figure 3.3.2.1: Schematic of process for GC-MS analysis



Figure 3.3.2.2: Shimadzu GC-MS equipment used in analysis of samples



Figure 3.3.2.3: GC-MS Column ZB-5MS

Table 3.3.2: GC-MS Analytical Conditions

| Parameter | Light Fractions | Heavy Fractions |
|---|---|---|
| Column oven temperature (°C) | 30 | 210 |
| Split ratio | 200 | 70 |
| Injection temperature (°C) | 280 | 280 |
| Carrier gas | Helium | Helium |
| Sample volume ($\mu l$) | 0.50 | 0.50 |
| Carrier gas pressure (kPa) | 46.60 | 100.10 |
| Carrier gas flowrate (ml/min) | 1.01 | 0.87 |

### 3.3.3 Method of Internal Standard

The method of internal standard was used to quantify groups of compounds in the oil samples.

Using the method of internal standards, quantification for the various functional organic groups was accomplished. These procedures were guided by the ASTM standards set out by the Manual of Hydrocarbon Analysis (Drews, 1998).

**Selection of internal standards and calibration**

The internal standards were selected to match as closely as possible the physical and chemical characteristics of the analytes of interest. Physical characteristics include volatility and molecular weight; while chemical characteristics include molecular structure, functional groups and polarity. Superior internal standards are deuterated analogs of the target analytes. However it is the relative cost and availability of the deuterated standards which prevent their use in general research (Drews, 1998).

The added amount of internal standard in the samples should yield a concentration close to that expected for target analytes. Best practice dictates that the concentration of the internal standard in the sample be within an order of magnitude of concentration of target analytes. If the potential concentration spans several orders of magnitude, it is good practice to consider using multiple concentrations of internal standards to cover the range. This was the approach taken in this study.

Further to this, an initial screening analysis was done for all samples. Observed in GC-MS chromatograms the concentrations of the quantifiable compounds varied considerably. Hence

a wide concentration range was used in the calibrations as the calibration range should always envelope the quantification range.

Solutions ranging from 5 to 1000ppm in concentration were prepared using 1-propanol as the solvent. This solvent was used as it did not change the original product distribution or concentration of the compounds. Each of these samples was spiked with a constant concentration of the internal standard.

Ethylbenzene was used as an internal standard for the cycloalkanes: benzene, cyclohexane and m-o-p-xylene, toluene.

Quantification techniques rely on the calibration procedure to be reproducible and accurate (i.e. sensitivity to volume of injected samples or final diluted volumes), in situations where the reproducibility of the calibration cannot be guaranteed the precision of the calibration may be compromised. It is however still possible to obtain an accurate standardization by referencing the analyte peak to another species in the injected sample, this species is called the internal standard. This is possible due to the fact that all samples experience the same conditions when injected into the gas chromatograph which negates the effect of any lack in reproducibility of the calibration procedure (McNair & Miller, 2011)

The internal standard chosen needs to meet the following criteria in order to be an effective standard (McNair and Miller, 2011):

- It should elute near the species of interest
- The internal standard peak should be clearly discernible
- It should be chemically similar to the species of interest while ensuring that it is chemically inert with all other species present
- It should be of a high purity

The relationship between the responses observed in a chromatograph and the amount of analyte or internal standard is given in Equations 3.3.3.1 to 3.3.3.2:

$$S_A = k_A \cdot M_A \qquad\qquad (3.3.3.1)$$

$$S_{IS} = k_{IS} \cdot M_{IS} \qquad\qquad (3.3.3.2)$$

Proportionality constants $k_A$ and $k_{IS}$ indicate the sensitivity of the analyte and internal standard to the detector respectively.

$$\frac{S_A}{S_{IS}} = \frac{k_A}{k_{IS}} \times \frac{M_A}{M_{IS}} \qquad\qquad (3.3.3.3)$$

Using the area of the respective peaks to quantify the responses and defining the ratio of the proportionality constants as $K_{A,IS}$ (relative response factor), Equation 3.3.3.3 is expressed as:

$$\frac{A_A}{A_{IS}} = K_{A,IS} \times \frac{M_A}{M_{IS}} \qquad\qquad (3.3.3.4)$$

In order to determine the relative response factor a calibration curve needs to be generated showing the relationship between the analyte and internal standard responses with the detector. This is done by preparing samples with known amounts of internal standard and analyte and observing the ratio between their respective responses on the resulting chromatograph, a calibration plot similar to Figure 3.3.3 results from the obtained data.
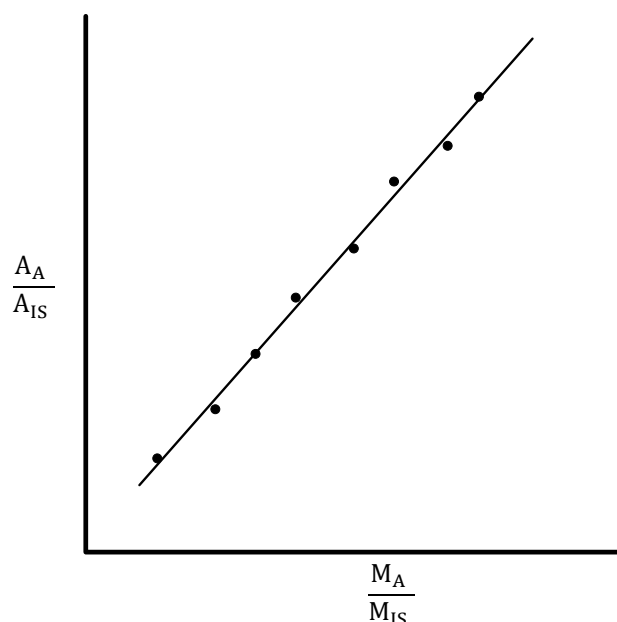


Figure 3.3.3: Illustrative example of calibration plot generated using internal standard gas chromatography quantification method (McNair and Miller, 2011).

Figure 3.3.3 shows the relationship described by Equation 3.3.3.4. The slope of the calibration plot is the relative response factor of the analyte and internal standard. The amount of analyte ($M_A$) in future samples to be analysed may be determined by adding a known mass of internal standard ($M_{IS}$) to the injected sample then observing the ratio between the respective responses in the chromatograph (Equation 3.3.3.5).

$$M_A = \frac{M_{IS}}{K_{A,IS}} \cdot \frac{A_A}{A_{IS}}$$
(3.3.3.5)

Klee (2014) describes the calibration plot as the response factor (or area ratio of internal standard to the area ratio of analyte) against the concentration (ppm).

# Chapter Four: Results and Discussion

**Chapter Overview:** Owing to the extensive experimental work carried-out, the experimental results obtained from the first and second stage processes were grouped into various data sets. An analysis of variance and regression performed on each group resulted in a best fit of these data sets to multilinear response functions, given the $2^3$ factorial design applied. In order to establish a baseline comparison, three main case studies were used where the first and second stage results were compared to similar investigations documented in literature. Results of these case studies demonstrate similarities of the experimental results to literature. The performance of the Co-Mo and Ni-Mo catalysts in comparison to each other and the first stage results, showed Ni-Mo to be superior to Co-Mo. The hydrocarbon classes and sulphur content in the oil are quantified.

In this chapter, the results of the liquid yields are presented, described and compared relative to a baseline. The baseline models detailed in the Baseline Development section of this chapter, were adapted from similar studies documented in literature.

The experiments and respective results were divided into the following groups:

**Group 1: First Stage**

- Group 1A     :     First stage blank (non-catalysed) runs
- Group 1B     :     First stage catalysed runs
      (with molybdenum doped $Fe_3O_4$ added)

**Group 2: Second Stage**

- Group 2A.1   :     Second stage using Ni-Mo for first stage blank run products
- Group 2A.2   :     Second stage using Co-Mo for first stage blank run products
- Group 2B.1   :     Second stage using Ni-Mo for first stage catalysed run products
- Group 2B.2   :     Second stage using Co-Mo for first stage catalysed run products

In total, 48 runs were conducted excluding the occurrence of any replications.

Robinson (2009) mentioned that in the coal-to-liquid process, the type and amount of solvent added in order to ensure adequate hydrogen transfer, reaction temperature, and space-time are important factors to consider. With the use of a hydrogen donor solvent such as Tetralin, the system pressure can be relaxed (Robinson, 2009). Both group 1 and group 2 experiments were carried-out under isobaric conditions of 100 barg.

The optimum range of operating conditions for the direct coal liquefaction process at a low pressure of 100 barg has not been investigated or documented in literature. A series of exploratory experiments were performed at temperatures of 523.15 K and 573.15 K for group 1 and temperature-staged with a 50 ℃ (or 50 K) increase for group 2, employing space-time values of 1800 and 3600 seconds and solvent: coal ratios of 2:1 and 3:1. This enabled

identification of the combination of operating conditions which would result in the highest liquid yield and selectivity to the hydrocarbon class.

Given the large amount of feedstock material required for the experiment; and taking into account the main process variables described by literature (Robinson, 2009), a $2^3$ factorial design was preferred.

The main performance criteria, % liquid yield ($Y_1$) was defined by equation 4.1 as follows:

$$Y_1 = \frac{M_{liquid}}{M_0} \text{ x } 100\% \qquad (4.1)$$

Where

$M_{liquid}$ =          mass of liquid product obtained after the reaction is complete [grams]

$M_0$    =          mass of initial reactor feed charge [grams]

For group 2, the selectivity to the alkane ($Y_2$) and cycloalkane ($Y_3$) production was determined from the GC-MS results detailed in the appendices section of the report.

Javed (2014) describes that the data generated from a $2^3$ factorial design can be fitted to a linear model such as the one described by equation 4.2.

$$Y = \beta_0 + \sum_i \beta_i x_i + \epsilon \qquad (4.2)$$

Where

$Y$      =          predicted response
$\beta_0$     =          intercept coefficient
$\beta_i$     =          coefficients of the linear terms
$x_i$     =          independent variables:
                  $X_1$ = reaction temperature in kelvin [K],
                  $X_2$ = amount of solvent in grams [g] per 100g coal,
                  $X_3$ = space time in seconds [s]

$\epsilon$      =          error term [dimensionless]

The factorial design experimental permutations and results for each group are given in Tables 4.1 to 4.3.

Table 4.1: Factorial design and experimental results for the first stage

| Run[a] | Manipulated Variables | | | | | | Response |
| | $X_1$ | | $X_2$ | | $X_3$ | | $Y_1$ |
| Group 1A | Temperature (K) | Level[b] | Space Time (s) | Level[b] | Solvent (g) | Level[b] | Liquid Yield % [c] |
|---|---|---|---|---|---|---|---|
| 1 | 523.15 | -1 | 1800 | -1 | 200 | -1 | 40.127 |
| 2 | 573.15 | +1 | 1800 | -1 | 200 | -1 | 40.253 |
| 3 | 523.15 | -1 | 3600 | +1 | 200 | -1 | 30.894 |
| 4 | 573.15 | +1 | 3600 | +1 | 200 | -1 | 29.251 |
| 5 | 523.15 | -1 | 1800 | -1 | 300 | +1 | 52.792 |
| 6 | 573.15 | +1 | 1800 | -1 | 300 | +1 | 38.105 |
| 7 | 523.15 | -1 | 3600 | +1 | 300 | +1 | 51.258 |
| 8 | 573.15 | +1 | 3600 | +1 | 300 | +1 | 50.119 |
| Group 1B | | | | | | | |
| 1 | 523.15 | -1 | 1800 | -1 | 200 | -1 | 42.263 |
| 2 | 573.15 | +1 | 1800 | -1 | 200 | -1 | 40.957 |
| 3 | 523.15 | -1 | 3600 | +1 | 200 | -1 | 38.237 |
| 4 | 573.15 | +1 | 3600 | +1 | 200 | -1 | 32.797 |
| 5 | 523.15 | -1 | 1800 | -1 | 300 | +1 | 51.987 |
| 6 | 573.15 | +1 | 1800 | -1 | 300 | +1 | 38.524 |
| 7 | 523.15 | -1 | 3600 | +1 | 300 | +1 | 54.768 |
| 8 | 573.15 | +1 | 3600 | +1 | 300 | +1 | 52.138 |

[a]1 = factorial design point; [b]-1=low level value, +1 = high level value; c = mass of liquid was obtained within +-0.01g accuracy

Table 4.2: Factorial design and experimental results for the second stage: Group 2A

| Run[a] | Manipulated Variables | | | | | | Response | | |
|---|---|---|---|---|---|---|---|---|---|
| | $X_1$ | | $X_2$ | | $X_3$ | | $Y_1$ | $Y_2$ | $Y_3$ |
| Group 2A.1 | Temperature (K) | Level[b] | Space Time (s) | Level[b] | Solvent (g) | Level[b] | Liquid Yield [c] % | Alkane [d] Selectivity % | Cycloalkane [d] Selectivity % |
| 1 | 573.15 | -1 | 1800 | -1 | 200 | -1 | 40.345 | 8.82 | 4.90 |
| 2 | 623.15 | +1 | 1800 | -1 | 200 | -1 | 60.115 | 5.55 | 2.74 |
| 3 | 573.15 | -1 | 3600 | +1 | 200 | -1 | 70.179 | 11.60 | 6.45 |
| 4 | 623.15 | +1 | 3600 | +1 | 200 | -1 | 51.675 | 7.16 | 2.94 |
| 5 | 573.15 | -1 | 1800 | -1 | 300 | +1 | 40.179 | 10.29 | 4.39 |
| 6 | 623.15 | +1 | 1800 | -1 | 300 | +1 | 57.809 | 13.64 | 4.40 |
| 7 | 573.15 | -1 | 3600 | +1 | 300 | +1 | 61.362 | 23.30 | 3.80 |
| 8 | 623.15 | +1 | 3600 | +1 | 300 | +1 | 73.169 | 24.46 | 3.55 |
| Group 2A.2 | | | | | | | | | |
| 1 | 573.15 | -1 | 1800 | -1 | 200 | -1 | 60.987 | 0.42 | 0.55 |
| 2 | 623.15 | +1 | 1800 | -1 | 200 | -1 | 62.257 | 0.13 | 0.05 |
| 3 | 573.15 | -1 | 3600 | +1 | 200 | -1 | 72.346 | 0.39 | 0.26 |
| 4 | 623.15 | +1 | 3600 | +1 | 200 | -1 | 52.303 | 0.26 | 0.89 |
| 5 | 573.15 | -1 | 1800 | -1 | 300 | +1 | 40.155 | 0.40 | 1.92 |
| 6 | 623.15 | +1 | 1800 | -1 | 300 | +1 | 60.133 | 0.39 | 2.15 |
| 7 | 573.15 | -1 | 3600 | +1 | 300 | +1 | 60.767 | 1.42 | 2.55 |
| 8 | 623.15 | +1 | 3600 | +1 | 300 | +1 | 73.121 | 1.47 | 2.94 |

[a]1 = factorial design point; [b]-1=low level value, +1 = high level value; c = mass of liquid was obtained within +-0.01g accuracy
d = selectivity based on concentration of compounds in the GC-MS chromatograms

Table 4.3: Factorial design and experimental results for the second stage: Group 2B

| Run[a] | Manipulated Variables | | | | | | Response | | |
|---|---|---|---|---|---|---|---|---|---|
| | $X_1$ | | $X_2$ | | $X_3$ | | $Y_1$ | $Y_2$ | $Y_3$ |
| Group 2B.1 | Temperature (K) | Level[b] | Space Time (s) | Level[b] | Solvent (g) | Level[b] | Liquid Yield [c] % | Alkane [d] Selectivity % | Cycloalkane[d] Selectivity % |
| 1 | 573.15 | -1 | 1800 | -1 | 200 | -1 | 38.947 | 6.45 | 3.87 |
| 2 | 623.15 | +1 | 1800 | -1 | 200 | -1 | 60.855 | 3.87 | 4.41 |
| 3 | 573.15 | -1 | 3600 | +1 | 200 | -1 | 72.841 | 13.64 | 5.89 |
| 4 | 623.15 | +1 | 3600 | +1 | 200 | -1 | 51.549 | 8.82 | 3.98 |
| 5 | 573.15 | -1 | 1800 | -1 | 300 | +1 | 39.431 | 9.15 | 5.55 |
| 6 | 623.15 | +1 | 1800 | -1 | 300 | +1 | 58.208 | 13.09 | 4.72 |
| 7 | 573.15 | -1 | 3600 | +1 | 300 | +1 | 60.952 | 25.57 | 2.55 |
| 8 | 623.15 | +1 | 3600 | +1 | 300 | +1 | 73.284 | 28.87 | 3.91 |
| Group 2B.2 | | | | | | | | | |
| 1 | 573.15 | -1 | 1800 | -1 | 200 | -1 | 60.201 | 0.57 | 0.68 |
| 2 | 623.15 | +1 | 1800 | -1 | 200 | -1 | 61.886 | 0.34 | 0.12 |
| 3 | 573.15 | -1 | 3600 | +1 | 200 | -1 | 72.176 | 0.53 | 0.28 |
| 4 | 623.15 | +1 | 3600 | +1 | 200 | -1 | 52.481 | 0.32 | 0.84 |
| 5 | 573.15 | -1 | 1800 | -1 | 300 | +1 | 40.319 | 0.67 | 2.12 |
| 6 | 623.15 | +1 | 1800 | -1 | 300 | +1 | 62.440 | 0.84 | 2.27 |
| 7 | 573.15 | -1 | 3600 | +1 | 300 | +1 | 59.941 | 1.54 | 2.78 |
| 8 | 623.15 | +1 | 3600 | +1 | 300 | +1 | 73.442 | 1.62 | 3.05 |

[a]1 = factorial design point; [b]-1=low level value, +1 = high level value; c = mass of liquid was obtained within +-0.01g accuracy
d = selectivity based on concentration of compounds in the GC-MS chromatograms

## 4.1 Statistical Analysis

The data organised in Tables 4.1 to 4.3 were analysed using the Analysis Of Variance (ANOVA) and regression tools in Microsoft Excel. As per the grouping, the results, adequacy and performance of the regression and ANOVA test are indicated in Tables 4.4 to 4.9.

Table 4.4: ANOVA results and regression statistics for the Group 1 yield models

| Statistics | Group 1A: Statistical Model | Group 1B: Statistical Model |
|---|---|---|
| $R^2$ | 0.991 | 0.992 |
| Adjusted $R^2$ | 0.776 | 0.779 |
| Standard error ($\epsilon$) | 7.027 | 6.943 |
| F-statistic | 95.679 | 108.328 |
| P-value | $3.526 \times 10^{-4}$ | $2.760 \times 10^{-4}$ |
| Regression mean square | 4723.990 | 5221.663 |
| Residual mean square | 49.373 | 48.202 |

The multilinear regression models, excluding the error term, to predict the liquid yield under the operating conditions described by Group 1A and 1B are given in equations 4.3 and 4.4 respectively:

$$Y_1 = 1.607 \times 10^{-2}X_1 - 9.642 \times 10^{-4}X_2 + 1.411 \times 10^{-1}X_3 \tag{4.3}$$

$$Y_1 = 1.844 \times 10^{-2}X_1 - 1.089 \times 10^{-3}X_2 + 1.230 \times 10^{-1}X_3 \tag{4.4}$$

Table 4.5: ANOVA results and regression statistics for the Group 2A yield models

| Statistics | Group 2A.1: Statistical Model | Group 2A.2: Statistical Model |
|---|---|---|
| $R^2$ | 0.980 | 0.980 |
| Adjusted $R^2$ | 0.771 | 0.772 |
| Standard error ($\epsilon$) | 10.490 | 10.858 |
| F-statistic | 79.856 | 82.684 |
| P-value | $5.030 \times 10^{-4}$ | $4.700 \times 10^{-4}$ |
| Regression mean square | 8787.327 | 9747.717 |
| Residual mean square | 110.039 | 117.891 |

The multilinear regression models, excluding the error term, used to predict the liquid yield under the operating conditions described by Group 2A.1 and 2A.2 are given in equations 4.5 and 4.6 respectively:

$$Y_1 = 5.931 \times 10^{-2}X_1 + 7.689 \times 10^{-3}X_2 + 1.477 \times 10^{-2}X_3 \tag{4.5}$$

$$Y_1 = 9.933 \times 10^{-2}X_1 + 4.980 \times 10^{-3}X_2 - 3.070 \times 10^{-2}X_3 \tag{4.6}$$

Table 4.6: ANOVA results and regression statistics for Group 2B yield models

| Statistics | Group 2B.1: Statistical Model | Group 2B.2: Statistical Model |
|---|---|---|
| $R^2$ | 0.976 | 0.980 |
| Adjusted $R^2$ | 0.766 | 0.772 |
| Standard error ($\epsilon$) | 11.514 | 10.876 |
| F-statistic | 66.758 | 82.679 |
| P-value | $7.140 \times 10^{-4}$ | $4.698 \times 10^{-4}$ |
| Regression mean square | 8849.719 | 9779.102 |
| Residual mean square | 132.564 | 118.278 |

The multilinear regression models, excluding the error term, used to predict the liquid yield under the operating conditions described by Group 2A.1 and 2A.2 are given in equations 4.7 and 4.8 respectively:

$$Y_1 = 6.053 \times 10^{-2}X_1 + 8.125 \times 10^{-3}X_2 + 8.022 \times 10^{-3}X_3 \qquad (4.7)$$

$$Y_1 = 9.872 \times 10^{-2}X_1 + 4.651 \times 10^{-3}X_2 - 2.529 \times 10^{-2}X_3 \qquad (4.8)$$

Table 4.7: ANOVA results and regression statistics for Group 2A alkane selectivity models

| Statistics | Group 2A.1: Statistical Model | Group 2A.2: Statistical Model |
|---|---|---|
| $R^2$ | 0.979 | 0.943 |
| Adjusted $R^2$ | 0.743 | 0.645 |
| Standard error ($\epsilon$) | 3.741 | 0.329 |
| F-statistic | 39.470 | 13.412 |
| P-value | $1.980 \times 10^{-3}$ | $1.486 \times 10^{-2}$ |
| Regression mean square | 552.515 | 1.454 |
| Residual mean square | 13.998 | 0.108 |

The multilinear regression models, excluding the error term, used to predict the selectivity under the operating conditions described by Group 2A.1 and 2A.2 are given in equations 4.9 and 4.10 respectively:

$$Y_2 = -3.778 \times 10^{-2}X_1 + 3.837 \times 10^{-3}X_2 + 9.392 \times 10^{-2}X_3 \qquad (4.9)$$

$$Y_2 = -3.130 \times 10^{-3}X_1 + 3.010 \times 10^{-4}X_2 + 6.060 \times 10^{-3}X_3 \qquad (4.10)$$

ANOVA results and regression statistics for Group 2A cycloalkanes selectivity models

| Statistics | Group 2A.1: Statistical Model | Group 2A.2: Statistical Model |
|---|---|---|
| $R^2$ | 0.918 | 0.957 |
| Adjusted $R^2$ | 0.685 | 0.740 |
| Standard error ($\epsilon$) | 1.558 | 0.460 |
| F-statistic | 18.590 | 37.100 |
| P-value | $8.208 \times 10^{-3}$ | $2.230 \times 10^{-3}$ |
| Regression mean square | 45.103 | 23.561 |
| Residual mean square | 2.426 | 1.058 |

The multilinear regression models, excluding the error term, used to predict the selectivity under the operating conditions described by Group 2A.1 and 2A.2 are given in equations 4.11 and 4.12 respectively:

$$Y_3 = 5.794 \times 10^{-3}X_1 + 1.774 \times 10^{-4}X_2 + 1.805 \times 10^{-3}X_3 \qquad (4.11)$$

$$Y_3 = -6.900 \times 10^{-3}X_1 + 2.330 \times 10^{-4}X_2 + 1.831 \times 10^{-2}X_3 \qquad (4.12)$$
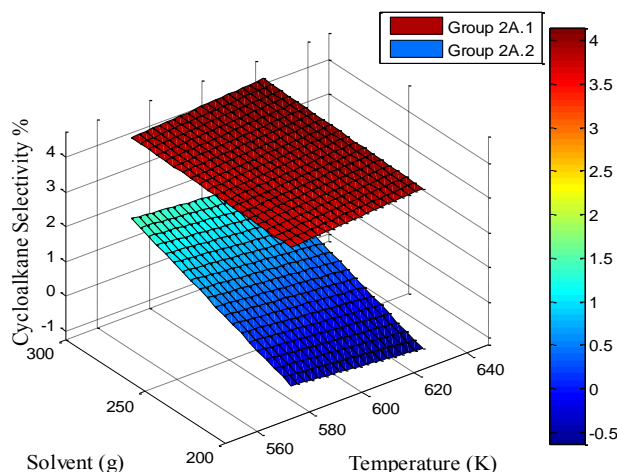


Figure 4.1.1: Comparative surface plots for models generated by equations 4.11 and 4.12

Table 4.9:
ANOVA results and regression statistics for Group 2B alkanes selectivity models

| Statistics | Group 2B.1: Statistical Model | Group 2B.2: Statistical Model |
|---|---|---|
| $R^2$ | 0.955 | 0.936 |
| Adjusted $R^2$ | 0.737 | 0.710 |
| Standard error | 4.298 | 0.299 |
| F-statistic | 35.558 | 24.419 |
| P-value | $2.419 \times 10^{-3}$ | $4.939 \times 10^{-3}$ |
| Regression mean square | 656.812 | 2.176 |
| Residual mean square | 18.471 | 0.089 |

The multilinear regression models, excluding the error term, used to predict the selectivity under the operating conditions described by Group 2B.1 and 2B.2 are given in equations 4.13 and 4.14 respectively:

$$Y_2 = -5.172 \times 10^{-2}X_1 + 5.965 \times 10^{-3}X_2 + 1.039 \times 10^{-1}X_3 \qquad (4.13)$$

$$Y_2 = 2.800 \times 10^{-3}X_1 + 2.140 \times 10^{-4}X_2 + 7.064 \times 10^{-3}X_3 \qquad (4.14)$$

Table 4.10:
ANOVA results and regression statistics for Group 2B cycloalkane selectivity models

| Statistics | Group 2B.1: Statistical Model | Group 2B.2: Statistical Model |
|---|---|---|
| $R^2$ | 0.951 | 0.936 |
| Adjusted $R^2$ | 0.731 | 0.711 |
| Standard error | 1.256 | 0.298 |
| F-statistic | 32.113 | 24.419 |
| P-value | $2.94 \times 10^{-3}$ | $4.938 \times 10^{-3}$ |
| Regression mean square | 50.648 | 2.176 |
| Residual mean square | 7.886 | 0.089 |

The multilinear regression models, excluding the error term, used to predict the selectivity under the operating conditions described by Group 2A.1 and 2A.2 are given in equations 4.15 and 4.16 respectively:

$$Y_3 = 1.005 \times 10^{-2}X_1 - 2.500 \times 10^{-4}X_2 - 1.920 \times 10^{-3}X_3 \qquad (4.15)$$

$$Y_3 = -7.220 \times 10^{-3}X_1 + 2.090 \times 10^{-4}X_2 + 1.969 \times 10^{-2}X_3 \qquad (4.16)$$

For a 95% confidence interval, analysis of the data showed that both the first and second stage experiments, fitted well to a first-order model passing through the origin. The rationale behind the fit to this model type is that neither a liquid yield nor selectivity to the alkane and cycloalkane hydrocarbon classes will result should the reaction not be initiated. Furthermore, numerous literature sources including Koltz et al. (1977) has carried out a fit of the data through the origin; and mention that there exists no theoretical basis for trying to fit the data with other mathematical models. The p-values for each of the single and interaction coefficients were greater than an alpha value of 0.05. The F-value and the corresponding p-values show a statistically significant regression. Overall the all models produced significant results that is the p-values were less than 0.05. The $R^2$ values were close to the perfect fit value of 1.

Based on the magnitude of the p-value and absolute t-value of the individual regression coefficients, for the first stage, the solvent: coal ratio was most significant followed by reaction temperature and then space time.

Since a linear regression model is not always appropriate for the data, it is necessary to assess the appropriateness of the models obtained by defining the residuals and examining the residual plots. Literature suggests that if the points in a residual plot are randomly dispersed around the

horizontal axis, a linear regression model is appropriate for the data. Thus, the random patterns observed in the residual plots below support the development of the multi-linear models in this study.

Surface plots were approximated to the two most significant factors. A comparative surface plot is given in Figure 4.1.1, emphasising the difference between Group 2A.1 and Group 2A.2 cycloalkane selectivity results. Individual surface plots are detailed in the Appendix A4 of the report. The alkane and cycloalkane % yield results were calculated on the basis of taking into consideration all related groups of compounds calibrated for in Appendix Cycloalkanes were grouped including benznen, toluene and xylene.

## 4.2 Second Stage Gas Analysis

Quantification of the second stage non-condensable gases via the MRU online VARIOplus gas analyser took place at a detection temperature range of 25.9-27.5℃ with Heavy Fuel Oil (HFO) being the fuel type selected for the gas to be processed.

For both Ni-Mo and Co-Mo the gas quality was similar. Typical methane ($CH_4$) concentrations ranged between 220 to 3200ppm with the latter favoured at 350℃ and for a reaction time of 60 minutes. Typical concentrations for carbon monoxide (CO) ranged between 20 to 304ppm, again with the latter favoured at 350℃ and for a reaction time of 60 minutes.

As pollutants, the global warming potential (GWP) gases are typically represented by methane and carbon dioxide. With only 0.32 % of a typical gas stream at most for methane and 0.03% for carbon monoxide, venting at this capacity may not pose a short-term hazard. However, owing to the methane content of this gas, consideration should be given to the use of this gas as a heating medium. The CO concentration of the gas stream should permit this gas to be recycled to the process in a closed loop system. Typically, syngas is composed of carbon monoxide. Documented is that catalytic coal liquefaction using syngas provides an improved thermal efficiency. This, also reducing the capital and operating costs by eliminating shift converters and purifying systems which are needed for the liquefaction process using hydrogen (Fu & Batchelder, 1975).

## 4.3 Baseline Development

This section presents baseline data and basic information gathered from documented literature of closely related studies. This was used to provide a comparison for assessing the performance of the experimental outputs of this project. The experimental outputs considered were the liquid yield and selectivity to specific hydrocarbon classes viz. alkanes and cycloalkanes.

Described in the methods section of this report, is that the main objective of first stage thermal dissolution process is to maximise on liquid yield. In the second stage, both maximising on liquid yield and obtaining a refined product distribution were important.

In this context, performance was considered to be directly related to the coal type and reacting system together with the operating conditions therein used.

### 4.3.1 Coal Type

Tingchen (2014) suggests that both the coal type and operating conditions have an effect on the liquid yield. Since the majority constituent of coal is carbon, Tingchen (2014) describes that the liquid yield is a function of the carbon content and hence the coal type.

Plot Digitizer ® was used to trace the liquid yield graphical function presented by Tingchen (2014) into a third order polynomial function. With the fit of the data to this function resulting in a $R^2$ value of 0.995, the liquid yield response can be represented by equation 4.3.1 below.

$$Y_1 = -6.600(X)^3 + 1.481(X)^2 - 109.292(X) + 2708.100 \qquad (4.3.1)$$

Where

$Y_1$ = liquid yield %

X = carbon content of the coal

The coal type used in this study had a carbon content of 72.86% (Roux, 2012). Using equation 4.3.1 this would then result in a liquid yield response of approximately 54.32%. In the first stage, this was obtained at operating conditions of 523.15 K (250 ℃) and 3:1 solvent: coal ratios.

Tingchen (2014) obtained data for the liquid yield responses at temperatures ranging from 400 ℃ to 623℃. This is indicative of the efficiency of this first stage process at the lower temperatures used.

### 4.3.2 Group 1A and 1B Baseline Development

### 4.3.2.1 Batch Reactor Performance

**Material balance**

Demonstrated in the material balance of a batch reactor given in equation 4.3.2.1, is that that temperature and time are the main operational variables affecting the performance of a batch reacting system.

$$\frac{dC}{dt} = C_{in} \ x \ (A exp(-\frac{E}{RT})) \qquad 4.3.2.1$$

Hence, at a constant feed concentration, the performance of the reactor was mainly determined by the reaction rate and hence temperature and time.

**Reaction mechanism**

The reaction mechanism used to determine the reaction rates is given in Figure 4.3.2 below.

Here, in the presence of a hydrogen donor solvent and hydrogen gas; products including gas, oil and solids are formed. This, in accordance with the actual products formed during the experiments.

**Gas**

$\uparrow$ $k_5$

**Coal** $\xrightarrow{k_1}$ Asphaltenes $\xrightarrow{k_2}$ **Oil** $\xrightarrow{k_3}$ **Solids**

$\downarrow$ $k_4$

**Oil**
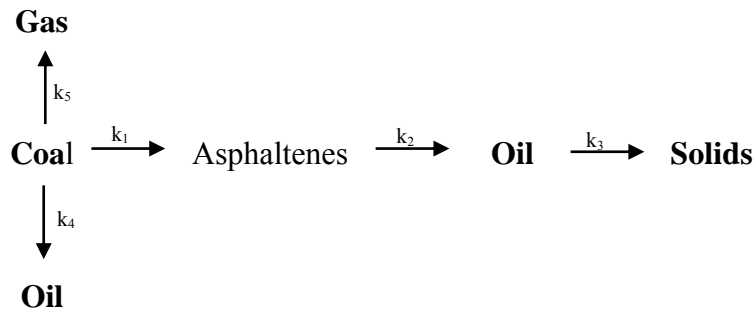
Figure 4.3.2: Reaction mechanism used in the development of the kinetic model for the first stage thermal dissolution process

Figure 4.3.2 describes a reaction mechanism containing first order reactions. Typically, the formation of pre-asphaltenes from coal and asphaltenes from pre-asphaltenes form the intermediate steps to the subsequent production of oil. However, studies including those published by Morita et al. (1992) and Cronauer et al. (1978) emphasise how the pre-asphaltene concentration reaches a maximum at an early stage of the reaction and that figure 4.3.2 is an acceptable mechanism for both long and short space times.

The major difference is in the early time behaviour of pre-asphaltenes, which is indicative that a higher order is needed to represent the pre-asphaltene concentrations (Cronauer et al., 1978). This, however, lies in contradiction to the simple reaction mechanism approach taken by a number of authors wherein first order reactions were used.

In this study, experimental data produced reasonable fits to linear, first order models. It was assumed that the steps to producing asphaltenes and pre-asphaltenes were relatively fast and; taking into consideration the increase in liquid yields from the blank to the catalysed runs; this would especially be so in the case of catalysed experiments. Soxhlet apparatus, typically used to separate asphaltenes and pre-asphaltenes from the liquid was not available. The formation of pre-asphaltenes was therefore excluded from the reaction mechanism.

**Rate Data**

As mentioned in the literature section of this work, many studies have been published using severe operating temperatures and pressures. Hence, in order to obtain the specific rate constants which are approximately related to the experimental conditions of this study, Arrhenius plots of first-order rate constants for coal dissolution were produced.

The Arrhenius equation is described by equations by 4.3.2.2. and 4.3.2.3.

$$k = A\exp\left(-\frac{E}{RT}\right) \qquad\qquad (4.3.2.2)$$

And taking the natural logarithm on both sides, results in:

$$\text{Ln } k = \left(-\frac{E}{R}\right)\left(\frac{1}{T}\right) + \text{Ln } A \qquad\qquad (4.3.2.3)$$

Where

k = rate constant $(\text{min}^{-1})$

E = Activation Energy $(\frac{J}{mol})$

A = Pre-exponential factor

$$y = mx + b \qquad\qquad (4.3.2.4)$$

Where

$y$ = any point up the y-axis that lies on the straight line graph

$x$ = any point along the x-axis that lies on the straight line graph

$(x, y)$ = co-ordinate pair that lies on the straight line graph

m = gradient

b = intercept

In accordance with the straight line equation 4.3.2.4, the gradient of the line is given by $(-\frac{E}{R})$ and the intercept by Ln A.

In order to assess the experimental outputs of Group 1A and Group 1B relative to literature, two case studies were considered.

**Group 1 Baseline Development**

**Case Study I: Group 1A Experimental Outputs versus Theoretical Results**

In this case study, rate data obtained from similar studies documented in literature was compared to the Group 1A liquid yield results. Using the reaction mechanism in Figure 4.3.2 and the rate data found in literature given in Table 4.3.2.1, the batch reactor system was simulated in MATLAB ®. The concentration profiles of the main products and comparative yield results are shown in Figures 4.3.3 and 4.3.4 respectively.

Table 4.3.2.1: Group 1A rate data obtained from Cronauer at al. (1978)

| Rate constant (min⁻¹) | |
|---|---|
| $k_1$ | $6.00 \times 10^{-2}$ |
| $k_2$ | $9.40 \times 10^{-3}$ |
| $k_3$ | $2.76 \times 10^{-3}$ |
| $k_4$ | $1.00 \times 10^{-2}$ |
| $k_5$ | $1.95 \times 10^{-2}$ |
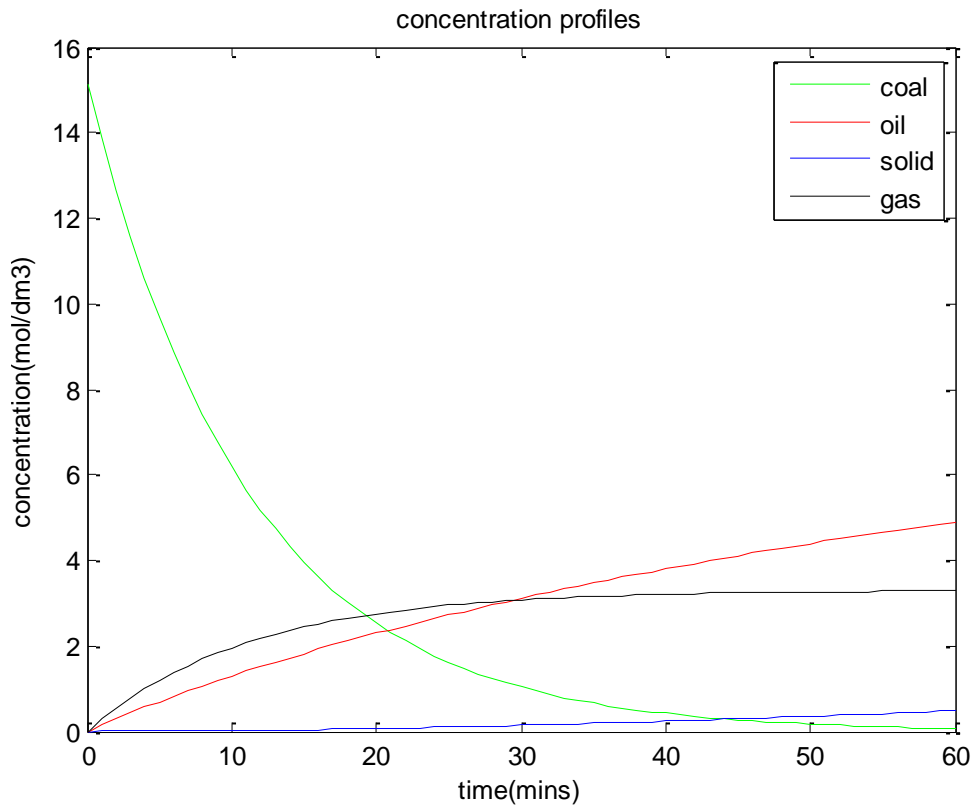
Figure 4.3.3:
MATLAB concentration profiles obtained using Case I rate data
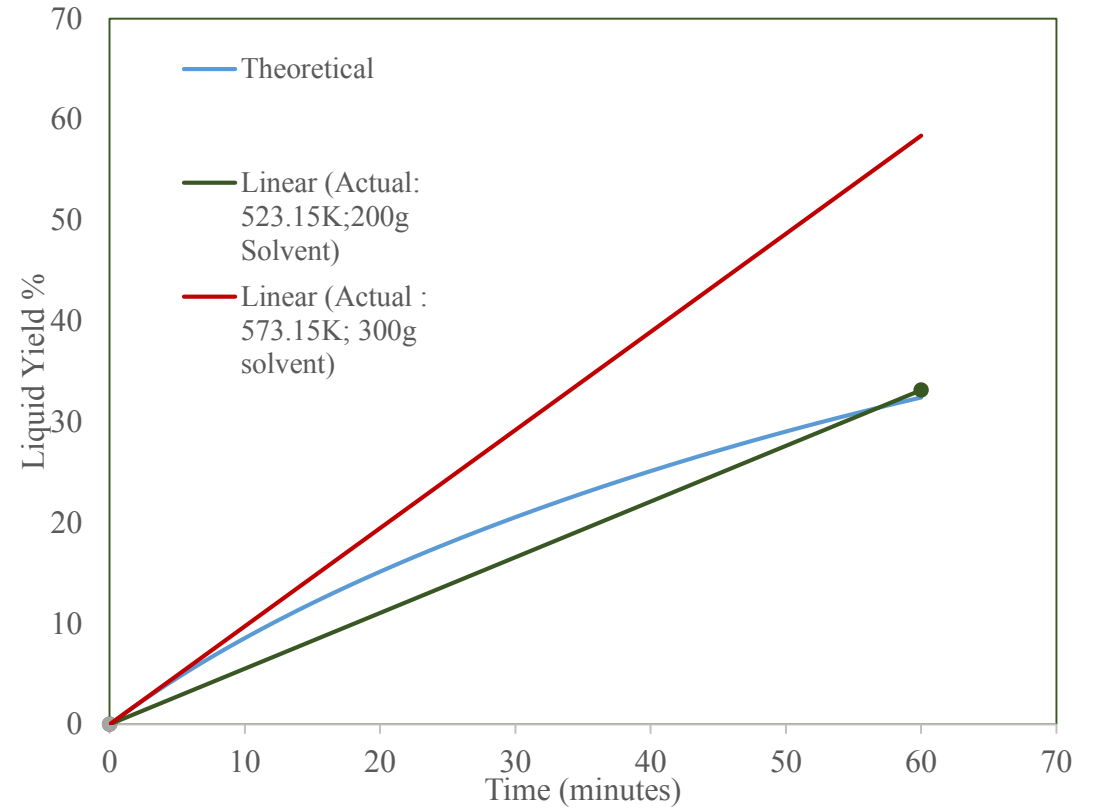


Figure 4.3.4: Comparative liquid yield results of actual vs theoretical data

Comparative yield results shown in Figure 4.3.4, indicate that the batch reactor system and operating conditions used in this study have a similar performance to literature for a solvent to coal ratio of 2:1 and a temperature of 523.15 K (250 °C).

A higher liquid yield resulted with the use of a 3:1 solvent to coal ratio.

Uncertainties lie in that, while literature provides a means of comparison to actual experimental values, the conditions at which the rate data were obtained were not identical with those used in obtaining the liquid yields of Group 1A. Scarce data exists for the Group 1A system. Theoretical yield values were however obtained at a higher temperature and pressure, which is a positive indication of the performance of the actual batch reactor system being operated at milder conditions.

**Case Study II: Group 1B Experimental Outputs versus Theoretical Results**

In order to make a comparison between literature and actual values, the estimation of the parameters of the Arrhenius equation took place under non isothermal conditions. The theoretical values of the liquid product calculated using the theoretical rate equations were in good agreement with the experimental values. This also provides an indication that the performance of the first stage batch reactor is in line to a theoretical performance.

The rate data obtained from literature was similar to the current study in the sense that batch reaction systems being pressurized with $H_2$ gas between 80 to 100 barg and using similar naphthalene derived HDS including decalin, methylnaphthalene and alike were used.

In terms of deriving the Arrhenius rate constants for the catalysed experiments, an approximation was made to relate the rate constants obtained from Morita et al. (1992) which made use of an iron-sulphide and molybdenum catalyst to the experimental results.

While there exists particular agreement between data from Morita et al. (1992) and experimental results, noteworthy is that data obtained from other sources is similar in terms of orders of magnitude which provides confidence in the rate data used.

With reference to table 4.3.2.2, reaction rates increase with an increase in temperature, a positive activation energy is therefore expected in the fit of the data to the Arrhenius relationship.

Table 4.3.2.2: Group 1B rate data obtained from literature

| Rate Constants ($s^{-1}$) | Literature | | |
|---|---|---|---|
| | Temperature (°C) | | |
| | 350 | 380 | 410 |
| $k_1^a$ | $7.850 \times 10^{-3}$ | $1.460 \times 10^{-2}$ | $2.570 \times 10^{-2}$ |
| $k_2^a$ | $1.880 \times 10^{-2}$ | $3.490 \times 10^{-2}$ | $6.130 \times 10^{-2}$ |
| $k_3^a$ | No data | No data | $2.760 \times 10^{-3}$ |
| $k_4^a$ | No data | No data | $2.910 \times 10^{-2}$ |
| $k_5^b$ | $1.95 \times 10^{-2}$ | | |

Table 4.3.2.3: Group 1B rate data at 250 °C and 300 °C

| Rate constant (min$^{-1}$) | | Arrhenius constants | |
| --- | --- | --- | --- |
| | | A (min$^{-1}$) | E (J/mol) |
| $k_1$ | 6.41 x 10$^{-3}$ | 5.060 x 10$^{-3}$ | 5.400 x 10$^2$ |
| $k_2$ | 1.54 x 10$^{-2}$ | 1.213 x 10$^{-2}$ | 5.378 x 10$^3$ |
| $k_3$ | 2.76 x 10$^{-3}$ | No data | |
| $k_4$ | 2.91 x 10$^{-2}$ | No data | |
| $k_5$ | 2.30 x 10$^{-2}$ | No data | |

Noteworthy, that in terms of the rate data obtained, there exists a small change in the data in relation to temperature changing from 250°C to 300°C.
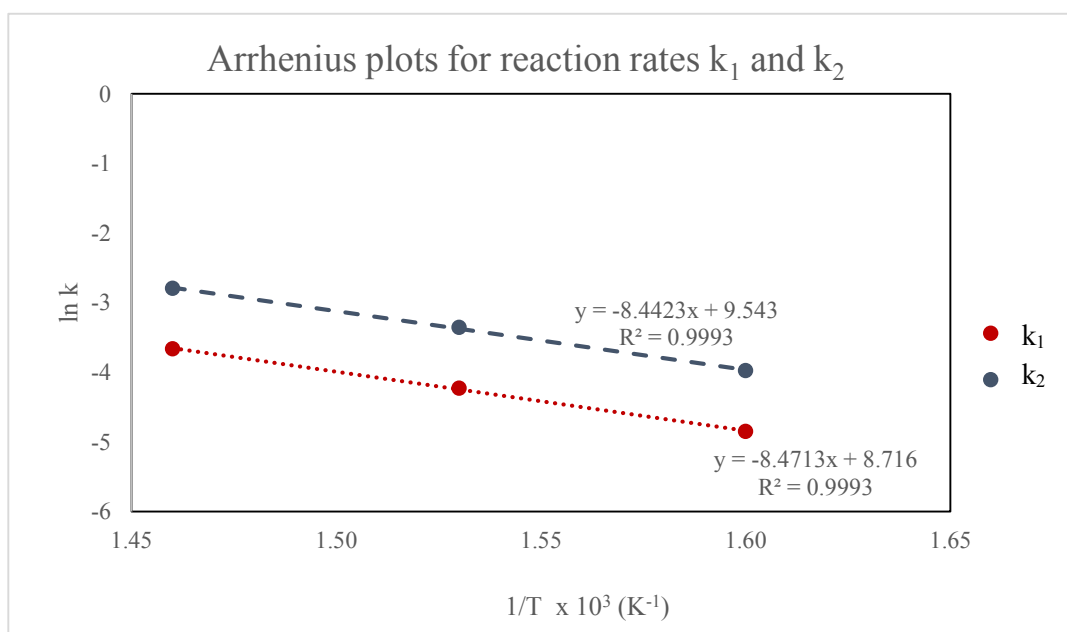


Figure 4.3.5: Linear Arrhenius plots used in determining rate constants at experimental temperature
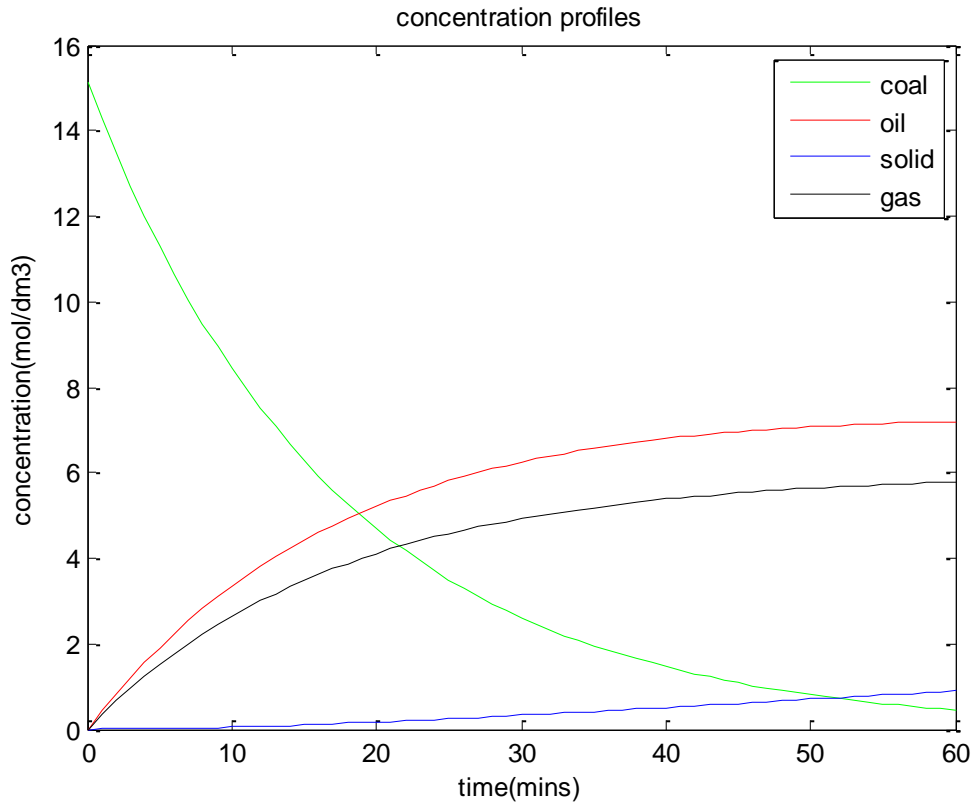
Figure 4.3.6 MATLAB concentration profiles of for first stage batch reactor for Case Study II
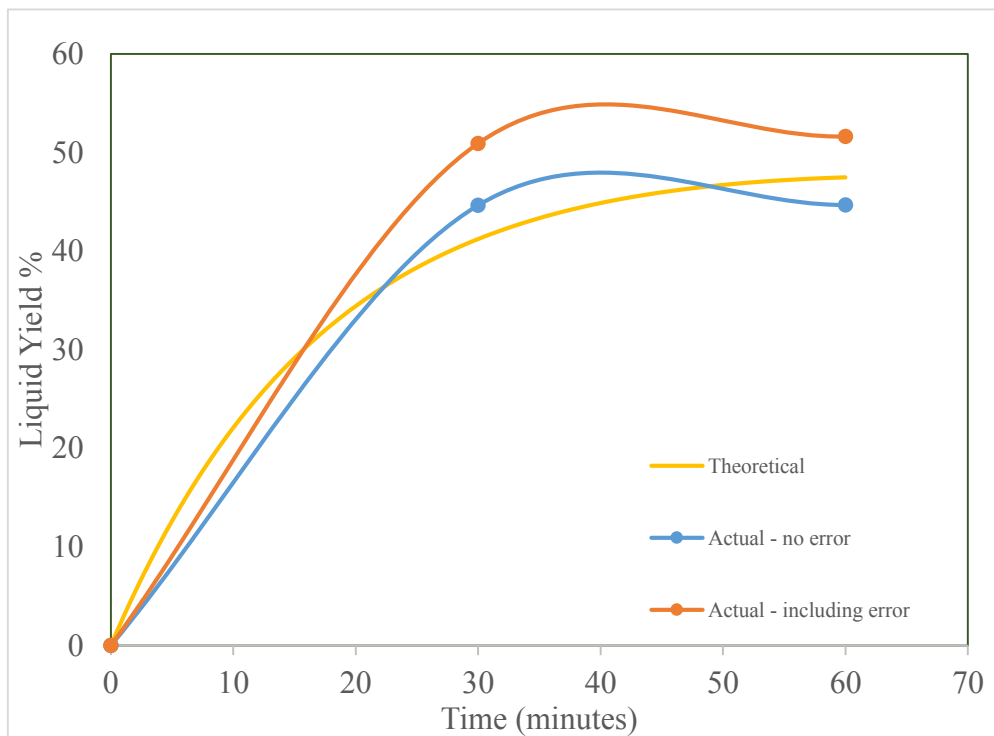


Figure 4.3.7: Theoretical vs. Actual for liquid yield comparison for case study II

Theoretical liquid yield results indicate that as per the rate plots, the liquid yield levels off after a while. At 30 minutes, a higher liquid yield is obtained experimentally. With reference to Figure 4.3.7, there exists evidence that the yield would too level off. This provides some evidence that, after 30 minutes, the molybdenum doped magnetite catalyst may be inactive.

Thus, in comparison to case study I, there exists a much higher rate of reaction as expected with the use of powdered catalysts (Gollakota et al., 1985).

### 4.3.4 Group 2 Baseline Development

### Case Study II: Group 2 Experimental Outputs versus Theoretical Results

While there exists data for Cobalt Molybdenum systems, typically batch type systems are used. A substitution of rate data into a batch reactor reveals a 64% liquid yield, which although higher than group 1, it is still lower than the liquid yield obtained from the second stage in a fixed-bed reactor counter-current configuration.

In terms of the reaction mechanism, there is agreement between the lack of a reaction step which accounts for the formation of solids and the lack of solid formation observed in the second stage. This reaction mechanism derived by Morita et al. (1992) when considering molybdenum type catalysts.

Based on the reputation of Cobalt Molybdenum and Nickel Molybdenum in hydrotreating systems, fixed bed reactors are typically used. Little kinetic data exists for hydrotreating reactions in the direct coal liquefaction process.

### 4.4 GC-MS Analysis

Thakur (1984) suggests that in coal liquefaction, catalyst selectivity is more important than the catalyst activity for controlling hydrogen consumption and product distributions. Once a product free from coal or pre-asphaltenes is obtained, the major task consists of upgrading or refining of coal liquids.

While activity is touched on in the section that follows, the major focus is on the improved product distribution obtained from the first to second stage process; as well as the application of the quantified compounds to industry.

### 4.4.1 Sulphur containing compounds

Literature suggests that the sulphur content of liquid fuel obtained from the hydrogenation of coal, ranges from 0.72 % to approximately 1 % (Tillman, 1979). These values are however below the concentration of sulphur containing compounds identified by GC-MS analysis. With reference to the figure, there exists evidence of a lesser hydro-desulphurisation performance of

the Co-Mo catalyst over the Ni-Mo catalyst. In the GC-MS analysis, sulphur compounds were only identified from day 11 of the catalysts being on stream in the fixed bed reactor.

Among other compounds, the presence of a sulphur is a sign of used catalysts. For Co-Mo catalysts, carbon deposition at lower system pressures, sintering and metal deposition are common causes for de-activation and hence the presence of sulphur (Fu & Batchelder, 1975).
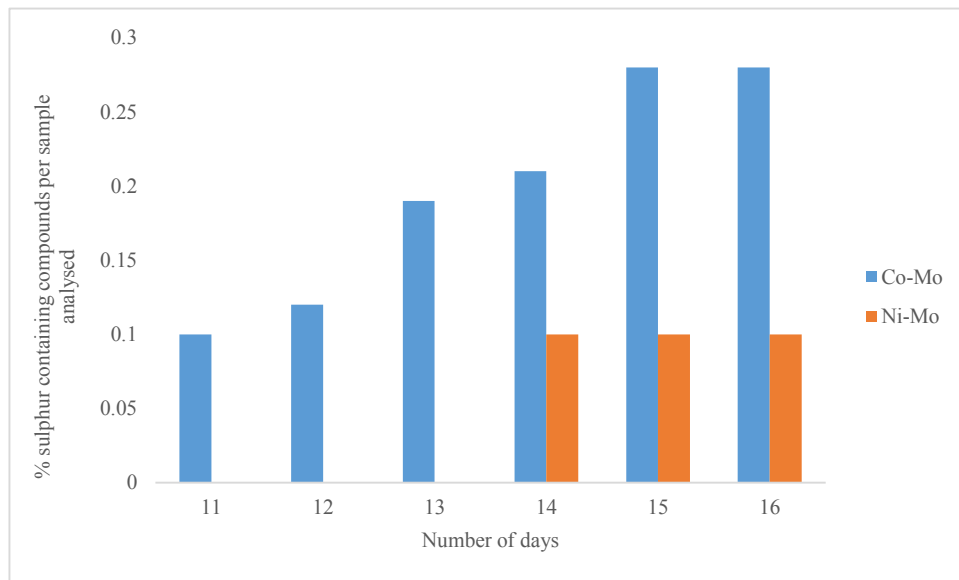


Figure 4.4.1: Sulphur content in second stage liquid product



Figure 4.4.2: Appearance of catalyst after 16 day on stream performance (Fresh catalyst: left and deactivated catalyst: right)

**4.4.2 Product Distributions**

Specific temperature profiles for the GC-MS analysis of the first and second stage liquid products were developed and detailed in the materials and methods section. Numerous literature sources including Mochida (2013) document a wide product distribution expected from hydrogenation of coal in the DCL process. In order to obtain a better split and separation of the numerous compounds formed by the processes, the liquid products were analysed both in terms of light and heavy fraction

Figure 4.4.2.1 shows the typical product distribution obtained with the use of Ni-Mo catalyst in the second stage. Table 4.4.2.1, the accompanying table to Figure 4.4.2.1 indicates that the formation of straight and branched chain alkanes is favoured over the other hydrocarbon classes.

Figure 4.4.2.2, include superimposed images of the GC-MS chromatograms comparing both the first and second stage processes for each catalyst type. The red chromatograms are those chromatograms obtained from the analysis of the second stage processes. Selectivity to the formation of alkanes, cycloalkanes and PAH compounds is increased with the use of Ni-Mo and Co-Mo catalysts. Well documented is that the extent of coal conversion is related to the hydrogen consumed in the process. As a measure of the hydrogen consumption by the coal and hence the conversion, the degree of tetralin dehydrogenation towards naphthalene has often been used (Cronauer et al., 1982).

Thus, the improved product distribution between stages 1 and 2 could be owing to an improved contact between hydrogen gas and liquid feed facilitated by the counter-current figuration of the second-stage and an increase in the activity of the Co-Mo and Ni-Mo catalysts. With reference to Table 4.4.2.2, further evidence of this conversion lies in the high concentration of naphthalene derived compounds identified in the second stage product distribution. An improved second-stage product distribution of Ni-Mo over Co-Mo and hence improved catalyst performance, could be owing to the higher sulphur content identified in the product distributions obtained with the use of Co-Mo catalyst.

As mentioned in the literature review (Section 2.6.3), this study focuses on desulphurization over denitrogneation. The temperature profile established and multiple internal standards specifically selected for the GC-MS work aimed to maximise the identification and quantification of sulphur compounds, alkanes, cycloalkanes and PAH compounds. Given the complex product distribution, further refining of the temperature profile and selection of another internal standard would be required. Literature states that a specific internal standard in GC-MS analysis or possibly the use of a GC-N (nitrogen-selective detector) would be required (Bradley et al., 1994). A GC-N may however prove ineffective for untreated distillates. However, in general, a qualitative analysis reveals some impure compounds containing nitrogen. Nitro benzoic acid, pyridine and carbamic acid were also identified in the second stage Ni-Mo product distributions. This may provide some positive insight into the denitrogneation performance of the catalysts not specifically aimed at in this study.

### 4.4.3 Theoretical Quantification of H2S Gas

According to Thomas (1982), the rate constant (k) for the decomposition of pyrite ($FeS_2$) contained within coal and in a solvent and hydrogen system is $8.60 \times 10^{-3}$ $min^{-1}$ for 0.9 wt% pyrite in a coal with a 3 wt% sulphur composition. This pyrite composition used in Thomas (1982) is almost one order of magnitude greater than the pyrite composition in the coal used in this study. The consistent activation energy calculated to be 88 kJ/mol Thomas (1982). As detailed in the literature section, a mechanism consistent with this data is the thermal decomposition of $FeS_2$ to produce pyrrohotite ($Fe_{1-x}S$) and S, followed by a reaction of the sulphur with the available hydrogen (from $H_2$, solvent or coal) to form $H_2S$.

As noted by Thomas (1982), the rate of pyrite decomposition is proportional to the rate of $H_2S$ formed. Also noted in this literature source is that the pyrite decomposition to pyrrohotite becomes significant at approximately 300 °C.

Thus higher pyrolysis temperatures and higher pyrite concentration in coal would favour a higher yield of $H_2S$ over milder liquefaction temperatures used in this study.

Other studies suggest that the necessity for $H_2S$ quantification is present in pyrolysis processes. Hydrogen sulphide is the principal sulphur species released during coal pyrolysis (Coburn et al., 1991). The iron-based catalysts could promote coal pyrolysis by markedly reducing the pyrolysis activation energy (Li et al., 2008).

Using the above rate data as an estimate, the conversion of pyrite to $H_2S$ would account for approximately 0.86 % of total pyrite composition per minute. (0.120 g/min of $H_2S$ release at 350°C). Thus after a 30 minute space time, only 25.80 % of pyrite is converted. After a 60 minute space time, 51.60 % of the pyrite is converted to $H_2S$. These results can be viewed as conservative estimates. This due to the rate of reaction having been determined using a coal with a pyrite composition almost within an order of magnitude greater than the pyrite composition of the coal used in this study.

In order to experimentally quantify the $H_2S$ release, gas-chromatography (GC) would be required. The following items of equipment would need to be fitted to each stage of operation:

- High pressure 6-port gas sampling valve
- Pressure reducing valve to ensure a lower operating pressure for GC analysis
- A flame photometric detector on the GC for detecting low levels of $H_2S$. $H_2S$ gas would then be required as a standard for calibration.

Thomas (1982) states that the $H_2S$ concentration was determined by GC analysis, performed with a Hewlett-Packard 5700A gas chromatograph using a teflon-lined aluminium column to reduce $H_2S$ absorption

Thus, given the low amounts of $H_2S$ expected, lower pyrite composition of the coal used and relatively mild operating temperatures, there exists little justification for the $H_2S$ quantification in this liquefaction study.

## GC-MS Results
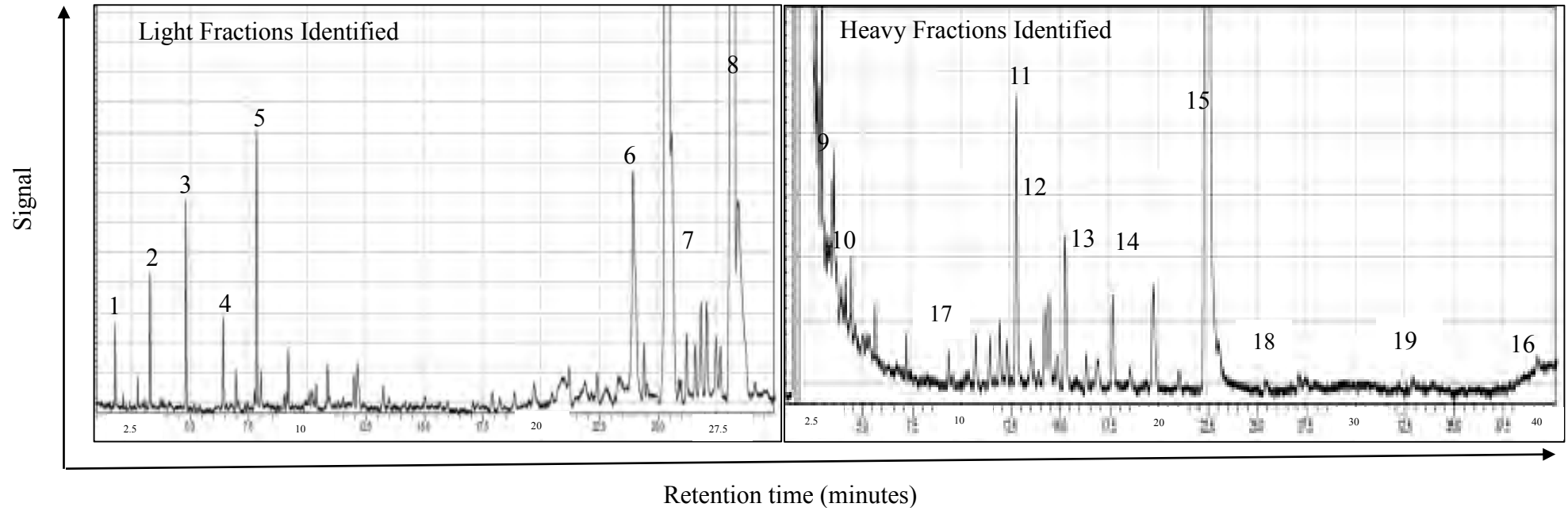


Figure 4.4.2.1: Product distribution of oil product from Ni-Mo run for Case 2B.1 (Light Fractions: Left and Heavy Fractions: Right)

Table 4.4.2.1: Accompanying product distribution information to Figure 4.4.2.1

| Peak identified: Compound | Retention time (mins) | Concentration (ppm) [a] | Peak identified : Compound | Retention time (mins) | Concentration (ppm) [a] |
|---|---|---|---|---|---|
| 1: Methyl-cyclopentane | 2.42 | Not-quantified | 9: Heptadecane | 3.54 | $1.92 \times 10^{-4}$ |
| 2: Toluene | 3.93 | 130.50 | 10 : Pentadecane, 8-hexyl | 4.41 | $8.17 \times 10^{-4}$ |
| 3: n- Nonane | 4.92 | 0.14 | 11: Naphthalene, 1,2,3, 4-tetrahydro-octyl | 12.77 | Not quantified |
| 4: Indane | 6.43 | 0.20 | 12: Eicosane | 15.67 | 2.24 |
| 5: cyclohexane | 7.97 | 1704.00 | 13: Tetriacontane | 17.62 | 0.20 |
| 6: Benzene, cyclopentyl | 24.08 | Not quantified | 14: Nonadecane, 9-methyl | 19.84 | Not quantified |
| 7: 1-methylenene-1H-indene | 26.23 | Not quantified | 15: Anthracene | 22.93 | 47.56 |
| 8: Bi-naphthalene | 28.13 | 571.79 | 16: Sulphurous acid | 39.4 | 6.93 |
| 17; 19: Carbamic acid | 8.43; 32.90 | Not quantified | 18: Nitrobenzoic acid | 25.89 | Not quantified |

(ppm) [a] = quantification was achieved using the respective calibration plots in Appendix B
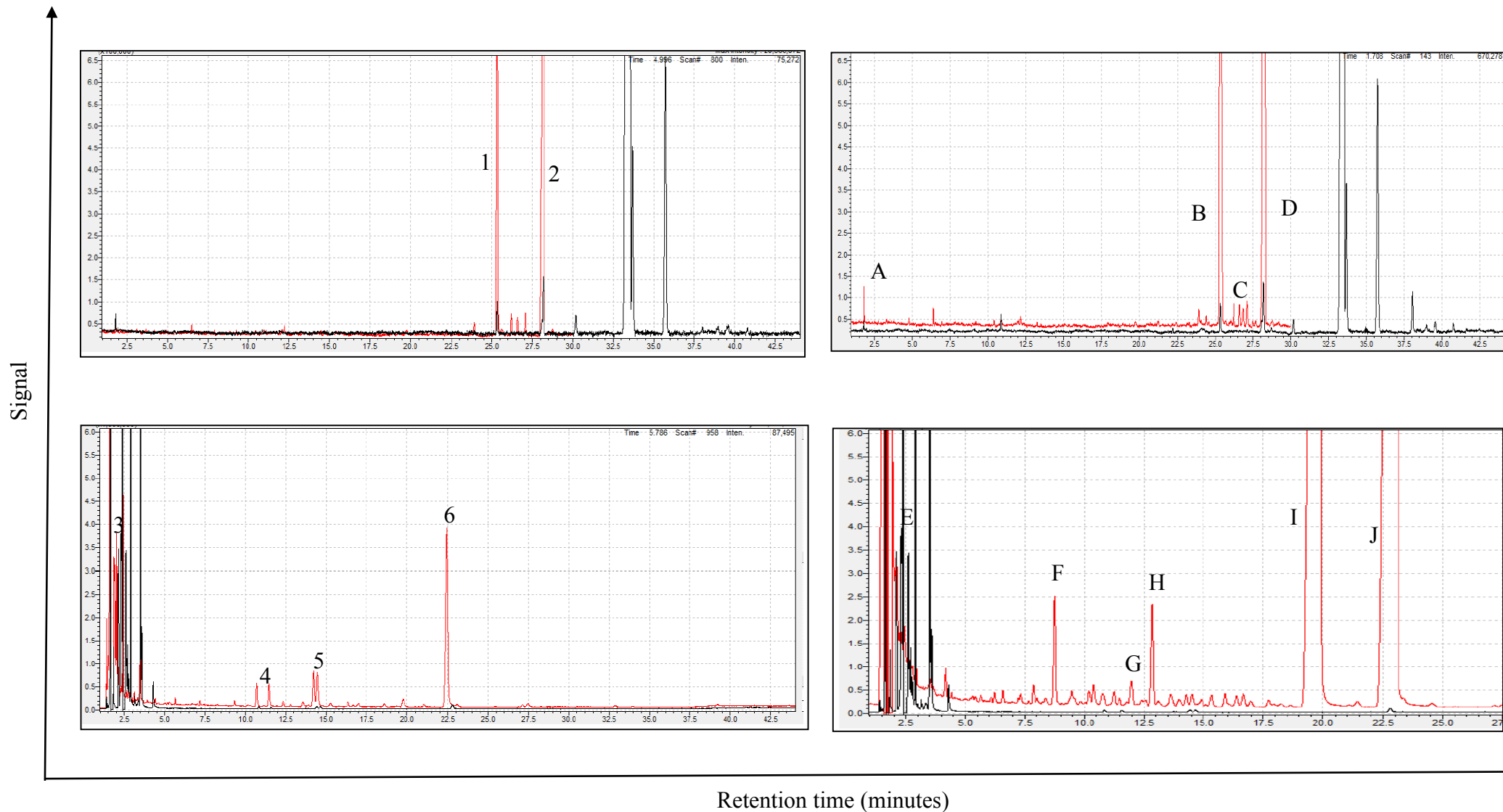
Figure 4.4.2.2: First stage (Black) versus second stage (Red) product distribution comparison
(Case 2A.2 vs. Case 1A Top; Case 2A.1 vs Case 1A: Bottom)

70

Table 4.4.2.2: Accompanying product distribution information to Figure 4.4.2.2

| Peak identified: Compound | Retention time (mins) | Concentration (ppm)[a] | Peak identified : Compound | Retention time (mins) | Concentration (ppm)[a] |
|---|---|---|---|---|---|
| 1: Dodecane | 25.24 | 0.18 | A: Heptadecane | 2.47 | $2.25 \times 10^{-3}$ |
| 2: Benzene | 28.41 | 935.69 | B : 2,2 -Binaphthalene | 25.53 | 185.35 |
| 3: Hexadecane | 2.39 | $5.97 \times 10^{-4}$ | C: Perylene | 25.57 | 150.04 |
| 4: Pentadecane 2, 6, 10, 14-tetramethyl | 12.15 | $9.42 \times 10^{-4}$ | D: Naphthalene | 27.56 | 623.13 |
| 5: xylene (m,o,p) | 14.79 | $9.57 \times 10^{-4}$ | E: Naphthalene | 1.78 | 524.35 |
| 6: Naphthalene | 22.54 | 690.00 | F: 2-methylhexacosane | 8.47 | Not quantified |
| | | | G: Eicosane | 12.34 | 0.10 |
| | | | H: 1,2-Binaphthalene | 12.82 | 166.93 |
| | | | I: 1,1-Binaphthalene | 19.78 | 872.32 |
| | | | J: Phthalic acid | 22.74 | Not quantified |

(ppm) [a] = quantification was achieved using the respective calibration plots in Appendix B

# Chapter Five: Conclusions

Chapter Overview: In this chapter, the main findings from the first and second stage investigations are summarised.

- Thermal dissolution of coal in a hydrogen donor solvent, followed by liquid product upgrading can be achieved in a two-step, temperature-staged process.

- Direct coal liquefaction can place at 100 barg, as opposed to documented low pressures of 130-210 barg (Robinson, 2009)

- At the experimental operating conditions, the first stage performs to yield a typical liquid product of approximately 50 %.

- Molybdenum doped magnetite performs to increase the liquid product yield. Under the given operating conditions, it the catalyst may be active for only 30 minutes.

- A second stage reactor is capable of upgrading the first stage liquid product in a counter-current gas-liquid catalytic fixed bed configuration.

- At temperatures of 300 °C and 350 °C, liquid yield of approximately 70% in the 2$^{nd}$ stage can be obtained

- Solid coke deposits were not found in the 2$^{nd}$ stage equipment or in the 2$^{nd}$ stage liquid product. This providing an indication that the reaction mechanism as provided by Morita et al. (1992) and that system pressure of 100 barg is sufficient for the process

- Exhaust gas from the second stage is composed of CO and $CH_4$. Based on the heating value of the methane and syngas potential of this exhaust gas, consideration should be given to feeding this gas back to the process in a closed loop system.

- Due to low pyrite concentration in the coal sample feed and mild operating temperatures, a theoretically quantified low amount of $H_2S$ gas was expected

- For 16 days on stream, the loss in activity of the second-stage catalysts was measured from day 11.

- For both Ni-Mo and Co-Mo, the presence of sulphur containing compounds in the liquid was below 0.3 %. However, Ni-Mo had an improved HDS performance over Co-Mo with only 0.1% of sulphur compounds quantified.

- Physical observations, included a marked colour change between first and second stage products. The lighter colour of the second stage is indicative of a more refined product

- Tetralin performs as a hydrogen donor solvent

- Evidence of the dehydrogenation of tetralin to naphthalene and thus hydrogen transfer, is provided by the high concentration of naphthalene derived compounds in the liquid and other saturated compounds

- Ni-Mo performs with a selectivity to long and branched chain alkanes over cycloalkanes and aromatics

- A qualitative analysis revealed some impure compounds containing nitrogen. Nitro benzoic acid, pyridine and carbamic acid were also identified in the second stage Ni-Mo product distributions in small quantities. This could provide some insight into the improved denitrogneation performance of the catalysts.

- Co-Mo performs with a selectivity to the production of aromatics and cycloalkanes

- The potential of the production of valuable compounds from the two-step, temperature-staged direct coal liquefaction process exists

## Chapter Six: Recommendations

Chapter Overview: In this chapter, in order to develop this topic beyond the scope described, recommendations for further related research work are listed.

- Exhaust gas from the second stage is composed of CO and $CH_4$. Based on the heating value of the methane and syngas potential of this exhaust gas, consideration should be given in future work to feeding this gas back to the process in a closed loop system.

- Due to the wide range of functional groups and hydrocarbon classes identified in the GC-MS product distribution, in future work, separation techniques including distillation may need to be employed to effect separation and the extraction of the more valuable content

# References

1. Akash, B. A. (2013). Thermochemical Liquefaction of Coal. *Internal Journal of Thermal and Environmental Engineering, Vol. 5, No. 1*, 51-60.

2. Birol, F. (2004). *World Energy Outlook.* Paris -France: International Energy Agency.

3. Bradley, C., Pauls, R., C, C. D., & Bambacht, M. E. (1994). *Characterization of nitrogeneous compounds in distillates derived from 2-stage coal liquefaction* . Naperville: Amoco Research Center.

4. Cronauer, D., McNeil, R., Young, D., & Ruberto, R. (1982). *Fuelvol. 61* , 610-619.

5. Cronauer, R., Roberto, R., & Shah, Y. (May 1978). Proceedings of the EPRI Contractors' Conference on Coal Liquefaction. (pp. 4-1). Palo Alto California: Electric Power Research Institute .

6. Drews, A. (1998). *Manual on hydrocarbon Analysis, 6th ed.* Pennsylvania, America: American Society for Testing and Materials (ASTM).

7. Fu, Y. C., & Batchelder, R. F. (1975). *Catalytic Liquefaction of Coal.* USA: U.S. Energy Research and Development Administration.

8. Gollakota, S. V., Guin, J. A., & Curtis, C. W. (1985). Parallel Theral and Catalytic Kinetics in Direct Coal Liquefaction. *Ind. Eng. Chem. Process Des.Dev., vol. 24, No. 4*, 1148-1154.

9. Javed, F. (2014, March 27). *Assignment 2: Overview of multivariable linear regression.* Retrieved from Lund University: http://www.maths.lth.se/matstat/kurser/fms072mas209/fms072_vt14/Notes%20on%20Assignment2.pdf

10. Klee, M. (2014). *GC Solutions 20: Calibration Curves - Part 2, Internal Standard Approach*. Retrieved from Separation Science Premier Learning for Analytical Scientists: http://www.sepscience.com/Techniques/GC/Articles/189-/GC-Solutions-20-Calibration-Curves--Part-2-Internal-Standard-Approach

11. Koltz, R. C., Baldwin, R. M., L, B. R., Golden, J. O., & H, G. J. (1977). Kinetics of coal hydrodesulphurisation in a batch reactor. In R. T. Ellington, *Liquid fuels from coal* (pp. 117-130). New York - London: Academic Press.

12. Li, X., Hu, S., Jin, L., & Hu, H. (2008). Role of iron-based catalyst and hydrogen transfer in direct coal liquefcation. *Energy Fuel, vol. 22*, 1126-1129.

13. Lokhat, D., Oliver, M., & Carsky, M. (2015). Preparation of iron oxide nanocatalysts and application in the liquid phase oxidation of benzene. *Polish Journal of Chemical Technology, Vol. 17, No. 2*, 43-46.

14. McNair, H. M., & Miller, J. M. (2011). *Basic Gas Chromatography* . USA: John Wiley and Sons.

15. Mochida, I. (2013). Chemicals from direct coal liquefaction. *American Chemical Society*, 1637-1672.

16. Morita, M., Sato, S., & Hashimoto, T. (1992). *Kinetics of Direct Liquefaction of Coal in the Presence of Mo-Fe Catalyst.* Yonezawa: Department of Chemical Engineering, Yamagata University, Japan.

17. Parkash, S., Cameron, A., & du Plessis, M. P. (1983). *Application of coal petrography in the liquefaction of sub-bituminous coals and lignites.* Alberta: Alberta Reserach Council.

18. Robinson, K. K. (2009). Reaction Engineering of Direct Coal Liquefaction. *Energies, vol. 2*, 976-1006.

19. Roux, H. J. (2012). *Petrographic evaluation of the monthly composite sample from Grootegeluk GG1.* Pretoria: Advanced Coal Technology.

20. Schobert, H. H. (1987). *Coal: The energy source of the past and future.* Washington: American Chemical Society.

21. Shui, H., Cai, Z., & Xu, C. C. (2010). Recent Advances in Direct Coal Liquefcation. *Energies*, vol 3; pp 155-170.

22. Song, C. S., Saini, A. K., & H, S. H. (1998; 38(3)). Enhancing low-severity catalytic liquefaction of low-rank coal by adding water. *American Chemical Society*, 1031-1038.

23. Speight, J. G. (2005). *Handbook of coal analysis.* New Jersey: John Wiley and Sons Incorporated.

24. Thakur, D. S. (1984). Catalyst Deactivation during Direct Coal Liquefaction: A Review. *Ind. Eng. Chem. Prod. Res. Dev., Vol. 23, No. 3*, 349-360.

25. Thomas, M. G., Granoff, B., Noles, G. T., & Baca, P. M. (1977). *Hydrogen Consumption in Non-Catalyzed Coal Liquefaction.* Albuquerque, New Mexico: Sandia Laboratories.

26. Thomas, M. G., Thomas, D. P., Stohl, F. V., & Stephens, H. P. (1982). Decomposition of pyrite under coal liquefcation conditions: a kinetic study. *Fuel, vol. 61*, 761-764.

27. Tillman, D. D. (1979). *Synthetic fuels from coal.* Australia: John Wiley and Sons.

28. Tingchen, L. (2014). Liquefaction of Coal. *Encyclopedia of life support systems (EOLSS), vol. 1*, 403-424.

29. University of York. (2014, February 17). *The Essential Chemical Industry Online*. Retrieved from Cracking and related refinery processes: http://www.essentialchemicalindustry.org/processes/cracking-isomerisation-and-reforming.html

30. Vlieger, J. (1988, April 19). Aspects of the chemistry of hydrogen donor solvent coal liquefaction

31. Williams and Larson. (2003). A comparisonm coal of direct and indirect liquefaction technologies for making fluid fuels from coal. *Energy for SUstainable Development, Volume VII, No. 4*.

32. Xu, B., & Kandiyoti, R. (1996). Two-stage Kinetic Model of Primary Coal Liquefaction . *Energy Fuels, 10(5)*, 1115-1127.

1. Appendix A1:

## MATLAB Code for Case Study I Theoretical Outputs

```
%Case I: Literature vs Group 1A Experimental Results
%Creating the function
Function [t,c] = call_caseI
%set time interval to make a smooth curve
tspan = (0:60);
%x=density of solid
%y=density of liquid
%z=denity of slurry
%c=concentration
%
for wt=50 % %wt fractions of coal in a 2:1 mixture on a 100g
basis
    w=0.5; %2:1 ratio
    x=833;%Bulk density of solid coal [=]kg/m3
    y=970;%Density of tetralin [=] kg/m3
    MMCoal=54.992; %Average coal molar mass kg/mol
    z=(100/(wt/x))+((100-wt)/y); % concentration of slurry
c1_0=((w*z)/MMCoal);%Initial concentration of coal in slurry
[=] mol/m3
end
c2_0=0;%Initial Asphaltenes concentration[=] mol/m3
c3_0=0;% Initial oil concentration [=] mol/m3
c4_0=0;%Initial Solids concentration [=] mol/m3
c5_0=0;%Initial Gas concentration [=] mol/m3
c0=[c1_0 c2_0 c3_0 c4_0 c5_0]; % creating a vector of the
initial concentrations
%caseI evaluates rhs of the ODE
[t,c]=ode45(@caseI,tspan,c0);
%Plotting the concentration profiles vs time and liquid yield
% vs time on
subplot (2,1,1)
plot(t,c(:,1),'g',t,c(:,3),'r',t,c(:,4),'b',t,c(:,5),'k')%plot
ting measurable yields
title('concentration profiles')
xlabel('time(mins)')
ylabel('concentration(mol/dm3)')
legend('coal','oil ','solid','gas');
subplot (2,1,2)
plot(t,((c(:,3)/c1_0)*100))
(c(:,3)/c1_0)*100 % outputting liquid yield %
title('Theoretical liquid yield%')
xlabel('time(mins)')
ylabel('Liquid yield %')
legend('theoretical');
function dcdt = caseI (t,c)
k1=0.06;%asphaltene production from coal
```

```matlab
k2=0.00940;%oil produced from asphaltenes
k3=0.00276;%solids produced from oil
k4=0.01;%oil produced directly from coal
k5=0.0195;%gas produced from coal
C_coal=c(1);
C_asphaltenes=c(2);
C_oil=c(3);
C_solid=c(4);%defined by dcdt(4)
C_gas=c(5);%defined by dcdt(5)
%Rate equations derived in terms of the rate mechanism in
Figure 4.3.2
dcdt(1)=-C_coal*(k1+k4+k5);
dcdt(2)=(C_coal*k1)-(C_asphaltenes*k2);
dcdt(3)=k4*C_coal+k2*C_asphaltenes-k3*C_oil;
dcdt(4)=k3*C_oil;
dcdt(5)=k5*C_coal;
dcdt=dcdt'; % outputting the results in a vector
end
end

%In a Separate Mfile Script
%House keeping
clc;
clear all;
%Calling the Case I Baseline Function
[t,c]=call_caseI;
```

**Appendix A2:**

**MATLAB Code for Case Study II Theoretical Outputs**

```matlab
%Case II: Literature vs Group 1B Experimental Results
%Creating the function
function [t,c] = call_caseII
%set time interval to make a smooth curve
tspan = (0:60);
%x=density of solid
%y=density of liquid
%z=denity of slurry
%c=concentration
for wt=50 % %wt fractions of coal in a 2:1 mixture on a 100g
basis
    w=0.5; %2:1 ratio
    x=833;%Bulk density of solid coal [=]kg/m3
    y=970;%Density of tetralin [=] kg/m3
    MMCoal=54.992;%Average coal molar mass kg/mol
    z=(100/(wt/x))+((100-wt)/y); % concentration of slurry
c1_0=((w*z)/MMCoal);%Initial concentration of coal in slurry
[=] mol/m3
```

```matlab
end
c2_0=0;%Initial Asphaltenes concentration[=] mol/m3
c3_0=0;% Initial oil concentration [=] mol/m3
c4_0=0;%Initial Solids concentration [=] mol/m3
c5_0=0;%Initial Gas concentration [=] mol/m3
c0=[c1_0 c2_0 c3_0 c4_0 c5_0]; % creating a vector of the
initial concentrations
%caseI evaluates rhs of the ODE
[t,c]=ode45(@caseII,tspan,c0);
%Plotting the concentration profiles vs time and liquid yield
% vs time on
subplot (2,1,1)
plot(t,c(:,1),'g',t,c(:,3),'r',t,c(:,4),'b',t,c(:,5),'k')%plot
ting measurable yields
title('concentration profiles')
xlabel('time(mins)')
ylabel('concentration(mol/dm3)')
legend('coal','oil ','solid','gas');
subplot (2,1,2)
plot(t,((c(:,3)/c1_0)*100))
(c(:,3)/c1_0)*100 % outputting liquid yield %
title('Theoretical liquid yield%')
xlabel('time(mins)')
ylabel('Liquid yield %')
legend('theoretical');
function dcdt = caseII (t,c)
k1=0.00641;%asphaltene production from coal
k2=0.0154;%oil produced from asphaltenes
k3=0.00276;%solids produced from oil
k4=0.0291;%oil produced directly from coal
k5=0.023;%gas produced from coal
C_coal=c(1);
C_asphaltenes=c(2);
C_oil=c(3);
C_solid=c(4);%defined by dcdt(4)
C_gas=c(5);%defined by dcdt(5)
%Rate equations derived in terms of the rate mechanism in
Figure 4.3.2
dcdt(1)=-C_coal*(k1+k4+k5);
dcdt(2)=(C_coal*k1)-(C_asphaltenes*k2);
dcdt(3)=k4*C_coal+k2*C_asphaltenes-k3*C_oil;
dcdt(4)=k3*C_oil;
dcdt(5)=k5*C_coal;
dcdt=dcdt'; % outputting the results in a vector
end
end
%In a Separate Mfile Script
%House keeping
clc;
clear all;
%Calling the Case II Catalysed Function
```

```
[t,c]=call_caseII;
```

## Appendix A3: MATLAB Code used to obtain various surface plots

```matlab
clc
clear all
% Coefficients for linear model
B1=-0.03778;
B2=0.003837;
B3 =0.09392;
x = linspace(573.15,623.15,20);
y = linspace(1800,3600,20);
r = linspace(200,300,20);
% [TempTemp,TimeTime,SolventSolvent]= meshgrid
(Temp,Time,Solvent);
[X,R]=meshgrid(x,r);
Z= (B1.*X)+(B3.*R);
surf(X,R,Z)
grid on
xlabel('Temperature (K)')
ylabel('Solvent (g)')
zlabel('Alkane Selectivity % Group 2A.1')
```

# Appendix A4

**Graphical Representation of Group 1A Statistical and Modelled Yield Results**
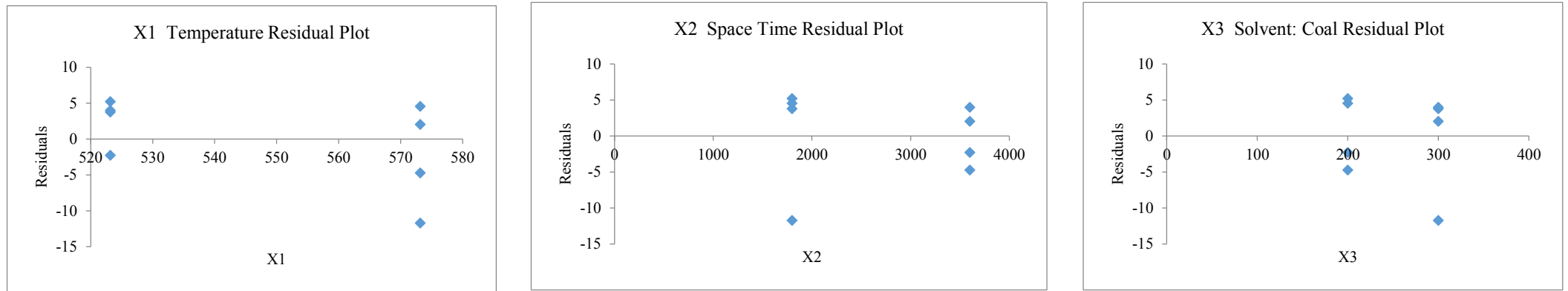


Figure A4.1.1 Residual plots for the regression of group 1A responses
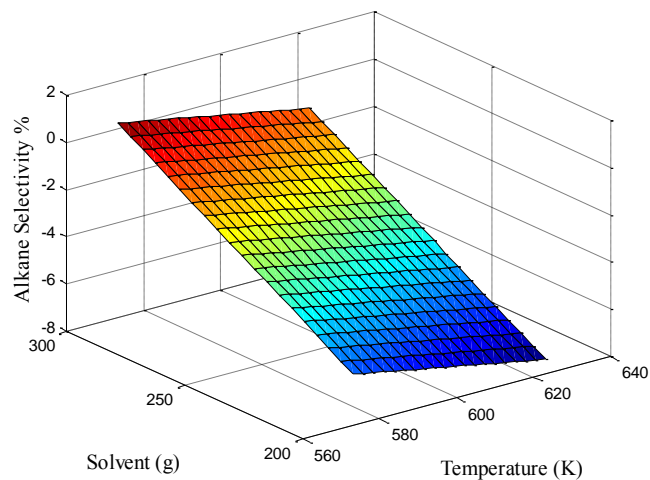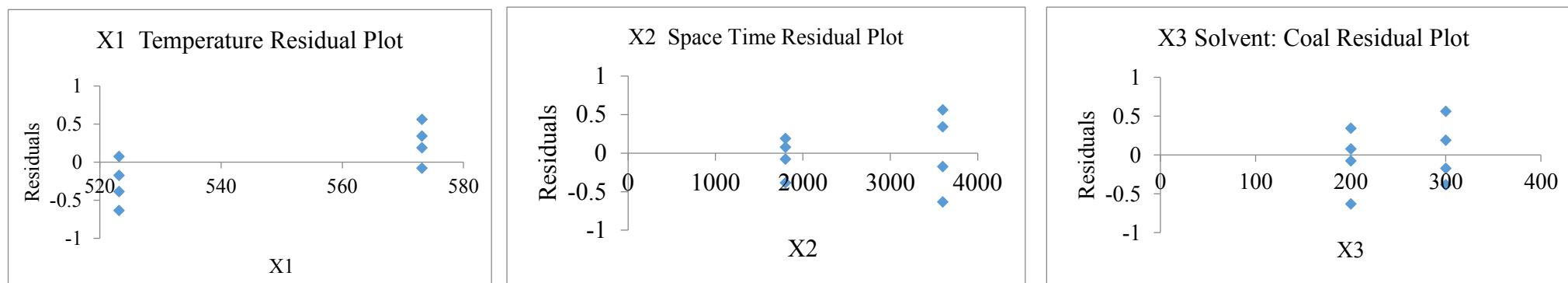(Left: Temperature (K); Middle: Space Time (seconds); Right: Solvent: Coal ratio (mass basis (g)))
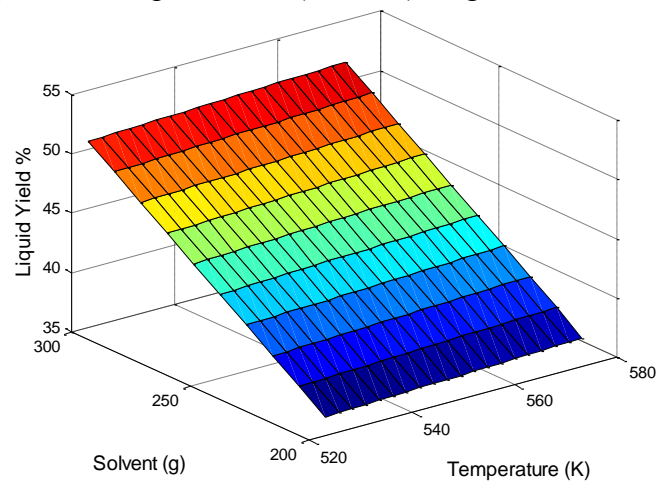


Figure A4.1.2: Approximated surface plot for Group 1A model

**Graphical Representation of Group 1B Statistical and Modelled Yield Results**
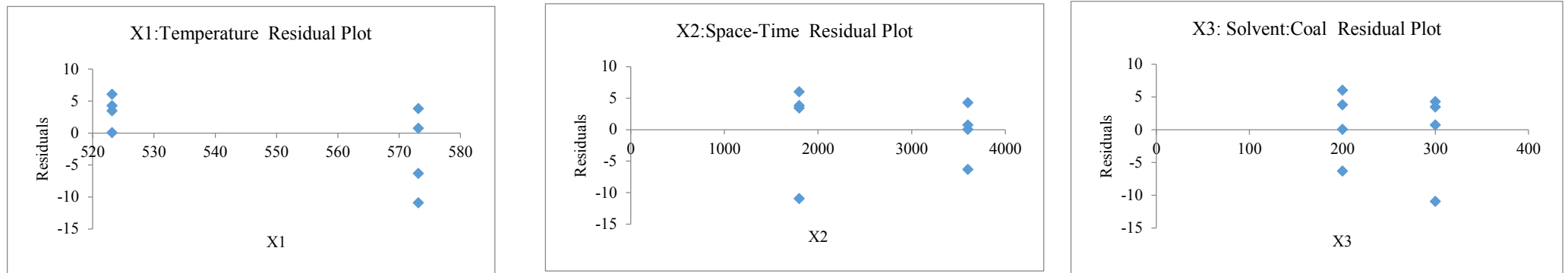


Figure A4.2.1 Residual plots for the regression of group 1B responses
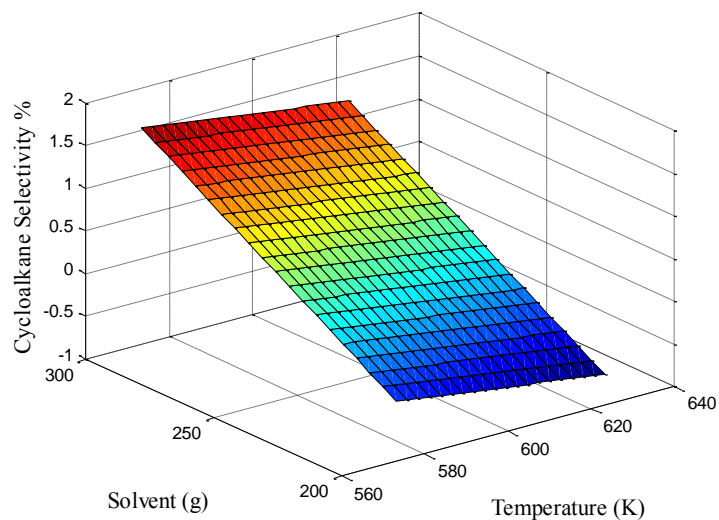(Left: Temperature (K); Middle: Space Time (seconds); Right: Solvent: Coal ratio (mass basis (g)))
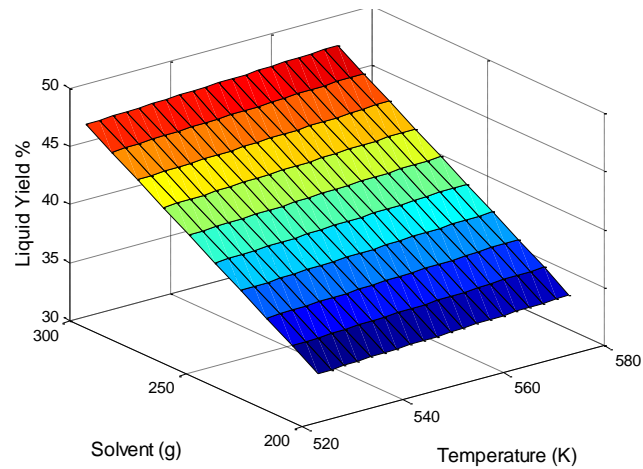


Figure A4.2.2: Approximated surface plot for Group 1B model

**Graphical Representation of Group 2A.1 Statistical and Modelled Results**
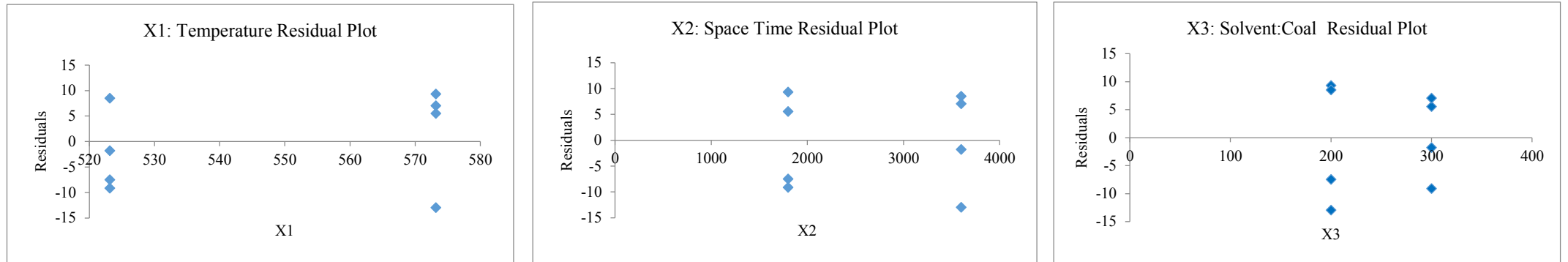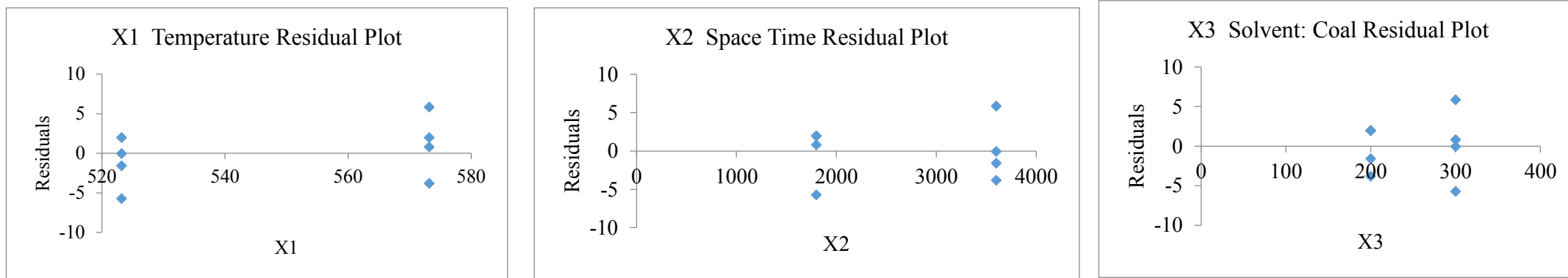


Figure A4.3.1 Residual plots for the regression of group 2A.1 responses
(Left: Temperature (K); Middle: Space Time (seconds); Right: Solvent: Coal ratio (mass basis (g)))
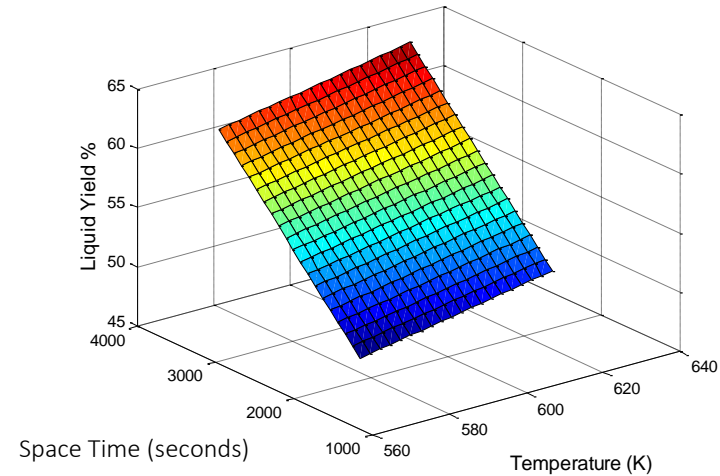


Figure A4.3.2: Approximated surface plot for Group 1B model

**Graphical Representation of Group 2A.2 Statistical and Modelled Yield Results**
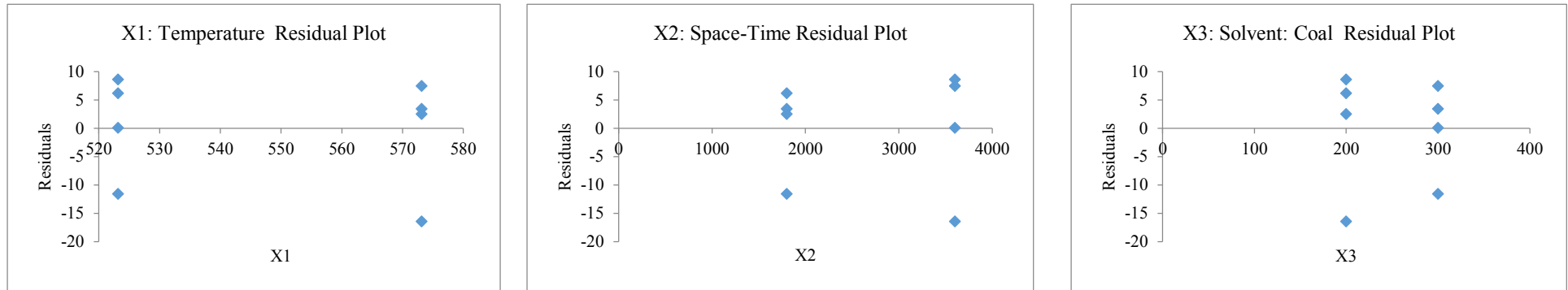


Figure A4.4.1 Residual plots for the regression of group 2A.2 responses
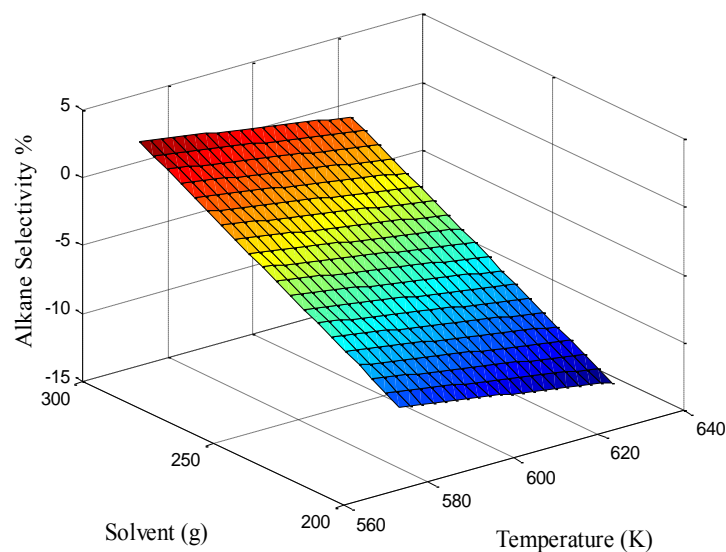(Left: Temperature (K); Middle: Space Time (seconds); Right: Solvent: Coal ratio (mass basis (g))
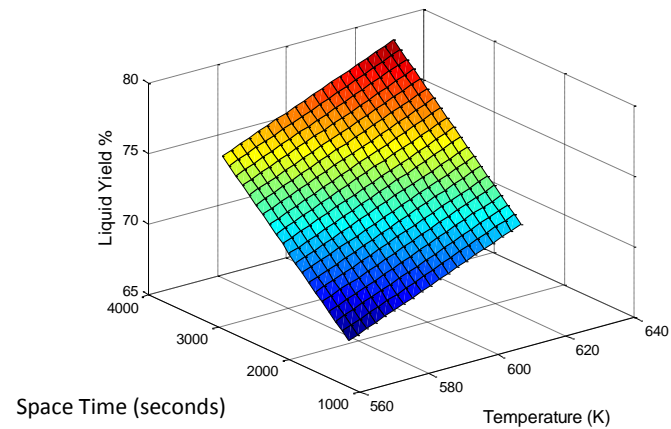


Figure A4.4.2: Approximated surface plot for Group 2A.2 model

**Graphical Representation of Group 2B.1 Statistical and Modelled Yield Results**
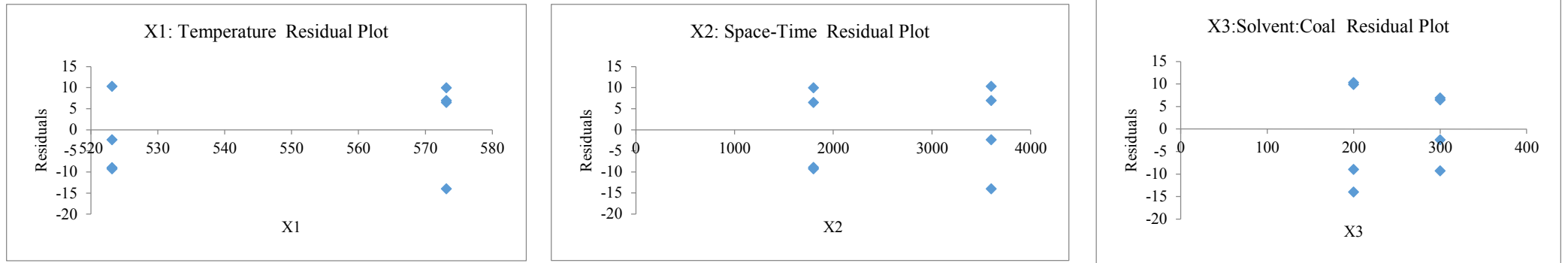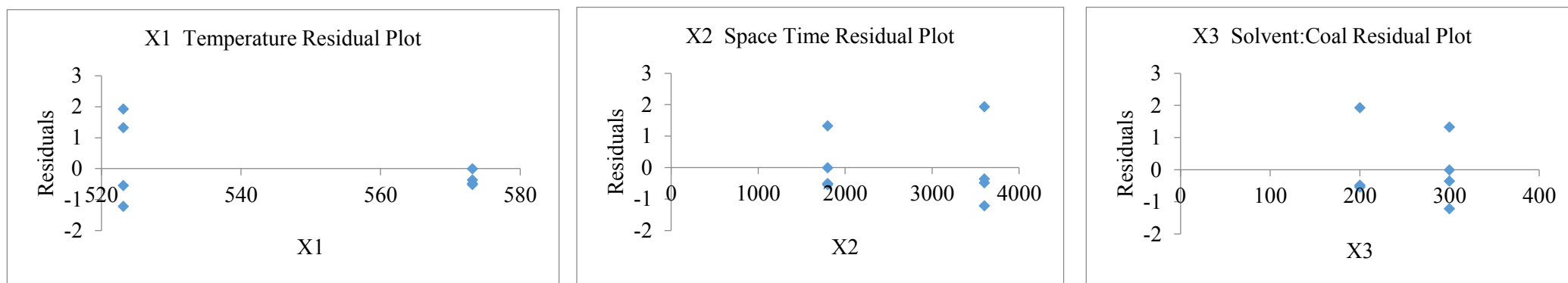


Figure A4.5.1 Residual plots for the regression of group 2B.1 responses
(Left: Temperature (K); Middle: Space Time (seconds); Right: Solvent: Coal ratio (mass basis (g)))
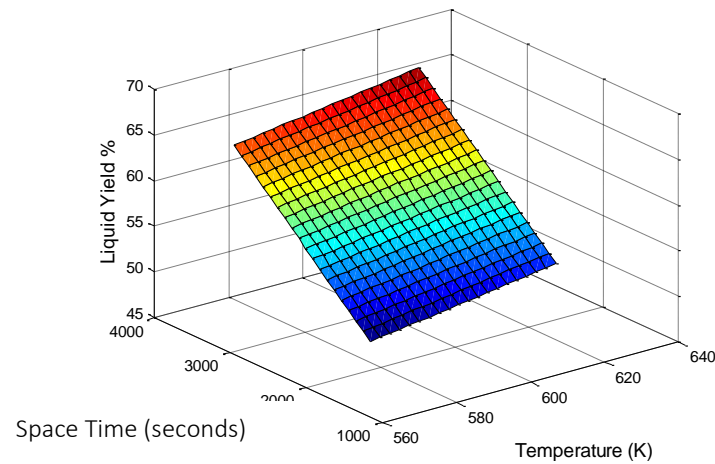


Figure A4.5.2: Approximated surface plot for Group 2B.1 model

**Graphical Representation of Group 2B.2 Statistical and Modelled Yield Results**
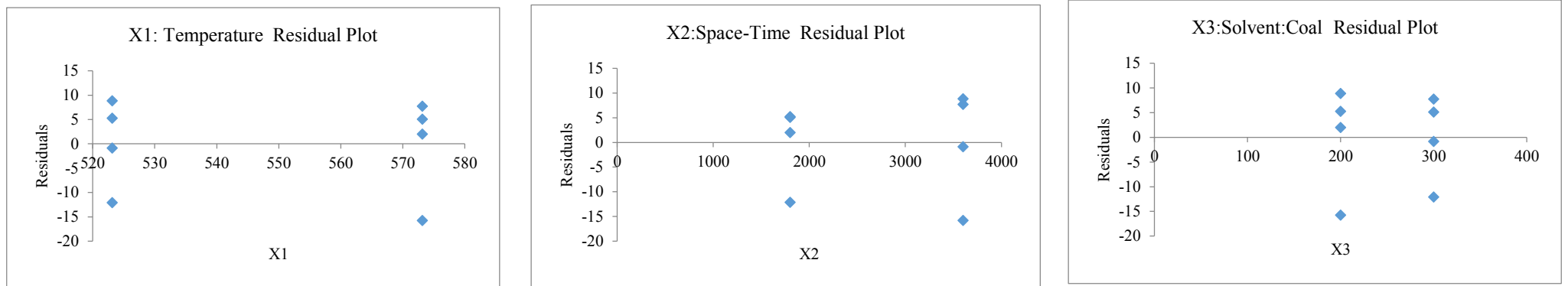


Figure A4.6.1 Residual plots for the regression of group 2B.2 responses
(Left: Temperature (K); Middle: Space Time (seconds); Right: Solvent: Coal ratio (mass basis (g)))
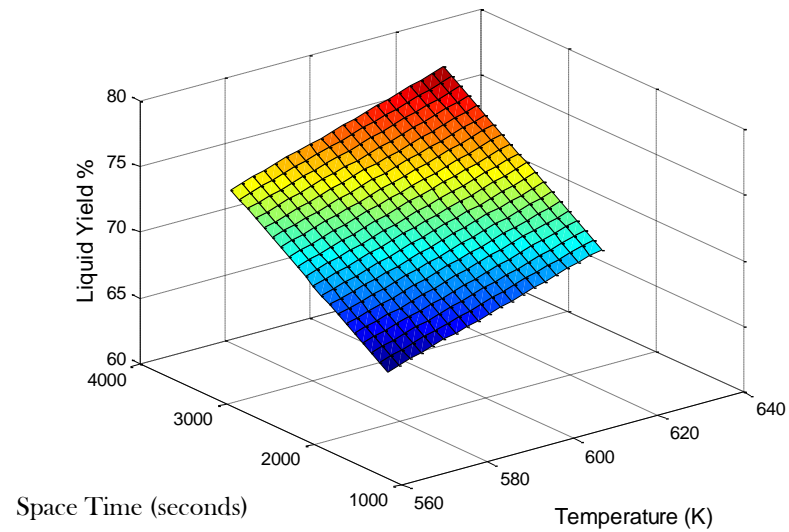


Figure A4.6.2: Approximated surface plot for Group 2B.1 model

**Graphical Representation of Group 2A.1 Statistical and Modelled Alkane Selectivity Results**
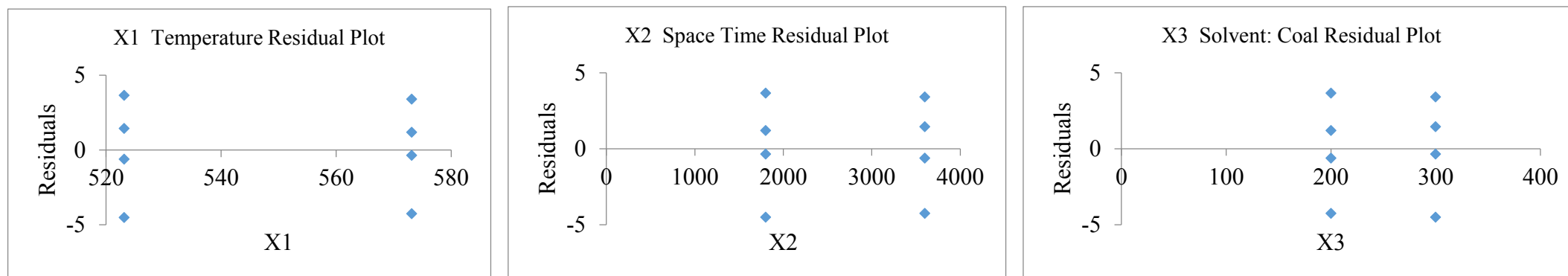


Figure A4.7.1 Residual plots for the regression of group 2A.2 alkane selectivity responses
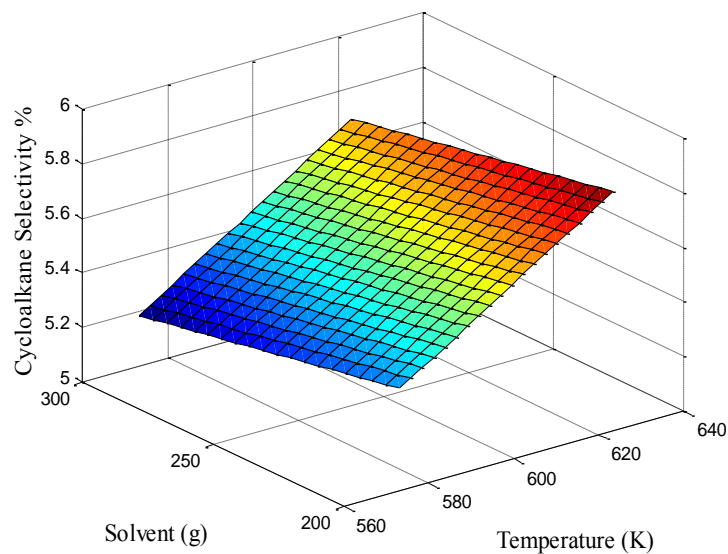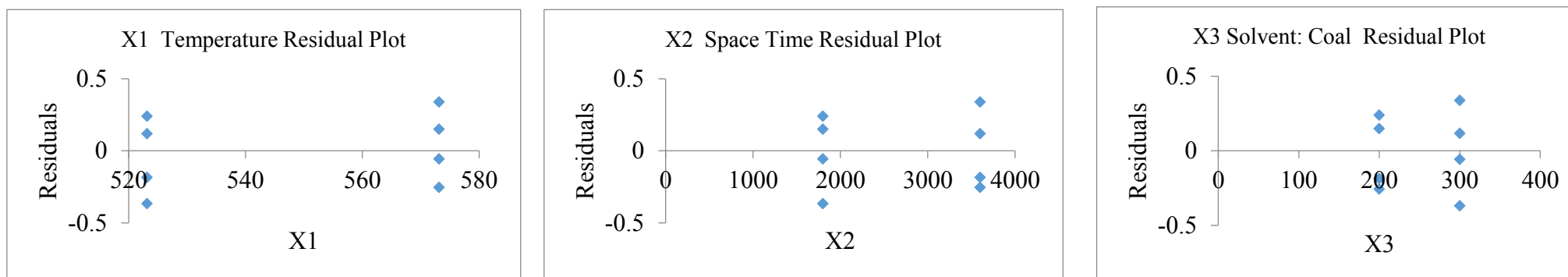(Left: Temperature (K); Middle: Space Time (seconds); Right: Solvent: Coal ratio (mass basis (g)))
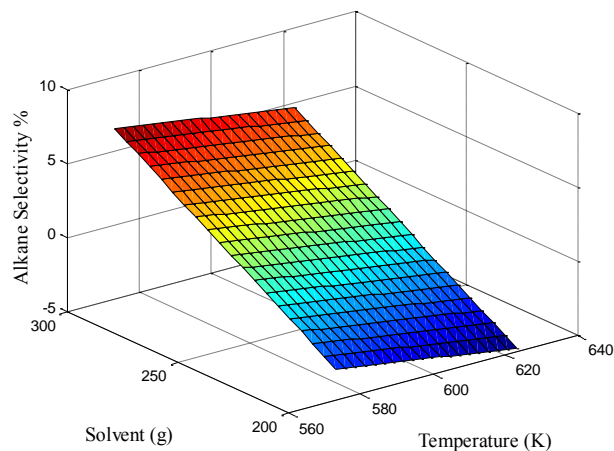


Figure A4.7.2: Approximated surface plot for Group 2A.1 alkane
selectivity model

**Graphical Representation of Group 2A.1 Statistical and Modelled Cycloalkane Selectivity Results**
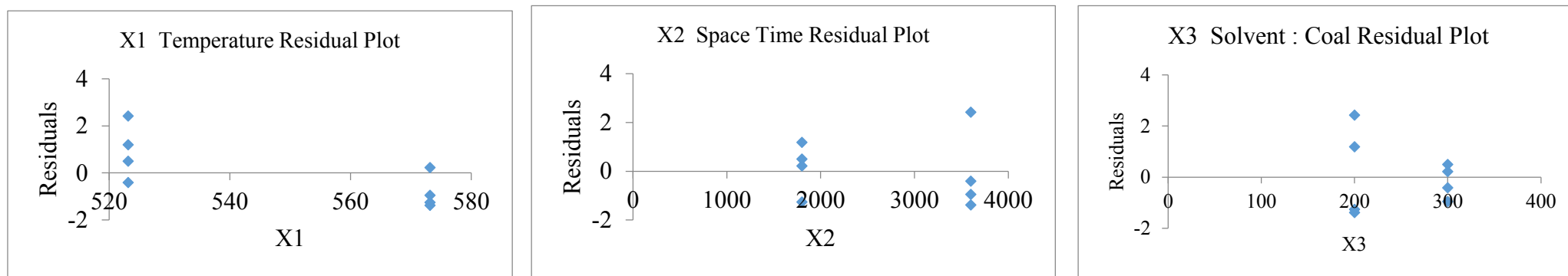


Figure A4.8.1 Residual plots for the regression of group 2A.2 cycloalkane selectivity responses
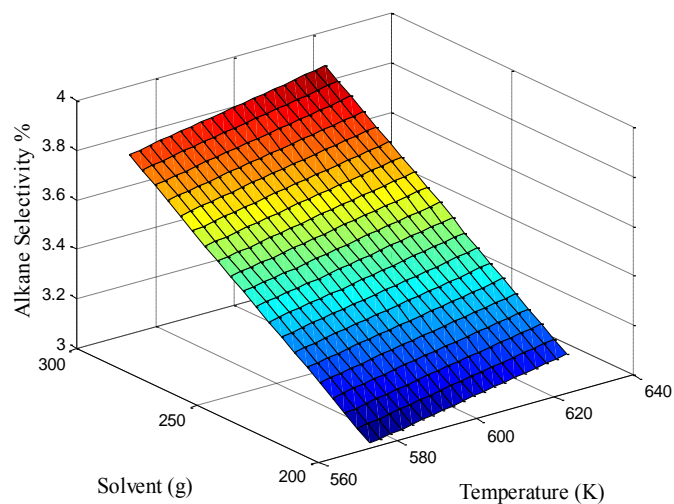(Left: Temperature (K); Middle: Space Time (seconds); Right: Solvent: Coal ratio (mass basis (g)))
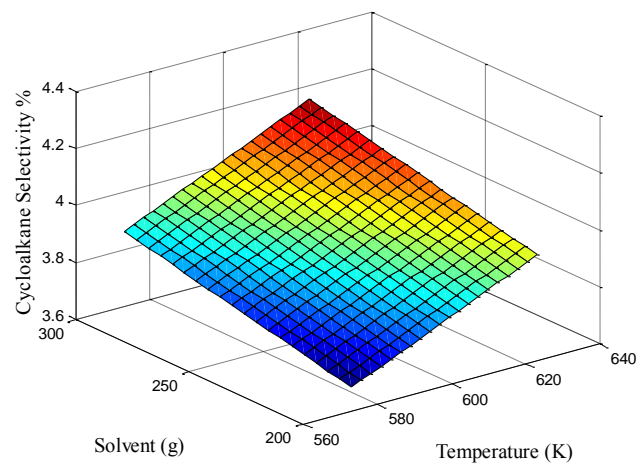


Figure A4.8.2: Approximated surface plot for Group 2A.2 cycloalkane selectivity model

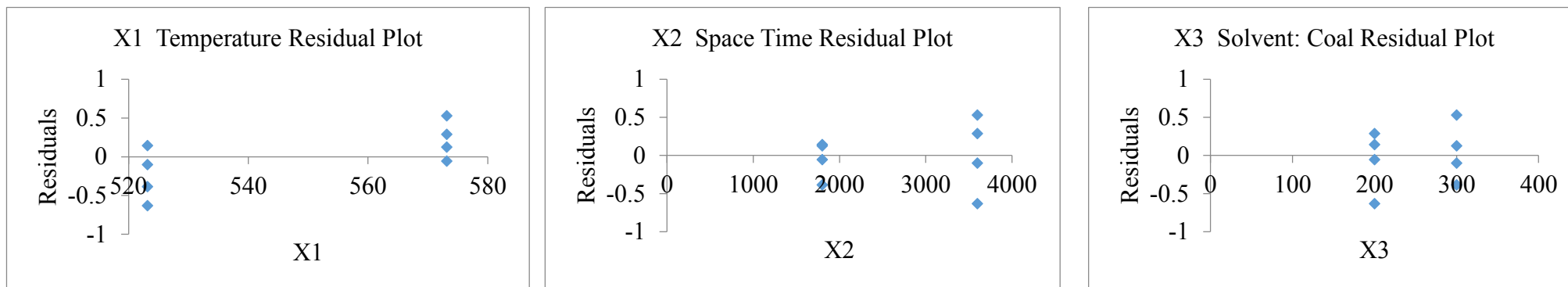**Graphical Representation of Group 2A.2 Statistical and Modelled Alkane Selectivity Results**
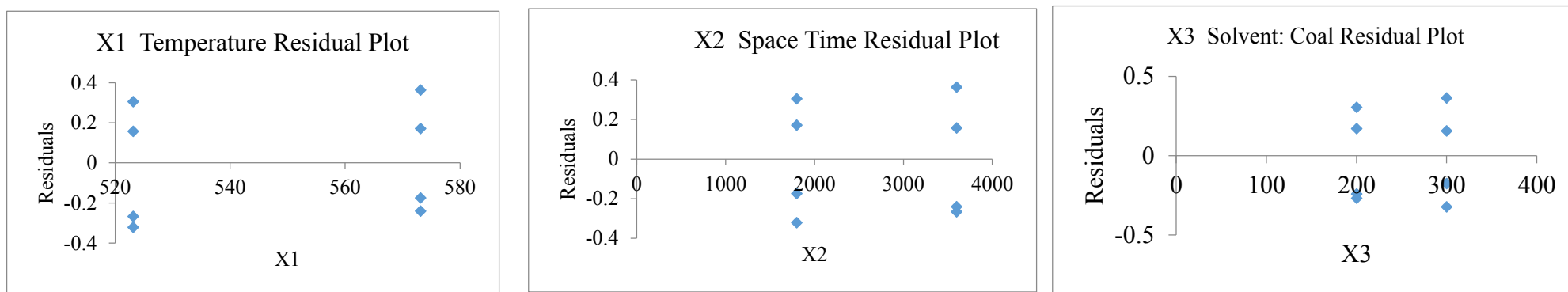


Figure A4.9.1 Residual plots for the regression of group 2A.2 alkane selectivity responses
(Left: Temperature (K); Middle: Space Time (seconds); Right: Solvent: Coal ratio (mass basis (g)))



Figure A4.9.2: Approximated surface plot for Group 2A.2 alkane selectivity model

**Graphical Representation of Group 2A.2 Statistical and Modelled Cycloalkane Selectivity Results**



Figure A4.10.1 Residual plots for the regression of group 2A.2 cycloalkane selectivity responses
(Left: Temperature (K); Middle: Space Time (seconds); Right: Solvent: Coal ratio (mass basis (g)))



Figure A4.10.2: Approximated surface plot for Group 2A.2 cycloalkane selectivity model

**Graphical Representation of Group 2B.1 Statistical and Modelled Alkane Selectivity Results**



Figure A4.11.1 Residual plots for the regression of group 2B.1 alkane selectivity responses
(Left: Temperature (K); Middle: Space Time (seconds); Right: Solvent: Coal ratio (mass basis (g)))



Figure A4.11.2: Approximated surface plot for Group 2A.2 alkane selectivity model

**Graphical Representation of Group 2B.1 Statistical and Modelled Cycloalkane Selectivity Results**



Figure A4.12.1 Residual plots for the regression of group 2B.1 cycloalkane selectivity responses
(Left: Temperature (K); Middle: Space Time (seconds); Right: Solvent: Coal ratio (mass basis (g)))



Figure A4.12.2: Approximated surface plot for Group 2B.1 cycloalkane selectivity model

**Graphical Representation of Group 2B.2 Statistical and Modelled Alkane Selectivity Results**



Figure A4.13.1 Residual plots for the regression of group 2B.2 cycloalkane alkane selectivity responses
(Left: Temperature (K); Middle: Space Time (seconds); Right: Solvent: Coal ratio (mass basis (g))



Figure A4.13.2: Approximated surface plot for Group 2B.2 alkane selectivity model

**Graphical Representation of Group 2B.2 Statistical and Modelled Cycloalkane Selectivity Results**



Figure A4.14.1 Residual plots for the regression of group 2B.2 cycloalkane alkane selectivity responses
(Left: Temperature (K); Middle: Space Time (seconds); Right: Solvent: Coal ratio (mass (g) basis))
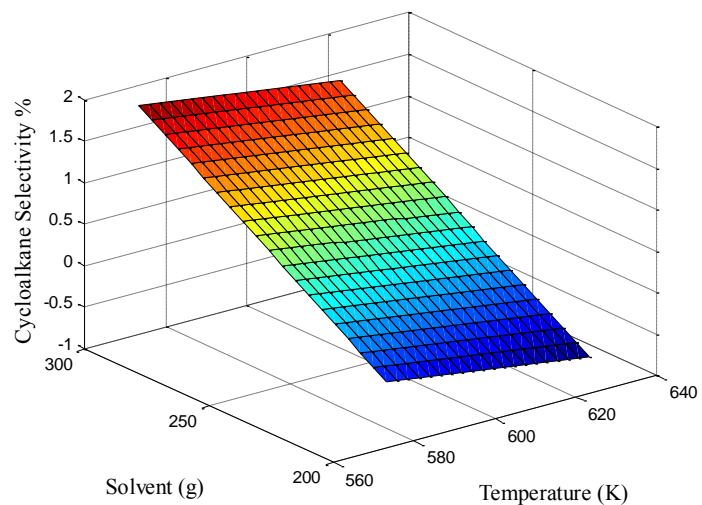


Figure A4.14.2: Approximated surface plot for Group 2B.2 alkane selectivity model

## Appendix B: GC-MS Analytical Work

Appendix B.1.1: GC-MS calibrations: straight and branched chain alkane and alkene compounds
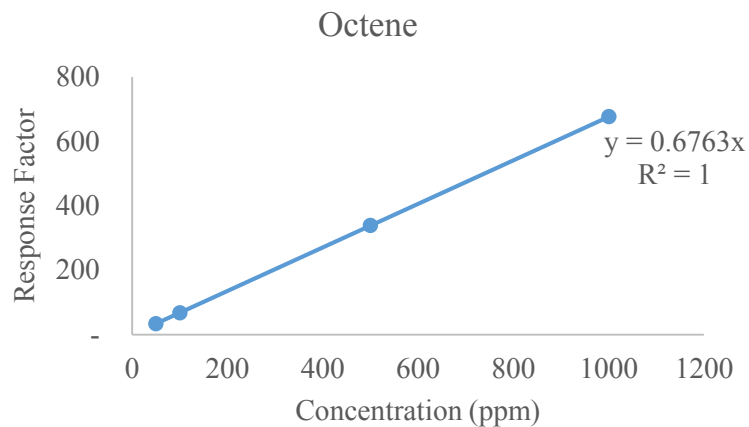


Figure B.1.1.1: Octene calibration plot

$y = 0.6763x$
$R^2 = 1$
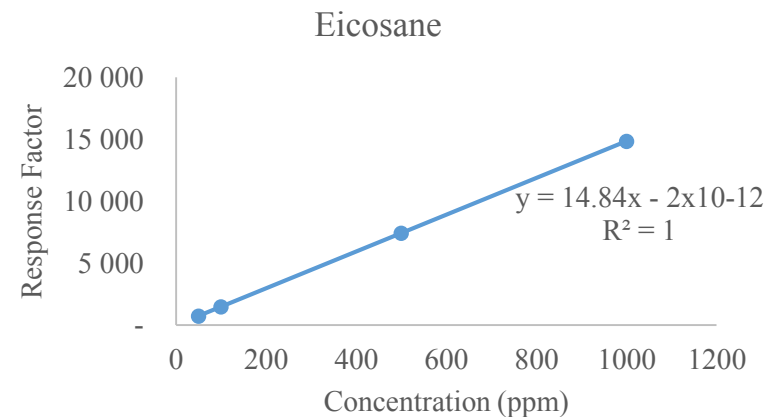


Figure B.1.1.2: Eicosane calibration plot

$y = 14.84x - 2x10\text{-}12$
$R^2 = 1$
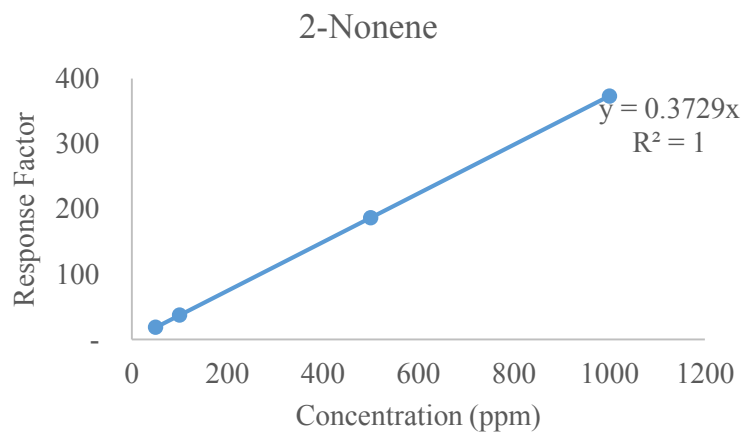


Figure B.1.1.3: 2-Nonene calibration plot

$y = 0.3729x$
$R^2 = 1$
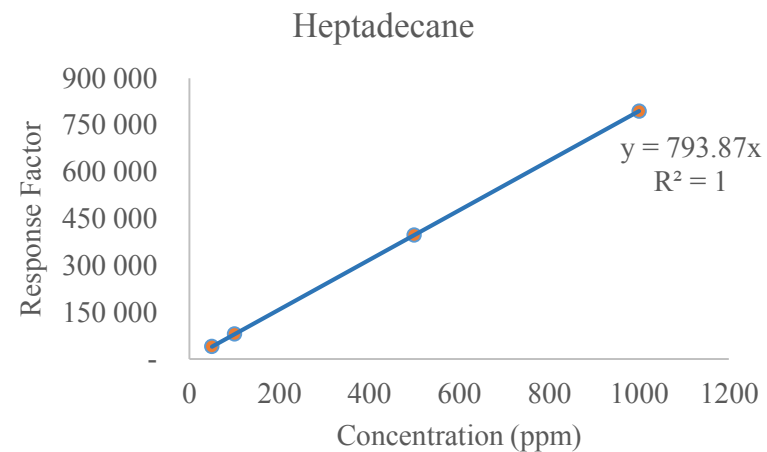


Figure B.1.1.4: Heptadecane calibration plot

$y = 793.87x$
$R^2 = 1$
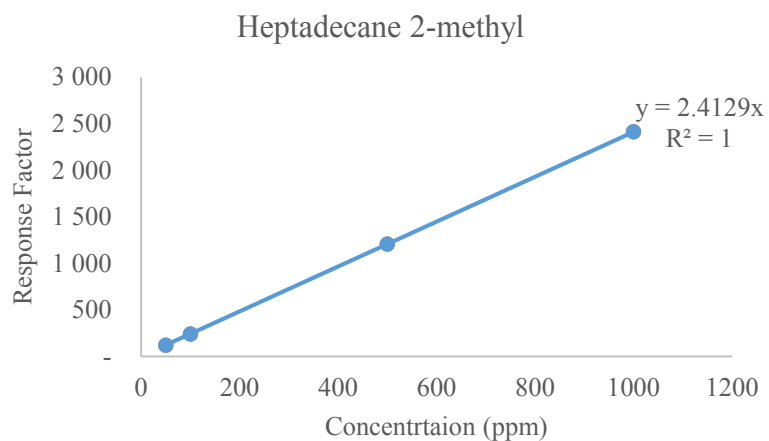
Figure B.1.1.5: Heptadecane 2-methyl calibration plot
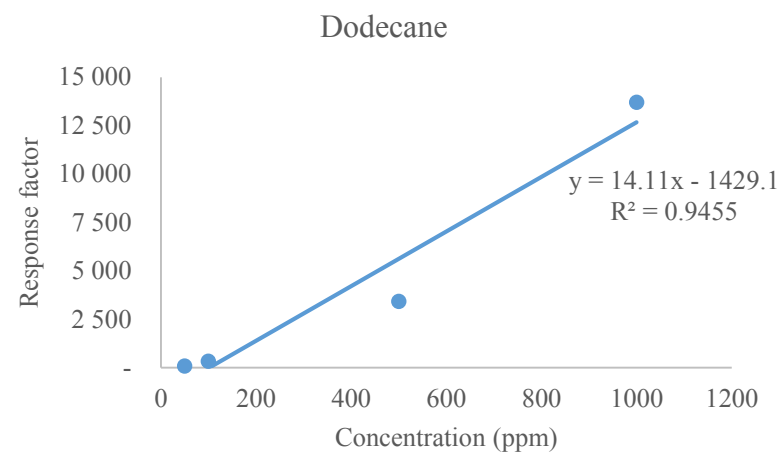


Figure B.1.1.6: Dodecane calibration plot
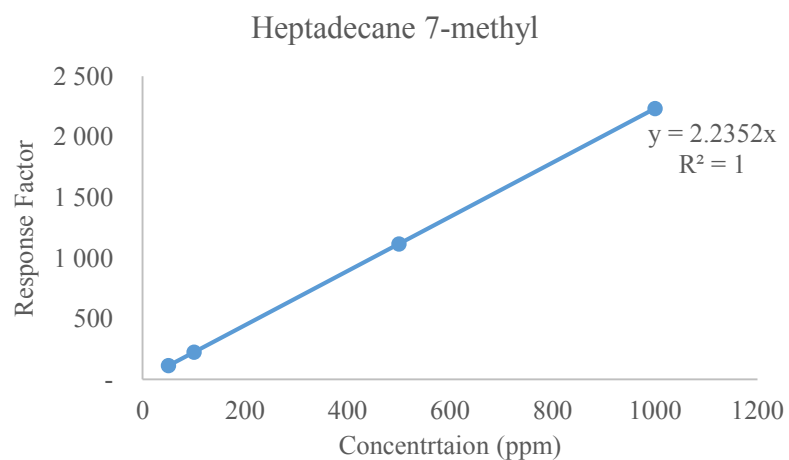


Figure B.1.1.7: Heptadecane 7-methyl calibration plot
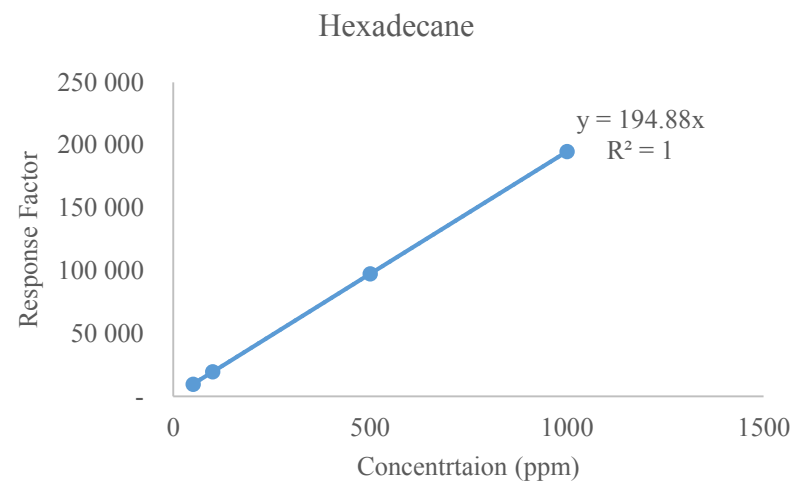


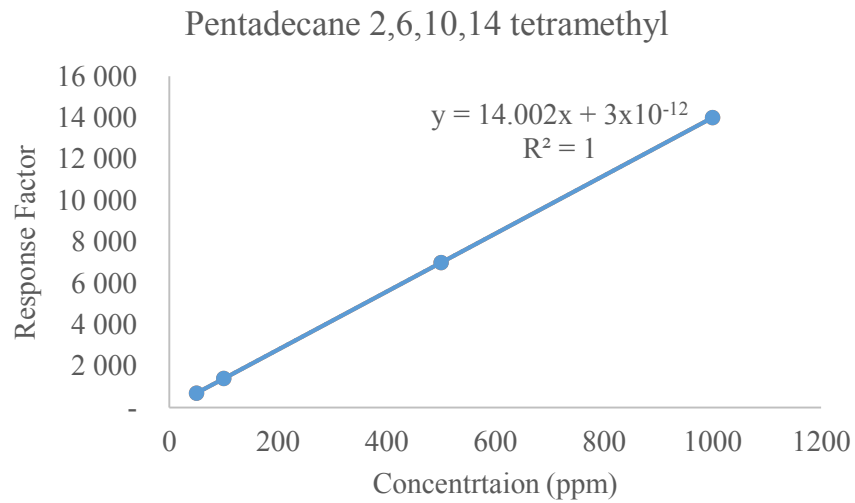Figure B.1.1.8: Hexadecane calibration plot

97

Figure B.1.1.9: Pentadecane, 2, 6, 10,14 tetramethyl calibration plot
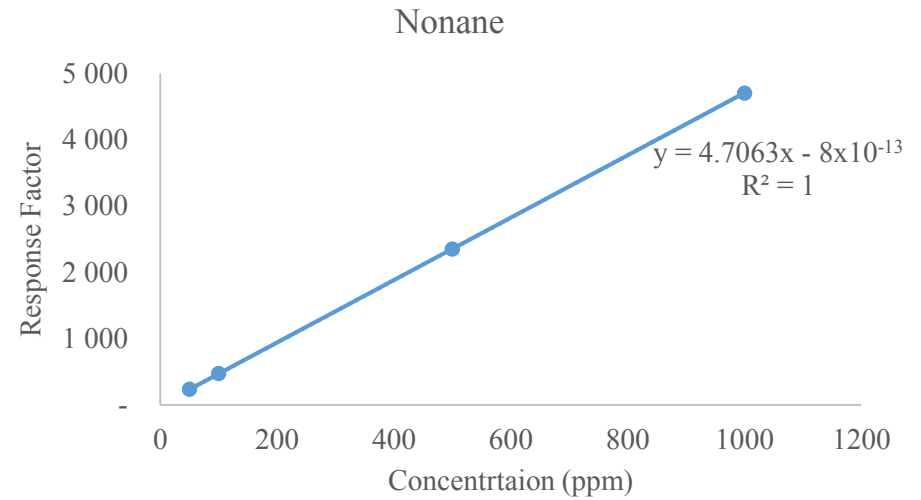


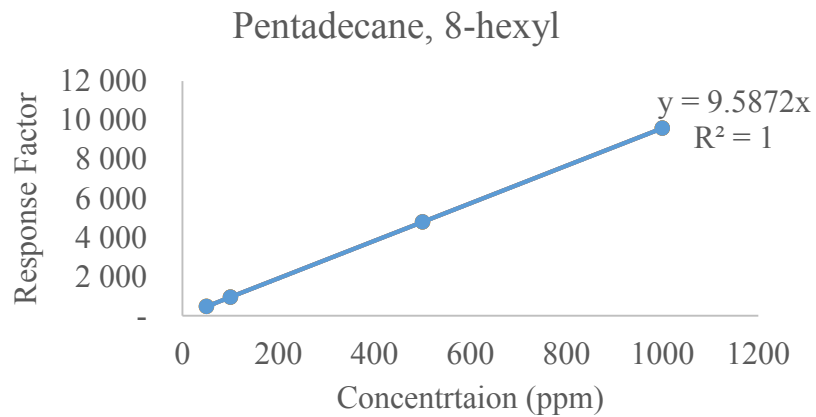Figure B.1.1.10: Nonane calibration plot



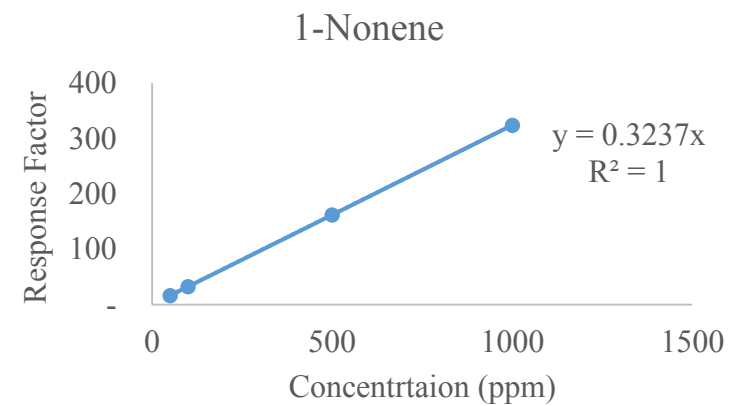Figure B.1.1.11: Pentadecane, 8-hexyl calibration plot



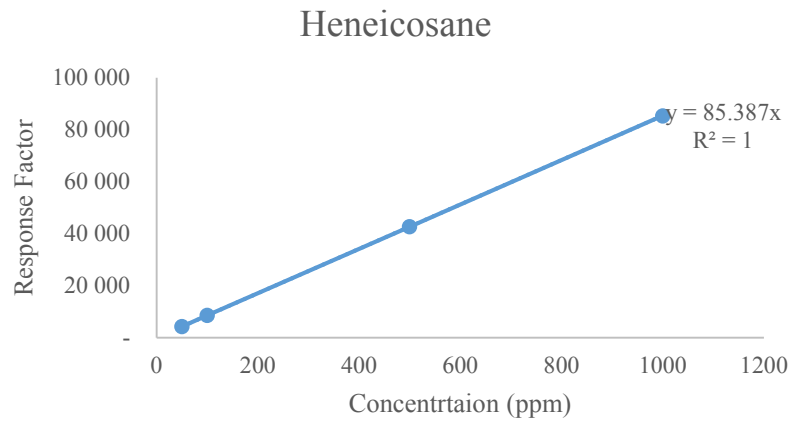Figure B.1.1.12: 1-Nonene calibration plot

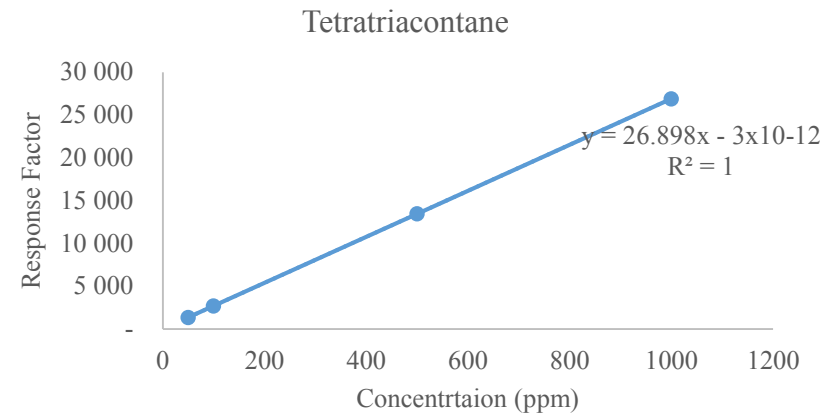Figure B.1.1.13: Heneicosane calibration plot


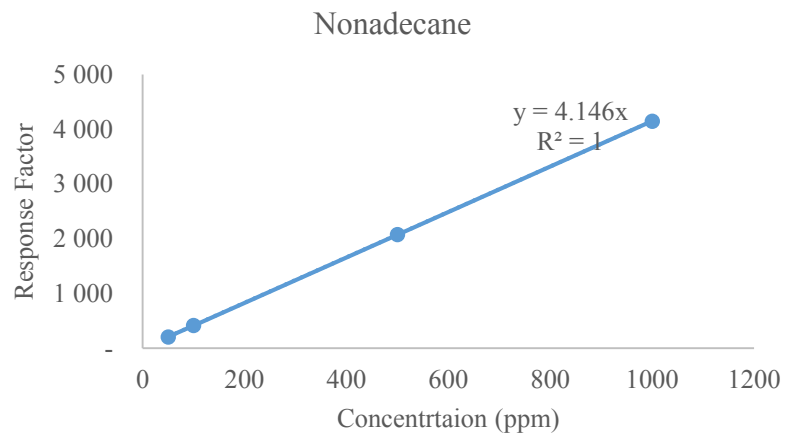
Figure B.1.1.14: Tetratriacontane calibration plot
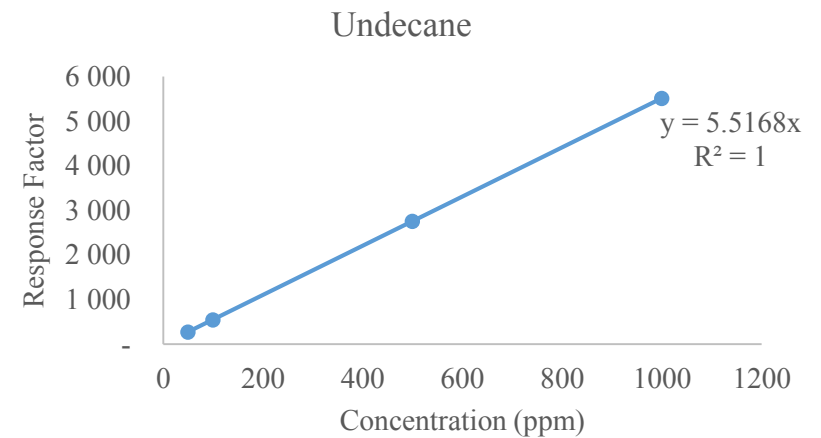


Figure B.1.1.15: Nonadecane calibration plot



Figure B.1.1.16: Undecane calibration plot
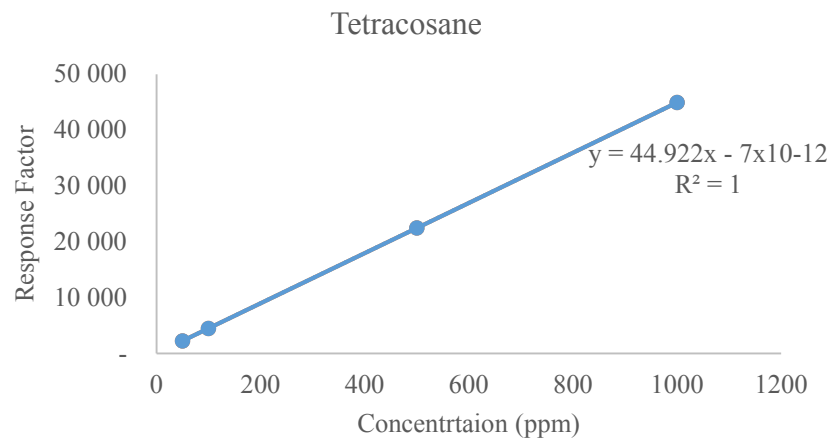
Figure B.1.1.17: Tetracosane calibration plot

**Appendix B.2.1: GC-MS Calibrations: Aromatics and Cycloalkanes**

### Toluene



$y = 0.0002x + 0.0039$
$R^2 = 0.9955$
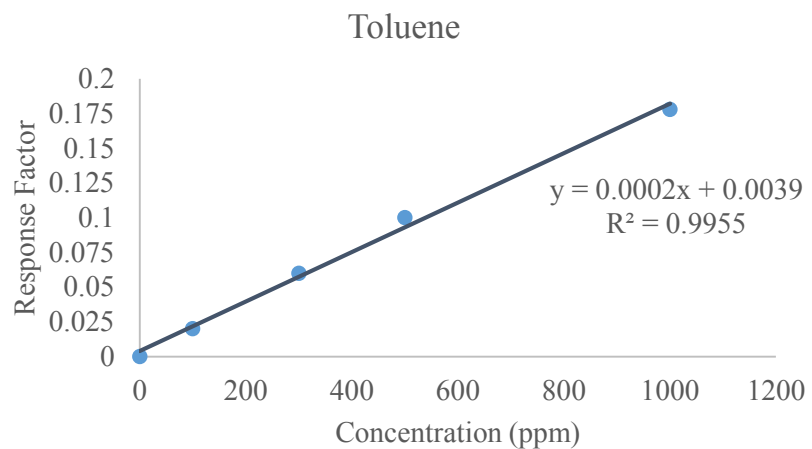
Figure B.2.1.1 Toluene Calibration Plot

### Benzene



$y = 0.0013x + 0.1589$
$R^2 = 0.938$
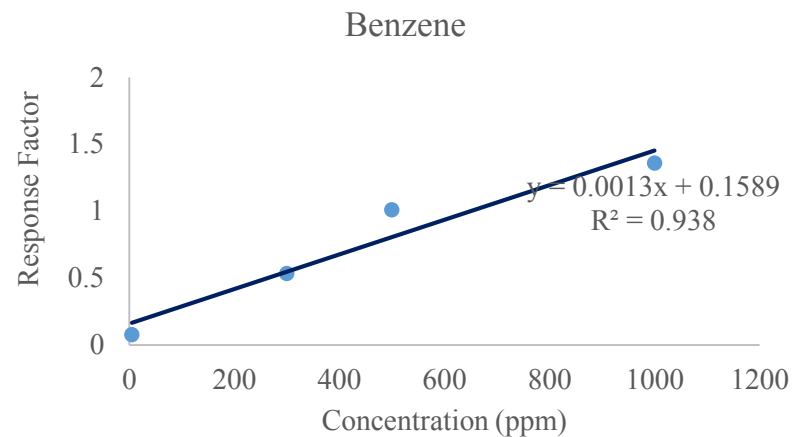
Figure B.2.1.2 Benzene Calibration Plot

### Cyclohexane



$y = 0.0003x - 0.0002$
$R^2 = 1$
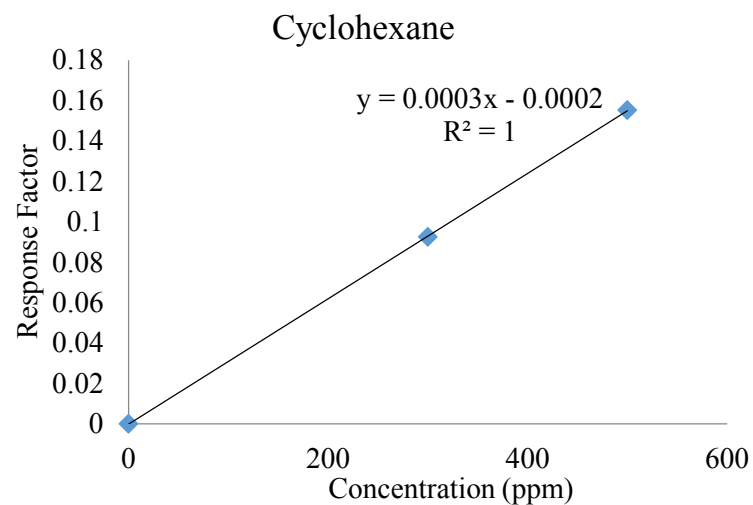
Figure B.2.1.3 Cyclohexane Calibration Plot

### o, p, m -xylene



$y = 0.0004x - 5x10{-17}$
$R^2 = 1$
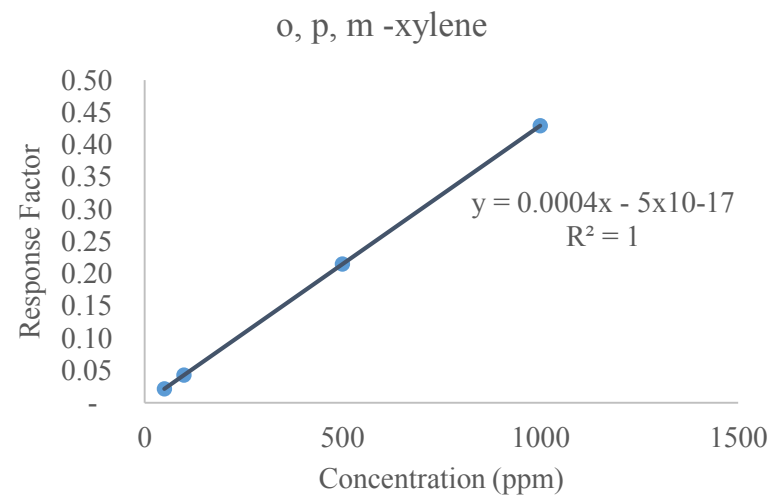
Figure B.2.1.4 Xylene

**Appendix B.3.1 GC-MS Calibrations: Polycyclic Aromatic Hydrocarbon (PAH) Compounds**



Figure B.3.1.1 Perylene Calibration Plot



Figure B.3.1.2 Anthracene Calibration Plot



Figure B.3.1.3: Naphthalene Calibration Plot



Figure B3.1.4: Binaphthalene Calibration Plot

Figure B3.1.5: Chyrsene Calibration Plot
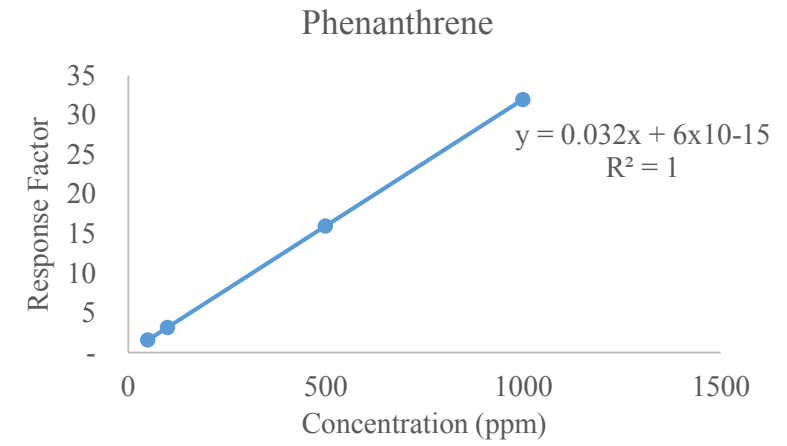


Figure B3.1.6: Phenanthrene Calibration Plot
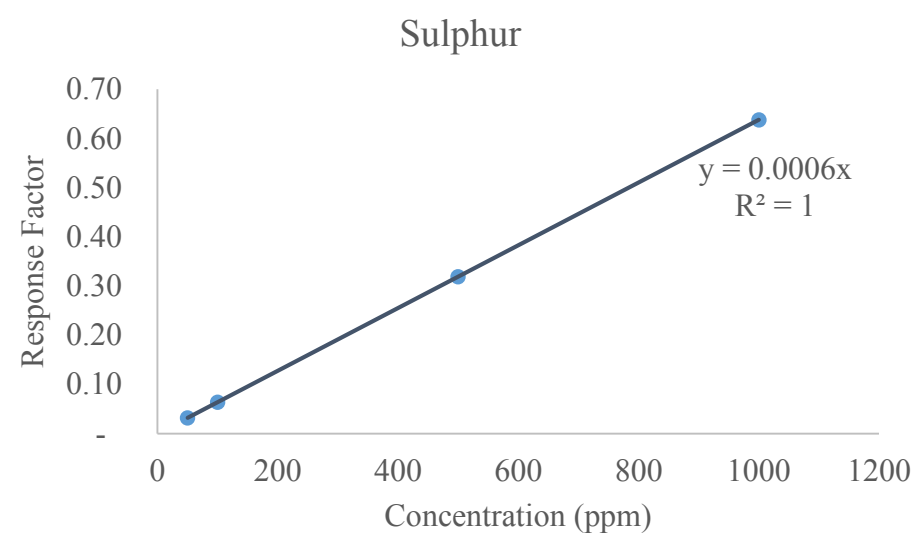


Figure B4.1.1: Sulphur Calibration Plot

Appendix C1: Chemical Hazard Table

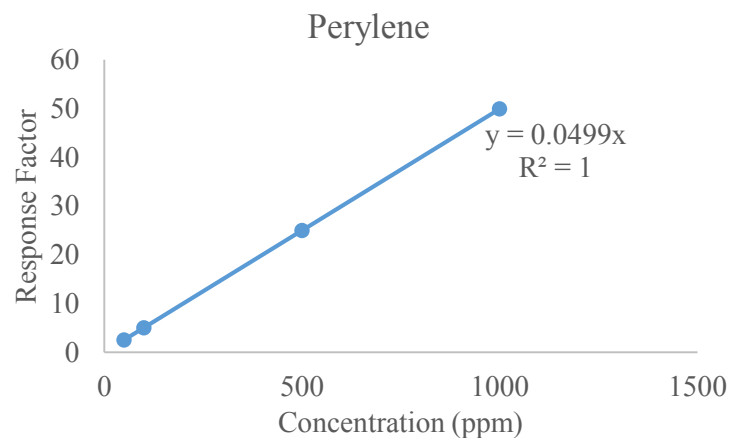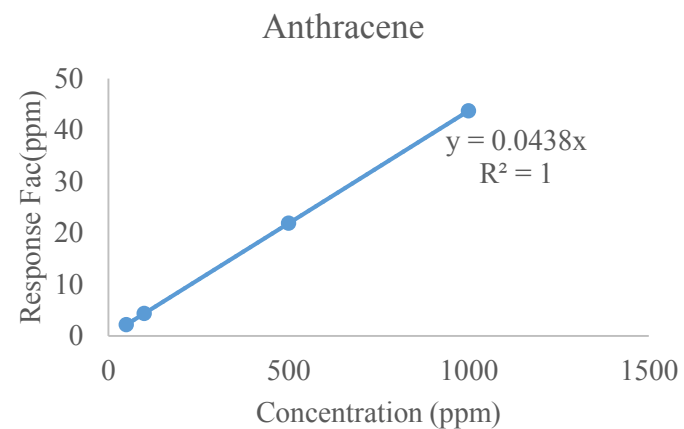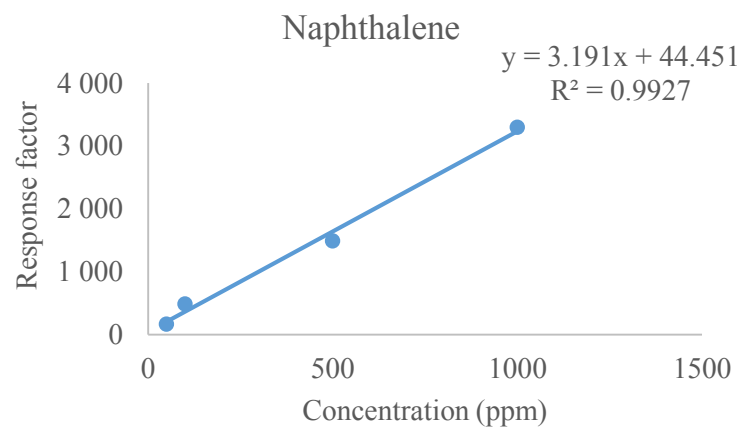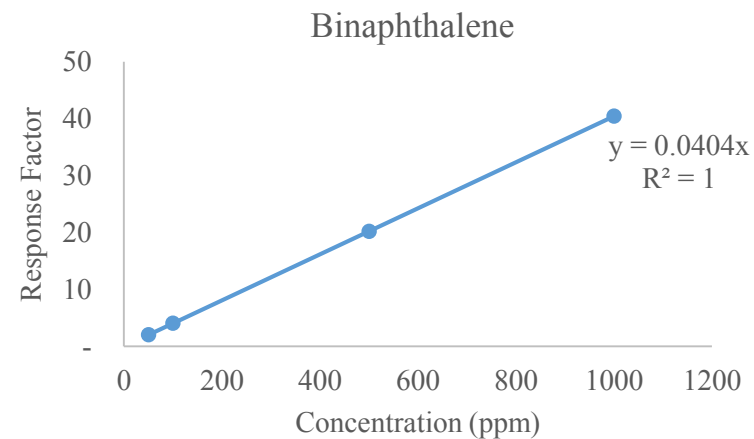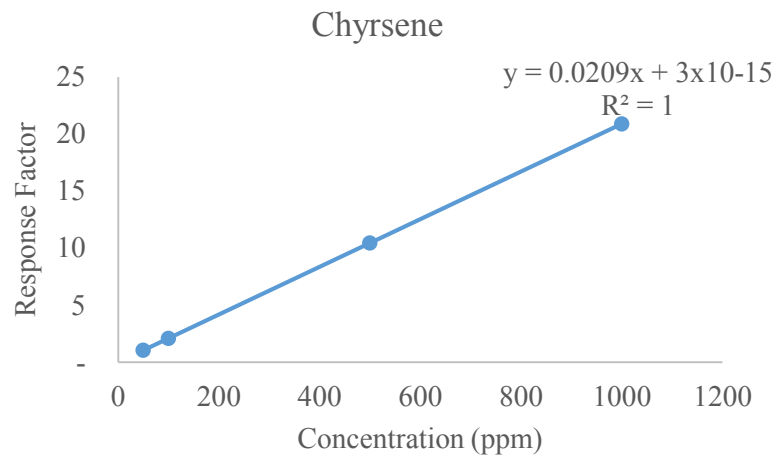| Chemical | Formula | Manufacturer | Purity | Main Hazards |
|---|---|---|---|---|
| Hexadecane | $C_{16}H_{34}$ | Sigma-Aldrich | ≥ 99% | Skin, eye and lung irritant<br><br>Hazardous decomposition products (carbon oxides) formed under fire conditions |
| Tetralin (1,2,3,4 – tetrahydronaphthalene) | $C_{10}H_{12}$ | Sigma-Aldrich | ≥ 97% | Eye - causes irritation or burns. Eye contact can result in corneal damage<br>Skin - Causes skin irritation or burns. Prolonged or widespread skin contact may result in the absorption of potentially harmful amounts of material<br>Inhalation: Material is irritating to mucous membranes and upper respiratory tract. May cause headache, nausea, vomiting, drowsiness, dizziness and central nervous depression. Prolonged exposure may cause a narcotic effect<br>Ingestion – Harmful if swallowed<br><br>As a combustible liquid, vapour may travel a considerable distance to a source of ignition and flash-back; forms an explosive mixture with air; container explosion may occur under fire conditions or when heated; contact with oxidisers may cause fire and or explosion; readily forms explosive peroxides on contact with air; may be sensitive to static discharge; emits toxic fumes (including Tetralin peroxides) under fire conditions |
| Sulfolane | $C_4H_8SO2$ | Sigma-Aldrich | 99% | May be harmful if swallowed<br>May damage fertility or unborn child<br>Hazardous decomposition products including carbon and sulphur oxides |
| Propan-1-ol | $CH_3CH_2CH_2OH$ | Merck | 99% | Damage to eyes, vapours may cause drowsiness and dizziness, may cause skin and respiratory tract irritation, aspiration hazard if swallowed – can enter lungs and cause damage<br><br>Flammable liquid and vapour |

Appendix C1: Chemical Hazard Table continued

| Chemical | Formula | Manufacturer | Purity | Main Hazards |
|---|---|---|---|---|
| 1-pentene | $C_5H_{10}$ | Fluka | 99% | Respiratory tract , skin and eye irritation, central nervous system, depression, difficulty breathing<br><br>Flammable liquid and vapour. Vapour may cause flash fire |
| Ethylbenzene | $C_8H_{10}$ | Fluka | ≥98% | Skin – irritant, sensitizer in case of contact<br>Possible carcinogenic effect<br>Toxic to central nervous system<br>Repeated or prolonged exposure to the substance can produce target organ damage<br>Flammable |
| Hydrogen | $H_2$ | Afrox | ≥ 99.99% | Flammable gas – burns in air very easily with ≤ 2ppm oxygen impurities.<br>Creation of static environment and potential hazard of explosion in a confined space |
| Acetone | $C_3H_6O$ | Sigma-Aldrich | ≥ 99.50% | Skin – irritant and potential permeator<br>Eye – irritant<br>Targeted organ damage suspected<br>Hazardous to central nervous system |
| 1,4-Dichlorobenzene-D4 | $C_6H_4Cl_2$ | Sigma-Aldrich | 99.9% | Skin – irritant<br>Eye – irritant (corneal) damage may occur<br>Harmful by inhalation, vapours can cause drowsiness and dizziness<br>Ingestion – Effects on CNS, targeted organ damage can occur |

Appendix C1: Chemical Hazard Table continued

| Chemical | Formula | Manufacturer | Purity | Main Hazards |
|---|---|---|---|---|
| HD Max 300 (Nickel Molybdenum Catalyst) | NiMo | Clariant | 10%≤ Molybdenum Trioxide Concentration < 20% 1≤Nickel Monoxide Concentration ≤ 10% <br><br> Form: Green extrusions | Eye – serious eye irritation <br> Skin – may cause an allergic skin reaction <br> Carcinogenicity – may cause cancer if inhaled <br> May cause damage to organs through prolonged or repeated exposure |
| HD Max 200 (Cobalt Molybdenum Catalyst) | CoMo | Clariant | 20%≤ Molybdenum Trioxide Concentration < 25% 10%≤ Cobalt Monoxide Concentration ≤ 2.5% <br><br> Form: Blue extrusions | Eye – serious eye irritation <br> Skin – may cause an allergic skin reaction <br> Carcinogenicity – may cause cancer if inhaled <br> May cause damage to organs through prolonged or repeated exposure and respiratory irritant <br> Very toxic to aquatic life with a long lasting effect |

**Appendix C2: Safety**

Due to the use of high temperature, pressure and hazardous chemicals, the following Personal Protective Equipment (PPE) was worn:

- Temperature and static resistant gloves were worn when working with the high temperature reacting systems; and in order to minimise the static shock created by the hydrogen charged system
- Latex gloves were worn when handling chemicals in the analytical laboratory
- Gas masks were worn when depressurizing the reactors as pungent odours resulted from the potential creation of aromatic and sulphurous compounds
- Dust masks were worn when handling the pulverised coal samples
- Safety boots and goggles were worn at all times
- Working spaces were demarcated with appropriate hazard signage in order to alert other laboratory users to the operational hazards of the process

Operationally, as described in Chapter 3, the following measures were taken to monitor and control any potential hazards of the process:

- Reactors were equipped with temperature controls and pressure gauges to manually monitor excessive values
- The first stage reactor was equipped with a rupture disc, designed to automatically burst open should the pressure exceed 138 barg (2000 psig)
- The second stage reactor was equipped with a pressure relief valve should the temperature exceed 180 barg

Appendix D1: Group 1 Raw Data

Table D1: Group 1 Raw Data

| Run | Manipulated Variables | | | | | | Raw data | | | | |
|---|---|---|---|---|---|---|---|---|---|---|---|
| | $X_1$ | Level | $X_2$ | Level | $X_3$ | Level | | | | | |
| Group 1A | Temperature (K) | Level | Space Time (s) | Level | Solvent (g) | Level | Total Feed Mass (g) | Liquid Yield % | Liquid mass (g) | Solid mass (g) | Gas Yield % |
| 1 | 573.15 | -1 | 1800 | -1 | 200 | -1 | 300 | 300 | 120.381 | 51.01 | 42.87 |
| 2 | 623.15 | +1 | 1800 | -1 | 200 | -1 | 300 | 300 | 120.759 | 35.23 | 48.00 |
| 3 | 573.15 | -1 | 3600 | +1 | 200 | -1 | 300 | 300 | 92.682 | 25.52 | 60.60 |
| 4 | 623.15 | +1 | 3600 | +1 | 200 | -1 | 300 | 300 | 87.753 | 44.46 | 55.93 |
| 5 | 573.15 | -1 | 1800 | -1 | 300 | +1 | 400 | 400 | 211.168 | 56.59 | 33.06 |
| 6 | 623.15 | +1 | 1800 | -1 | 300 | +1 | 400 | 400 | 152.42 | 38.1 | 52.37 |
| 7 | 573.15 | -1 | 3600 | +1 | 300 | +1 | 400 | 400 | 205.032 | 35.37 | 39.90 |
| 8 | 623.15 | +1 | 3600 | +1 | 300 | +1 | 400 | 400 | 200.476 | 24.4 | 43.78 |
| Group 1B | | | | | | | | | | | |
| 1 | 573.15 | -1 | 1800 | -1 | 200 | -1 | 300 | 300 | 126.789 | 34.21 | 46.33 |
| 2 | 623.15 | +1 | 1800 | -1 | 200 | -1 | 300 | 300 | 122.871 | 36.65 | 46.83 |
| 3 | 573.15 | -1 | 3600 | +1 | 200 | -1 | 300 | 300 | 114.711 | 21.72 | 54.52 |
| 4 | 623.15 | +1 | 3600 | +1 | 200 | -1 | 300 | 300 | 98.391 | 37.73 | 54.63 |
| 5 | 573.15 | -1 | 1800 | -1 | 300 | +1 | 400 | 400 | 207.948 | 51.71 | 35.09 |
| 6 | 623.15 | +1 | 1800 | -1 | 300 | +1 | 400 | 400 | 154.096 | 35.16 | 52.69 |
| 7 | 573.15 | -1 | 3600 | +1 | 300 | +1 | 400 | 400 | 219.072 | 37.62 | 35.83 |
| 8 | 623.15 | +1 | 3600 | +1 | 300 | +1 | 400 | 400 | 208.552 | 25.62 | 41.46 |

Appendix D2: Group 2A Raw Data

Table D2: Group 2A Raw Data

| Run | Manipulated Variables | | | | | | Raw Data[1] | | |
| | X$_1$ | | X$_2$ | | X$_3$ | | | | |
| Group 2A.1 | Temperature (K) | Level | Space Time (s) | Level | Solvent (g) | Level | Liquid Yield % | Liquid mass (g) | Gas Yield % |
| 1 | 573.15 | -1 | 1800 | -1 | 200 | -1 | 38.947 | 5.53 | 61.053 |
| 2 | 623.15 | +1 | 1800 | -1 | 200 | -1 | 60.855 | 8.64 | 39.145 |
| 3 | 573.15 | -1 | 3600 | +1 | 200 | -1 | 72.841 | 10.34 | 27.159 |
| 4 | 623.15 | +1 | 3600 | +1 | 200 | -1 | 51.549 | 7.32 | 48.451 |
| 5 | 573.15 | -1 | 1800 | -1 | 300 | +1 | 39.431 | 5.60 | 60.569 |
| 6 | 623.15 | +1 | 1800 | -1 | 300 | +1 | 58.208 | 8.27 | 41.792 |
| 7 | 573.15 | -1 | 3600 | +1 | 300 | +1 | 60.952 | 8.66 | 39.048 |
| 8 | 623.15 | +1 | 3600 | +1 | 300 | +1 | 73.284 | 10.41 | 26.716 |
| Group 2A.2 | | | | | | | | | |
| 1 | 573.15 | -1 | 1800 | -1 | 200 | -1 | 60.201 | 8.55 | 39.799 |
| 2 | 623.15 | +1 | 1800 | -1 | 200 | -1 | 61.886 | 8.79 | 38.114 |
| 3 | 573.15 | -1 | 3600 | +1 | 200 | -1 | 72.176 | 10.25 | 27.824 |
| 4 | 623.15 | +1 | 3600 | +1 | 200 | -1 | 52.481 | 7.45 | 47.519 |
| 5 | 573.15 | -1 | 1800 | -1 | 300 | +1 | 40.319 | 5.73 | 59.681 |
| 6 | 623.15 | +1 | 1800 | -1 | 300 | +1 | 62.440 | 8.87 | 37.56 |
| 7 | 573.15 | -1 | 3600 | +1 | 300 | +1 | 59.941 | 8.51 | 40.059 |
| 8 | 623.15 | +1 | 3600 | +1 | 300 | +1 | 73.442 | 10.43 | 26.558 |

[1] Liquid Feed is approximately 15 ml (14.4g)

Appendix D3: Group 2B Raw Data

Table D3: Group 2B Raw Data

| Run[a] | Manipulated Variables | | | | | | Raw Data[1] | | |
| | $X_1$ | | $X_2$ | | $X_3$ | | | | |
| Group 2B.1 | Temperature (K) | Level | Space Time (s) | Level | Solvent (g) | Level | Liquid Yield % | Liquid mass (g) | Gas Yield % |
| 1 | 573.15 | -1 | 1800 | -1 | 200 | -1 | 38.947 | 5.61 | 61.053 |
| 2 | 623.15 | +1 | 1800 | -1 | 200 | -1 | 60.855 | 8.76 | 39.145 |
| 3 | 573.15 | -1 | 3600 | +1 | 200 | -1 | 72.841 | 10.49 | 27.159 |
| 4 | 623.15 | +1 | 3600 | +1 | 200 | -1 | 51.549 | 7.42 | 48.451 |
| 5 | 573.15 | -1 | 1800 | -1 | 300 | +1 | 39.431 | 5.68 | 60.569 |
| 6 | 623.15 | +1 | 1800 | -1 | 300 | +1 | 58.208 | 8.38 | 41.792 |
| 7 | 573.15 | -1 | 3600 | +1 | 300 | +1 | 60.952 | 8.78 | 39.048 |
| 8 | 623.15 | +1 | 3600 | +1 | 300 | +1 | 73.284 | 10.55 | 26.716 |
| Group 2B.2 | | | | | | | | | |
| 1 | 573.15 | -1 | 1800 | -1 | 200 | -1 | 60.201 | 8.67 | 39.799 |
| 2 | 623.15 | +1 | 1800 | -1 | 200 | -1 | 61.886 | 8.91 | 38.114 |
| 3 | 573.15 | -1 | 3600 | +1 | 200 | -1 | 72.176 | 10.39 | 27.824 |
| 4 | 623.15 | +1 | 3600 | +1 | 200 | -1 | 52.481 | 7.56 | 47.519 |
| 5 | 573.15 | -1 | 1800 | -1 | 300 | +1 | 40.319 | 5.81 | 59.681 |
| 6 | 623.15 | +1 | 1800 | -1 | 300 | +1 | 62.440 | 8.99 | 37.56 |
| 7 | 573.15 | -1 | 3600 | +1 | 300 | +1 | 59.941 | 8.63 | 40.059 |
| 8 | 623.15 | +1 | 3600 | +1 | 300 | +1 | 73.442 | 10.58 | 26.558 |

[1] Liquid Feed is approximately 15 ml (14.4g)